

A novel pseudo-azeotrope mosquito repellent mixture

by

Homa Izadi

A thesis submitted in partial fulfilment of the requirements for the degree

Doctor of Philosophy

in the

Department of Chemical Engineering

Faculty of Engineering, the Built Environment and Information Technology

University of Pretoria

Pretoria

A novel pseudo-azeotrope mosquito repellent mixture

Author: Homa Izadi

Supervisor: Prof Walter W. Focke

Degree: PhD (Chemical Technology)

Department: Chemical Engineering

ABSTRACT

Repellents play a key role in preventing mosquito-borne diseases such as malaria by reducing human-vector contact. The general mechanism of action relies on providing a repelling vapour around the applied area on the skin. Thus, the proper evaporation rate and consistency of the composition of the released vapour are factors determining the performance of repellent formulations. The formulation should evaporate fast enough to provide a sufficient level of repellence during its life time. However, if evaporation proceeds too fast, then it will be depleted rapidly so that activity is lost within a short period of time, which makes the repellent inefficient.

Several controlled-release approaches have been developed to improve both the protection time and level. However, these techniques have inherent drawbacks from the industrial point of view. Moreover, these techniques mostly focus only on reducing the release rate, while the consistency of the vapour composition has not been addressed.

In the present study, a novel approach towards controlling the evaporation behaviour of repellents is proposed. It is based on engineering the molecular interactions in order to design negative pseudo-azeotrope formulations. Negative pseudo-azeotrope mixtures are less volatile than the pure parent components and they do not undergo separation during evaporation.

The feasibility of the idea was investigated by studying the molecular structure of generally available repellents. Among known molecular interactions, hydrogen bonding has the most likely impact on the formation of azeotropes and in particular pseudo-azeotropes. Thus, established repellents were classified based on their chemical structures and their capability to take part in hydrogen bonding. Next, a simple spectroscopic method for anticipating pseudo-azeotropes formation was developed. Binary compositions of nonanoic acid and ethyl butylacetylaminopropionate (IR3535) showed a potential for forming pseudo-azeotrope mixtures. Hence IR3535 and nonanoic acid were selected as model compounds to test the hypothesis.

An experimental technique to confirm pseudo-azeotrope formation and to locate the composition of the probable pseudo-azeotrope point was required. To this end, an oven test was designed. The temporal mass loss, under an isothermal program, of a series of evaporating mixtures was measured. Simultaneously, the Fourier transform infrared (FTIR) spectra of the liquid remaining was recorded. Inverse analysis techniques were used to determine the composition of remaining liquid mixtures from the recorded FTIR spectra. The oven tests revealed that, as vaporisation progressed, the composition of the liquid remaining and the emitted vapour converged to a fixed IR3535 content of ca. 75 mol%. Mixtures close to this composition also featured the lowest volatility. Oven test also showed that the composition of the liquid mixtures diverged from the fixed IR3535 content of ca. 10 mol%. Mixtures close to this composition featured the highest volatility. These observations showed that IR3535 and nonanoic acid forms two pseudo-azeotrope compositions, i.e. a negative pseudo-azeotrope at an IR3535 content of ca. 75 mol%, and a positive pseudo-azeotrope at IR3535 content of ca. 10 mol%.

Thermogravimetric analysis (TGA) and differential scanning calorimetry (DSC) were applied to check these results. TGA confirmed that the negative pseudo-azeotrope mixture is less volatile while the positive pseudo-azeotrope is more volatile than the parent compounds. The DSC results revealed that in comparison with the pure compounds, negative pseudo-azeotrope had a lower boiling point onset while the positive pseudo-azeotrope had a higher boiling point.

Although negative pseudo-azeotrope repellent formulations have the desired lower constant release rate, their repellent activity needed to be tested. This is due to the fact that mixing the

ingredients to formulate a negative pseudo-azeotrope results in interactions among the components. As a consequence, the inherent repellence effect of the compounds might have been impaired in the mixture.

The modified arm-in-cage test was used to test the repellence of the controlled-release repellent formulation i.e. the negative pseudo-azeotrope of the IR3535 + nonanoic acid system. Results showed that the mixture featured improved performance with respect to both repellence efficacy and persistence. Moreover, the negative pseudo-azeotrope also exhibited a knock down effect, even resulting in mortality of most of the test mosquitoes.

The presence of two pseudo-azeotrope points at different composition in the IR3535 + nonanoic acid system is a rare occurrence, analogous to double azeotropy. Thus, molecular simulation techniques were used to explore the nature of system and the interactions responsible for this unique behaviour. Gibbs-Monte Carlo simulation results suggest that variations in the sizes of the molecular clusters present in the liquid at various compositions might be responsible. They revealed that IR3535 and nonanoic acid in neat form are both highly structured liquids. The break-down in the structure of IR3535 at high concentrations of the acid may be the origin of increased evaporation rate and formation of the positive pseudo-azeotrope. On the other hand, negative pseudo-azeotrope may be resulted from formation of bulkier clusters at the ration of 3:1 (IR3535: nonanoic acid).

Key words: Repellents, controlled-release, evaporation, pseudo-azeotrope, hydrogen bonding, molecular interactions

DEDICATION

This thesis work is dedicated to my husband, Erfan, who has been a constant source of support and encouragement during the challenges of my life. Thanks for your unconditional love! I am truly thankful for having you in my life!

ACKNOWLEDGEMENTS

I would like to express my sincere gratitude to the following people since without their support this study would not have been possible:

- Prof Walter Focke for the continuous support of my PhD study and related research, for his patience, encouragement, and motivation. His guidance helped me in all the time of research and writing of this thesis.
- Dr Jannie Pretorius for the insightful discussions and valuable advices in the study conducted in chapter 5.
- Mrs Suzette Seymore for assisting me in many different ways and handling the paperwork and ordering the reagents.
- Mr Ollie del Fabbro and Mrs. Isbe van der Westhuizen for their patience during experimental setups and TGA runs.
- To all my former and present colleagues at University of Pretoria for making an enjoyable working environment.
- My parents Hadi and Nasrin, and my in-laws Mohammad and Zohreh for their unwavering support and being there for me throughout the duration of my study.
- Last but certainly not the least, God Almighty for his step-by-step guidance through all the difficulties. I will keep on trusting.

Contents

Abstract.....	i
Dedication.....	iv
Acknowledgements.....	v
List of figures.....	xii
List of tables.....	xvii
List of abbreviations	xix
1. Motivation of the study.....	2
1.1. Current vector control methods.....	2
1.1.1. Pre-bite vector elimination.....	2
1.1.2. Personal protection.....	3
1.1.3. Post-bite elimination	3
1.2. The need for more commitment to repellents	4
1.3. Problem statements	4
1.4. Aims and objectives	6
1.5. Dissertation outline	8
2. Literature review.....	11
2.1. Mosquito repellent methods.....	11
2.2. Topical repellents	11

2.3.	Topical repellent's mechanism of action	12
2.3.1.	Olfaction system of mosquitoes	12
2.3.2.	Mode of action of repellents	13
2.4.	Factors affecting the effectiveness of repellents	13
2.4.1.	Vapour pressure	13
2.4.2.	Other factors.....	14
2.5.	Current efforts to develop topical repellents	15
2.5.1.	Discovery of new repellents.....	15
2.5.2.	Enhancement of efficacy of repellents.....	16
2.6.	Synergy, magic of mixing	18
2.7.	Transesterification.....	19
2.8.	Azeotropes and pseudo-azeotropes	20
2.8.1.	Thermodynamics of azeotropes	21
2.9.	Repellent selection rules for formation of pseudo-azeotrope mixtures.....	23
2.9.1.	Chemical structure of repellents	23
2.10.	Possible intermolecular interactions	32
2.11.	Prediction of pseudo-azeotrope formation	33
2.11.1.	Vibrational spectroscopy.....	35
2.11.2.	Ultraviolet–visible (UV-Vis) spectroscopy.....	36
2.12.	Review of azeotrope determination methods	39

2.12.1.	Inverse analysis technique.....	41
2.12.2.	Differential scanning calorimetry.....	42
2.13.	Molecular simulation techniques.....	43
2.13.1.	Introduction to molecular simulation.....	43
2.13.2.	Monte Carlo method.....	45
2.13.3.	Practical implementation.....	46
2.13.4.	Force field	48
2.13.5.	Introduction of molecular potentials to AUA force field.....	49
2.14.	Evaluation of repellence	54
2.14.1.	Arm in cage test.....	54
2.14.2.	Ethical considerations	55
3.	Experimental.....	58
3.1.	Reagent and suppliers.....	58
3.2.	Instrumentation.....	58
3.2.1.	FTIR spectroscopy	58
3.2.2.	Raman spectroscopy	58
3.2.3.	UV-Vis spectroscopy	58
3.2.4.	TGA	59
3.2.5.	DSC.....	59
3.2.6.	Density	60

3.3.	Method development: Part 1- Oven test.....	60
3.3.1.	The inverse composition identification method.....	61
3.4.	Method development: Part 2 - Repellence test.....	62
3.4.1.	Animal preparation	62
3.4.2.	Test Repellents	62
3.4.3.	Test Procedure	62
4.	Results	65
4.1.	Vibrational spectroscopy.....	65
4.2.	UV-Vis spectroscopy	70
4.3.	Oven test.....	74
4.4.	TGA.....	77
4.5.	DSC	78
4.6.	Repellence test.....	79
5.	Discussions	83
5.1.	Vibrational spectroscopy.....	83
5.2.	UV-Vis spectroscopy	85
5.3.	Oven test.....	90
5.4.	TGA.....	91
5.5.	DSC	91
5.6.	Repellence test.....	92

6. Molecular simulations	95
6.1. Insertion of missing parameters to AUA.....	95
6.2. Validation of the added parameters.....	98
6.3. Ensemble	98
6.4. Radial distribution functions	101
6.4.1. Nonanoic acid	101
6.4.2. IR3535.....	103
6.4.3. Mixtures	106
7. Conclusion	118
8. References	120
9. Appendices	141
9.1. Appendix A: Validated A and B parameters for $K= 2.75$ used for electric charge calculation based on EEM.....	141
9.2. Appendix B: Informed consent forms to practice in the repellence study	142
1) Introduction:	142
2) What is this research about and why is it being done?	142
3) Why are you invited to participate in this study?	143
4) How many people will take part in this research study?	143
5) How long will you take part in this research study?.....	143
6) What procedures are involved in this research study?	143

7) What are the risks and discomforts of this research study?.....	144
8) What benefits are there for taking part in this study?.....	144
9) Are there reasons that your participation may end early?	144
10) What will happen when the research study is over?.....	145
11) Will you have to pay to take part in this research study?	145
12) What privacy and confidentiality procedures apply to the information gathered about you in this study?	145
13) Who can answer your questions about the research and your rights as a research subject?	145
14) Consent to participate in this research study	145
9.3. Appendix C: The initial compositions of mixtures used in the oven test	147
9.4. Appendix D: Compositions used for constructing the training set for inverse mapping	148
9.5. Appendix E: Considerations to minimize some of the possible sources of deviation of Beer-Lambert law	149
9.6. Appendix F: GIBBS-Monte Carlo flowchart for calculation of density of liquids.	150
9.7. Appendix G: Measured density of IR3535 over a range of temperature	151
9.8. Appendix H: Validation of AUA model based on the reported density of N, N-dimethylacetamide	153
9.9. Appendix I: Validation of AUA model based on the reported radial distribution function of N, N- dimethylacetamide.....	154
9.10. Appendix J: GIBBS-Monte Carlo flowchart for calculation of single phase properties of IR3535-nonanoic acid binary mixtures.....	155

LIST OF FIGURES

Figure 1. FTIR spectra of nonanoic acid and IR3535.....	65
Figure 2. Raman spectra of nonanoic acid and IR3535.....	65
Figure 3. FTIR spectra of binary mixtures of nonanoic acid and IR3535 at various concentrations. The indicated IR3535 concentrations refer to the IR3535 content of the liquid phase.	67
Figure 4. Raman spectra of binary mixtures of nonanoic acid and IR3535 at various concentrations. The indicated IR3535 concentrations refer to the IR3535 content of the liquid phase.	68
Figure 5. The position of the peak assigned to carbonyl bond in cyclic dimer structure as a function of IR3535 molar concentration in the FTIR spectra.....	69
Figure 6. Frequency new-formed peak as a function of IR3535 molar ratio in the FTIR spectra.....	69
Figure 7. UV-Vis spectrum of nonanoic acid.....	70
Figure 8. UV-Vis spectrum of IR3535.....	70

Figure 9. UV-Vis spectra of nonanoic acid-IR3535 mixtures (with nonanoic acid as reference) at various compositions. The indicated IR3535 concentrations refer to the IR3535 content of the mixtures.....71

Figure 10. Intensity of the main peak of figure 9 at its maxima versus IR3535 molar concentration.....71

Figure 11. ΔAbs of IR3535-nonanoic acid mixtures at different concentrations73

Figure 12. Deviation from Beer-Lambert law at $\lambda_{1max} = 247$ nm and $\lambda_{2max} = 253$ nm ...73

Figure 13. Evaporation profile of IR3535 and nonanoic acid binary mixtures obtained in oven test. The indicated concentrations refer to the primary IR3535 content of the liquid phase. ..74

Figure 14. Mole fraction of IR3535 remained in the liquid phase as a function of the fraction of mixture released. The indicated concentrations refer to the primary IR3535 content of the liquid phase.75

Figure 15. Mole fraction of IR3535 remained in the liquid phase as a function of time. The indicated concentrations refer to the primary IR3535 content of the liquid phase.....76

Figure 16. Mole fraction of IR3535 in the released vapour as a function of time. The indicated concentrations refer to the primary IR3535 content of the liquid phase.77

Figure 17. TGA evaporation profiles of selected binary mixtures compared with pure nonanoic acid and pure IR3535. The indicated concentrations refer to the initial IR3535 content of the liquid phase.78

Figure 18. DSC profiles of IR3535-nonanoic acid binary mixtures in comparison with pure IR3535 and pure nonanoic acid. The indicated concentrations refer to the primary IR3535 content of the liquid phase. 79

Figure 19. Protection of negative pseudo-azeotrope, IR3535 and DEET tested 3 to 360 minutes after application on skin 81

Figure 20. Two major electronic excitations of a carbonyl group (Reusch, June 2010) 86

Figure 21. Comparing the measured (○) densities of IR3535 with values (▲) calculated using the AUA model 98

Figure 22. Adopted move attempts for internal and rigid moves, Insertion test and volume moves in the first stage run to equilibrate the density 100

Figure 23. Adopted move attempts for internal and rigid moves, Insertion test and volume moves 101

Figure 24. Partial radial distribution functions of the carbonyl oxygen atom in the nonanoic acid molecule 102

Figure 25. Snapshot of dimer ring configuration in nonanoic acid at P = 1 atm, T = 323 K. The short contacts are shown with dash blue lines 102

Figure 26. Deconvolution of the peak related to H(OH)-O(OH) in partial radial distribution function of nonanoic acid as calculated presently 103

Figure 27. Partial radial distribution functions of either nitrogen or oxygen with methyl groups in IR3535..... 104

Figure 28. Snapshot of IR3535 aggregation in IR3535 at $P = 1 \text{ atm}$, $T = 323 \text{ K}$. IR3535 molecules are shown by red, blue, and grey lines for oxygen, nitrogen and carbon atoms, respectively. The short contacts are shown with dashed blue lines 105

Figure 29. Two typical aggregations of IR3535 molecules. Red, blue, and grey lines represent oxygen, nitrogen and carbon atoms, respectively. The short contacts are shown with dashed blue lines. 106

Figure 30. Partial radial distribution functions $H(OH) - O(CO)$ in the nonanoic acid molecule at various concentrations of IR3535. The indicated concentrations refer to the IR3535 content of the liquid phase. 107

Figure 31. Partial radial distribution functions $H(OH) - O(OH)$ in the nonanoic acid molecule at various concentrations of IR3535. The indicated concentrations refer to the IR3535 content of the liquid phase. 108

Figure 32. Partial radial distribution functions $C(CO) - O(CO)$ in the nonanoic acid molecule at various concentrations of IR3535. The indicated concentrations refer to the IR3535 content of the liquid phase. 109

Figure 33. Partial radial distribution functions $O(CO) - O(CO)$ in the nonanoic acid molecule at various concentrations of IR3535. The indicated concentrations refer to the IR3535 content of the liquid phase. 110

Figure 34. Partial radial distribution functions of $H(OH) - O(sp^2\text{-ester})$ at various concentrations of IR3535. The indicated concentrations refer to the IR3535 content of the liquid phase. 110

Figure 35. Partial radial distribution functions involving C(CO-acid) - O(sp²-ester) at various concentrations of IR3535. The indicated concentrations refer to the IR3535 content of the liquid phase 111

Figure 36. Partial radial distribution functions H (OH) - O(sp³-ester) at various concentrations of IR3535. The indicated concentrations refer to the IR3535 content of the liquid phase. 112

Figure 37. Snapshot of IR3535-nonanoic acid (3:1) aggregation at P = 1 atm, T = 323 K. Red, blue, and grey spheres represent oxygen, nitrogen and carbon atoms, respectively. The short contacts are shown with dash blue lines 113

Figure 38. Partial radial distribution functions H(OH) - O(sp²-amide) at various concentrations of IR3535. The indicated concentrations refer to the IR3535 content of the liquid phase 114

Figure 39. Partial radial distribution functions for nitrogen at various concentrations of IR3535. The indicated concentrations refer to the IR3535 content of the liquid phase 115

Figure 40. Partial radial distribution functions O(sp²-ester) - N at various concentrations of IR3535. The indicated concentrations refer to the IR3535 content of the liquid phase 115

Figure 41. Partial radial distribution functions O(sp²-amide) - O(sp³-ester) at various concentrations of IR3535. The indicated concentrations refer to the IR3535 content of the liquid phase 116

LIST OF TABLES

Table 1. Chemical structure and boiling point and boiling points of some of the known insect repellents, containing amide group.	25
Table 2. Structure and boiling point of some of the known insect repellents, containing piperidine functional group.	26
Table 3. Structure and boiling point of some of the known insect repellents, containing diol functional group.	27
Table 4. Structure and boiling point of some of the known insect repellents, containing phthalate ester moiety.	28
Table 5. Structure and boiling point of some of the known insect repellents, containing carboxylic acid functional group.	29
Table 6. Structure and boiling point of some of the known insect repellents, containing ester functional group.	31
Table 7. Three-minute mosquito repellence screening results for DEET and binary mixtures of IR3535 and nonanoic acid. Protection was measured after a three-minute exposure period	79
Table 8. Time lag repellence tests using DEET, IR3535 and negative pseudo-azeotrope containing 75% IR3535	80

Table 9. Added stretching parameters of the anisotropic united atoms intermolecular potential for tertiary amides	95
Table 10. Added bending parameters of the anisotropic united atoms intermolecular potential for tertiary amides	95
Table 11. Added torsion parameters of the anisotropic united atoms intermolecular potential for tertiary amides (In units of K)	96
Table 12. Applied charges for tertiary amides	97

LIST OF ABBREVIATIONS

ASTM	American Society for Testing and Materials
AUA force field	anisotropic united atom force field
AUA	anisotropic united-atom
CPT	complete protection time of repellents
DDT	dichlorodiphenyltrichloroethane
DEET	N,N-diethyl-meta-toluamide
DSC	differential scanning calorimetry
EDs	effective doses
EEM	electronegativity equalization method
EPA	environmental protection agency
EPA	environmental protection agency
EOS	equation-of-state
FTIR	Fourier transform infrared
GE	Gibbs energy
GEMC	Gibbs ensemble Monte Carlo
GDI	Gibbs-Duhem integration
GRN	gustatory receptor neuron

HB	hydrogen bond
HBA	hydrogen bond acceptor
HBD	hydrogen bond donor
IRS	indoor residual spraying
IR	infrared
IR3535	Insect repellent 3535 (trade name for ethyl butylacetylaminopropionate)
ITWL	Insecticide treated wall linings
IVM	Integrated Vector Management
NPT	Isothermal–isobaric ensemble. The number of molecules, the pressure and the temperature are kept constant.
LOO-CV	leave-one-out cross validation
LOS	length of stay
LLITN	long-lasting insecticide-treated net
MCMC	Markov chain Monte Carlo
MedeA	material design
NRTL	non-random two-liquid
NMR	nuclear magnetic resonance
OBP	odorant binding protein
OR	odorant receptors

ORN	olfactory receptor neuron
Pmd	para-menthane-3,8-diol
PLSR	partial least squared regression
QSPR	quantitative structure–property relationship
TGA	thermogravimetric analysis
UV-Vis	ultraviolet–visible
UA force field	united atom force field
UA	united atoms
UNIQUAC	universal quasi-chemical
VLE	vapour liquid equilibrium
VLE	vapour/liquid equilibrium
WHO	World Health Organization

Chapter 1

MOTIVATION AND AIM OF STUDY

1. Motivation of the study

Malaria is a deadly disease transmitted to people through the bites of infected female mosquitoes (WHO, 2014). The disease itself is caused by parasitic protozoans, a group of single-celled micro-organisms. Almost half of the world population is at risk of malaria while most deaths occurs among children and pregnant women (WHO, 2008).

For decades, the fight against malaria has been pursued through the implementation of various elimination and eradication programs. There is a growing realization that no single control method in any given setting is sufficient to eradicate malaria. Rather, an entire package of appropriate techniques should be considered (Griffing *et al.*, 2014). In the hope of reducing the great burden of malaria, elimination programs consider three main priorities: (i) Diagnose the infected cases and treat all people carrying parasites; (Chen et al.) Provide vector control to reduce vector-human contact; and (iii) Implement chemoprevention to avoid new infections in human beings (WHO, 2015).

Due to the lack of effective vaccines, the emergence of drug resistance and exorbitant costs of antimalarials, the main focus of malaria elimination programs is still on effective vector control interventions (Karunamoorthi, 2011b).

1.1. Current vector control methods

Several vector control strategies have been suggested to control the spread of malaria. The World Health Organisation (WHO) introduced integrated vector management (IVM) and recommended the use of a combination of techniques to attack vectors at different stages of their life cycle (WHO, 2004). These vector control strategies fall into three main categories: Pre-bite elimination, personal protection, post-bite elimination.

1.1.1. Pre-bite vector control

The goal of pre-bite vector elimination is to reduce the number of adult mosquitos by targeting specific stages of the vector life cycle. For instance, the environmental management approach attempts to make the potential breeding sites for mosquitoes unsuitable for the development of mosquito larvae (WHO, 1982, Walker and Lynch, 2007, Grieco *et al.*, 2005). Larvicidal

techniques target the aquatic stages of *Anopheles* mosquitoes (Fillinger and Lindsay, 2006, Gu *et al.*, 2008, Utzinger *et al.*, 2001, Fillinger *et al.*, 2009, Killeen, 2003, Killeen *et al.*, 2002a, Killeen *et al.*, 2002b, Shousha, 1948). Adulticidal is a method that aims to reduce the number of adult mosquitoes through ground-based or aerial application of pesticides (Bonds, 2012, Conlon, 2011). Biological vector population control relies on vector pathogens such as specific bacteria (Federici *et al.*, 2003, Federici *et al.*, 2007), Fungi (Couch, 1972, ES, 1985), predators (Bukhari *et al.*, 2013, Karunamoorthi, 2011a) or competitors (Duquesne *et al.* 2011).

Mating with infertile males, results in the emergence of infertility in the female mosquitoes. Sterilisation of male mosquitoes by exposing the pupae or adult mosquitoes to high-energy radiation is reportedly an effective technique to decrease the fecundity of the mosquitoes (Helinski *et al.*, 2009). This technique is most effective when it is applied at the time when the number of the mosquitoes reaches a seasonal minimum.

1.1.2. Personal protection

With 30 to 60 percent reduction in malaria morbidity, personal protection becomes a very effective strategy for malaria prevention. It also helps to prevent the development of drug resistance (Touré, 2001). Long-lasting insecticide-treated nets (LLITNs) are among the highly accepted personal protection tools available due to the advantages they provide. LLITNs are inexpensive and simple to implement. Unlike normal insecticide-treated bed nets, LLITNs do not need to be re-treated. They utilize less insecticide and a smaller amount is released to contaminate water resources (Guillet *et al.*, 2001). The main limiting factor of LLITNs is that protection is provided only during the sleeping time span. Moreover, mosquitoes develop resistance against insecticides over time (Dabiré *et al.*, 2006). On the other hand, repellents are considered a key component to control malaria by providing personal protection outdoors (Fradin, 2001, Curtis, 1992). A wide variety of mosquito repellent products with a varying lengths of stay (Singleton *et al.*) and diverse levels of effectiveness are available.

1.1.3. Post-bite elimination

Post-bite elimination techniques aim to kill mosquitoes after they have fed to prevent transmission of infection to other people. For instance, Indoor Residual Spray (IRS), which involves coating the surfaces with residual insecticides, targets the fed mosquitos trying to rest

on indoor surfaces. Dichlorodiphenyltrichloroethane (DDT) is the most effective among the WHO-approved IRS insecticides (WHO, 2006a). However, serious concerns have been raised about the long-term safety of use of DDT as it is a persistent organic pollutant.

Net-like insecticide treated wall linings (ITWLs) covering interior house walls is a potential alternative to IRS that overcomes some of the inherent limitations, e.g. its dependence on DDT as well as the problem of insecticide dusting (Kruger *et al.*, 2015).

1.2. The need for a greater commitment to repellents

Based on the techniques reviewed in Section 1.1, vector control remains the cornerstone for malaria elimination. Pre-bite and post-bite vector control interventions offer promising results. However, they should be done under the guidance and control of higher authorities or organisations rather than being managed by individuals. Personal protection provides supplementary protection to pre-bite and post-bite vector control by involving individuals in malaria control. WHO recommended LLITN is an effective intervention, able to provide personal protection. However, owing to the development of resistance, it could also become ineffective. Moreover, LLITNs target mosquitoes that feed indoors, while a significant proportion of malaria infections is due to exposure to vector mosquitoes when people are active outdoors, i.e. not subject to protection by LLITNs.

Repellents are accepted vector control interventions. They provide effectively outdoor personal protection. However, most repellents on the market suffer from some limitations. These include health side-effects, adverse environmental impacts, and short residual activity. In view of this perspective, exploration of novel alternatives and development of innovative ways to improve the existing repellents are warranted.

1.3. Problem statements

Repellents are considered a key component to control malaria as they provide personal protection outdoors (Fradin, 2001, Curtis, 1992). To be effective, repellents are expected to satisfy several basic requirements such as minimal adverse influence, commercial availability, low cost, effective repellence, low odour, stability, and an appropriate evaporation rate (Reifenrath, 2002).

DEET is considered the gold standard mosquito repellent on the market. It is the most widely used repellent over the last few decades (Fradin, 1998). Despite the outstanding effectiveness of DEET, it nevertheless suffers from several problems. Adverse human side effects, include insomnia, mood disturbances, impaired cognitive function, skin hypersensitivity, eye irritations, headache, weakness, fatigue, muscle and joint pain, tremors, shortness of breath and in some cases seizures and even death have been reported (Goodyer and Behrens, 1998, Bell *et al.*, 2002, Abou-Donia *et al.*, 2001). Moreover, more and more scientific evidence indicates that DEET is somewhat toxic to birds, fish and aquatic invertebrates (Weeks *et al.*, 2012). DEET also has a potential to penetrate into soil and contaminate the ground water (Miller, 2000). On the other side of the coin, the relatively high cost of DEET and the need for repeated application to the skin at high concentrations precludes its use in poor tropical countries where malaria is most prevalent (Turner *et al.*, 2011).

Because of these concerns, the search for alternatives to DEET has become an important goal for the repellent industry. Numerous studies attempted to address this issue through two main approaches: (1) searching for novel active ingredients with high intrinsic repellence, and (2) enhancing the physical and chemical properties of available repellents.

Efforts to introduce new active repellent to market have been hampered by numerous issues including the huge cost of safety assessment (Gupta and Bhattacharjee, 2007). This fact encourages one to consider enhancement of available repellents. Several studies have aimed to keep the release rate of repellent formulations under control (Debboun *et al.*, 2014).

Fast repellent evaporation rates result in inefficient use. After a short period of application, the active becomes depleted and protection is lost. On the other hand, a minimum evaporation rate is required in order to provide effective repellence (Reifenrath *et al.*, 1989). Moreover, there is always the risk of alteration of the repellent mixture's composition during its evaporation due to the volatilities differences among the formulation constituents. This can have a negative effect on the efficacy of the formulation and limits its performance. A constant effective repellent composition is preferred to provide active ingredients in the released vapour during the full protection time.

Excellent progress has been made in the development of a wide variety of delivery forms that implement physical barriers. Microcapsules (Solomon *et al.*, 2012, Massey and Langley, 2015) and microporous polymers (Tang *et al.*, 2016) have been proposed to control the evaporation rate of repellents. However, these techniques have several inherent drawbacks from the standpoint of industrial application.

Addition of other ingredients, e.g. non-volatile solutes and perfume fixatives, is an alternative strategy to moderate the release rate of repellents. However, there is still limited scientific understanding of basic principles for combining and formulating repellent compounds to reach desired properties such as controlled release, reduced absorption, abrasion resistance, synergism, user acceptance and, etc. (Louis and Raj, 2006). Advancing repellent science requires more than the focussed study of specific formulations or individual active ingredients alone. Advances in the basic knowledge of combining and formulating repellents are also needed.

1.4. Aims and objectives

The aim of the current study was to develop methods to control the release rate of repellent formulations at a constant, reduced level. Towards this end, the concept of utilizing negative pseudo-azeotrope repellent mixtures is proposed. The hypothesis behind this approach is the fact that such pseudo-azeotrope mixtures should reduce the rate of evaporation compared to the constituents and, in addition, guarantee a constant vapour composition.

Although the azeotrope phenomenon is well-known in thermodynamics (Kiva *et al.*, 2003b, Lei *et al.*, 2005), to the best of authors' knowledge, the concept has not yet been considered in the repellent technology and its application has not yet been justified in this field. Therefore, a main objective of this study is to introduce this concept to the repellent community. The second object of the current work is to develop a work plan to design and characterize negative pseudo-azeotrope mixture of repellents with the desired properties.

Therefore, the management of the intermolecular interactions, e.g. hydrogen bonding interactions, as a method to design negative pseudo-azeotropes was investigated. Specifically, combinations of IR3535 and nonanoic acid were used to test the hypothesis.

The specific objectives were as follows:

- Check the feasibility of the idea, i.e. formation of negative pseudo-azeotrope mixtures, between known repellents, based on a study of their chemical structure
- Explore simple rules to select proper repellents based on their capability to entering into hydrogen bonding interactions
- Develop rough-and-ready experimental methods for preliminary checking of the selected pairs
- Develop accurate tests to ascertain formation of negative pseudo-azeotropes and also to locate the corresponding composition
- Characterize the repellent formulation by thermal analysis, e.g. TGA and DSC techniques
- Perform molecular simulations to identify the nature of the pseudo-azeotrope mixtures
- Perform bioassay tests to check the efficacy of the selected repellent formulation

1.5. Dissertation outline

This dissertation is divided into six chapters. Chapter 1 gives a general overview of the role of vector control techniques in decreasing the burden of malaria. The most effective available vector control methods are briefly reviewed and the importance of repellents among them is justified. One of the main challenges of repellent industry is to keep the release rate under control and attempts of meeting this basic requirement are presented. This is followed by a novel hypothesis based on pseudo-azeotrope formation to bridge one of the gaps in current controlled release methods. Finally, the aims and objectives of the current study are presented.

Chapter 2 is the literature review. It starts by giving a brief explanation of the mosquito repellent methods. This is followed by information on commercially available topical repellents, their mechanisms of action and the factors affecting their effectiveness. The Chapter also reviews the difficulties of introducing novel repellent compounds to the market and the approaches taken to enhance the properties of the current repellent compounds. Application of chemical additives to enhance repellent formulations and the phenomenon of synergy in repellent mixtures is briefly explained. This Chapter also provides a brief overview of the concept of an azeotrope and pseudo-azeotrope mixtures. The chemical structure of repellents and their possible intermolecular interactions are also reviewed. A brief review of the techniques used to characterize the intermolecular interactions, azeotrope formation and repellent activity of repellent mixtures is presented.

Chapter 3 is divided into four parts. The first part provides information on all the reagents used in this study. The second part explains all the experiments that were carried out, including the experimental conditions, the mixture preparation and the instrumentation used for characterisation. The third part gives information on the development of the inverse technique and oven test methods. The fourth part present the details of repellence testing, including the test procedure and preparation of the test mosquitoes.

Chapter 4 details the results. This chapter presents the liquid phase FTIR, Raman and UV spectroscopic results of binary mixtures of the understudy model compounds, i.e. IR3535 and

nonanoic acid. This is followed by the oven test, thermogravimetry and DSC results for the mixtures. Finally, the repellence test results are presented.

Chapter 5 presents a discussion of the results. This Chapter provides detailed comments on all the results presented in Chapter 4.

Chapter 6 reveals the information provided by molecular simulation techniques that were done in order to obtain a deeper understanding of the nature of the pseudo-azeotrope mixtures comprising IR3535 and nonanoic acid.

This is followed by the Conclusion Section of Chapter 7.

The References provide a record of the literature consulted in the course of this study, which was also used to elucidate the findings of the study.

The Appendices contain complementary and supplementary data generated during the study.

Chapter 2

LITERATURE REVIEW

2. Literature review

2.1. Mosquito repellent methods

Repellence is defined as “any stimulus which elicits an avoiding reaction” (Dethier *et al.*, 1960, Dethier, 1948). Mosquito repellents may be classified on the basis of their application into the following categories (Xue *et al.*, 2014):

- Topical repellents which are applied to selected parts of the skin and clothes
- Area repellents which are dispensed into the atmosphere of a space to inhibit the ability of mosquitoes to locate and track a target (Nolen *et al.*, 2002)
- Plants, such as *Corymbia citriodora* (Seyoum *et al.*, 2003) which can repel mosquitoes from their surrounding area
- Energy-emitting repellents which are purported to disrupt insect activities by producing ultrasound (Okorie *et al.*, 2015) or emitting electromagnetic energy (Canfield *et al.*, 2015)
- Treated fabrics such as treated clothes, curtained and bed nets which are impregnated with insecticides and repellents
- Systemic repellents which are taken orally and which include garlic, vitamin B1 and vitamin B12 (Xue *et al.*, 2014)

Among the described classes of repellents, topical repellents are the most common (Xue *et al.*, 2014).

2.2. Topical repellents

Despite difficulties in distribution to poor communities (McElroy *et al.*, 2009), topical repellents are a key component of personal protection (Curtis, 1992, Fradin and Auerbach, 2001).

A wide range of repellents have been identified. They are classified, according to their source of origin, into synthetic or plant-based repellents. Each of these compounds has a different intrinsic protection which varies over different mosquito species (Lupi *et al.*, 2013).

The most widely used synthetic active ingredients in commercial products are DEET, IR3535 (ethyl butylacetylaminopropionate) and picaridin (1-piperidinecarboxylic acid 2-(2-hydroxyethyl)-1-methylpropylester; KBR 3023) (Stanczyk, 2011).

Although the synthetic repellents can provide a satisfactory level of protection, the relatively high price, the smell and greasy feeling, and even safety concerns may discourage the public to use some of them (Service, 2008).

Plant-based repellents such as citronella oil and *p*-menthane-3,8-diol (PMD) were investigated as potential alternatives (Moore *et al.*, 2002, Frances *et al.*, 2005, Park *et al.*, 2005, Zhu *et al.*, 2006, Muller *et al.*, 2009). However, they usually provide less effective protection in terms of efficiency and persistence (Fradin and Day 2002, Frances *et al.*, 2005).

2.3. Topical repellent's mechanism of action

Generally topical repellents provide vapour around the applied area to repel mosquitoes (Satpute, 2015). The emitted vapour exerts its impact through interactions with olfactory and gustatory receptors in mosquitoes (Dickens and Bohbot, 2013). There are many unanswered questions about the mode of action of repellents. However, thanks to electrophysiological studies and molecular simulations, some effects of repellents on olfactory and gustatory processes have been determined (Dickens and Bohbot, 2013).

The olfaction system of mosquitoes and some of the theories of repellents' mode of actions are briefly discussed in Sections 2.3.1 and 2.3.2 respectively.

2.3.1. Olfaction system of mosquitoes

Mosquitoes' olfactory systems contain thousands of sensilla, the hair-like structures on the antennae and maxillary palps of mosquitoes. Each sensilla contains a few olfactory receptor neurons (ORNs). It has been shown that active semiochemicals pass through the outer membrane of the sensilla (McIver, 1982). Odorant binding proteins (OBPs) transfer semiochemicals from sensilla to olfactory receptors (Nutting and Horsley). Binding of semiochemicals to ORs renders depolarization of the cell and as a consequence an action potential is sent to the brain through the olfactory nerve (Davis, 1976, Davis and Sokolove,

1976). This process results in behavioural changes such as attraction or repulsion in mosquitoes.

Electrophysiological studies and molecular studies have provided valuable information about the mode of action of repellents, i.e. the particular response of mosquitoes' peripheral olfaction system to the compound which cause repulsion.

2.3.2. Mode of action of repellents

The main modes of actions of repellents are as follow:

- Masking responses of olfactory receptor neurons (ORNs) to attractants (Turner and Ray, 2009)
- Activating specific ORNs or specific odorant receptors (Nutting and Horsley) to confuse the mosquitoes (Turner *et al.*, 2011)
- Reduction of the released attractants and changing the chemical composition of human emanations (Dogan *et al.*, 1999, Ditzen *et al.*, 2008)
- Stimulation of the gustatory receptor neuron (GRN) and changing the feeding behaviour (Hao *et al.*, 2008)
- Modulation of activity of specific ORNs and ORs to their ligands and inhibit responses of ORs to attractants (Bohbot and Dickens, 2010)

2.4. Factors affecting the effectiveness of repellents

The efficacy of repellents depends mainly on factors such as:

- The intrinsic repulsion of the compound
- The vapour pressure of repellent
- Environmental factors such as wind, humidity, temperature
- Individual factors such as perspiration and susceptibility to mosquito bites
- Mosquito species, age and density
- Repellent formulation

Some of these factors are discussed in sections 2.4.1 and 2.4.2.

2.4.1. Vapour pressure

As mentioned in Section 2.3, topical repellents exert their effect through releasing vapour around the applied area. Thus to be effective, the formulation should be sufficiently volatile to repel the mosquitoes (Garson and Winnike, 1968). Vapour pressure is related to the volatility of repellents and as a consequence, is a critical factor in terms of efficacy of repellent formulations. Graham (Graham, 2006) has described vapour pressure as “the property causing a chemical to evaporate” and is defined as “the pressure of the vapour in equilibrium with the liquid or solid state; measured in J m^{-3} ” (Graham, 2006).

A large set of repellents are volatile and have a high vapour pressure, while other repellents feature a low vapour pressure. At high mosquito densities, a low concentration of a highly volatile repellent in the formulation may provide sufficient protection, whereas a high concentration of low vapour pressure repellents in the liquid is required to provide enough vapour for protection. On the other side, the high evaporation rate of volatile repellents may mean that they will function for a short period of time only. A less volatile repellent can provide protection for a longer time period. However, it is noteworthy that the use of high concentrations of low vapour pressure repellents on the skin increases the risk of dermal absorption (Feldmann and Maibach, 1970).

2.4.2. Other factors

Many other factors play a role in the level of efficacy of repellents. For instance, topical mosquito repellents may be formulated in various forms such as lotions, sprays, cream, oils and grease sticks. The form, in which topical repellent is formulated, influences the efficacy of the product (Lupi *et al.*, 2013).

Individual factors including proper application of the repellent, i.e. frequency and uniformity of application, the inherent attractiveness of host to mosquitos and the level of physical activity are also important factors (Govere *et al.*, 2007).

The density of the mosquito population as well as the nature of the species, age and size of mosquitos can also affect the effectiveness of repellents (Govere *et al.*, 2007). The efficacy of repellents may also be influenced by a set of external factors such as temperature, level of humidity and wind speed. In warm, humid climates or at windy environment, the protection

time of repellents is usually lower. Each 10°C increase in temperature can lead to as much as a 50% reduction in protection time (Maibach *et al.*, 1974).

Moreover, repellents may lose their effectiveness by perspiration, abrasion, and skin penetration (Rueda *et al.*, 1998, Kroeger *et al.*, 1997).

2.5. Current efforts to develop topical repellents

Two main approaches have been taken to develop topical repellent formulations including: (1) Searching for novel active ingredients with high intrinsic repellence, and (2) enhancing the physical and chemical properties of available repellents. These approaches are briefly described in Sections 2.5.12.5.2.

2.5.1. Discovery of new repellents

Various studies have shown that repellent activity of chemical compounds is related to its chemical structure and stereo-electronic properties (Nakayama *et al.*, 1985, Nakayama and Richards, 1987, Bhattacharjee *et al.*, 2000, Suryanarayana *et al.*, 1991b). Therefore, structural studies of repellents aid the design and development of more efficient repellents. Numerous efforts are being made to develop a general structure-activity framework to guide new synthetic repellent studies (Gupta and Bhattacharjee, 2007).

Beside high intrinsic repellence, a broad range of mosquitoes, the ideal topical repellent would last for at least eight hours, cause no toxicity and skin irritation, show resistance against abrasion, humidity and sweat, and be cosmetically-acceptable (Gupta and Bhattacharjee, 2007).

Efforts to find such repellents have been hampered by the numerous factors that affect the efficacy of repellents. Various modes of action have been suggested for repellents and certain modes of action for a wide range of known repellents are still unknown (Gupta and Rutledge, 1993). Moreover, diverse species of mosquitoes may respond differently to a particular repellent (Gupta and Bhattacharjee, 2007). As mentioned before, the vapour pressure of the repellent also affects its efficacy. Other factors such as lipophilicity of the compound, the molecular size, the potential to skin penetration, resistance to water, etc., should all be

considered (Suryanarayana *et al.*, 1991a). Finding that ideal repellent is delayed by the complex correlation between the above-mentioned factors and efficacy of repellents (Gupta and Bhattacharjee, 2007).

Moreover, discovery of new repellent active ingredients is a complicated process. Promising active ingredients have to pass through numerous filters to be tested for the human and probable environmental side effects. It takes about 10 years and, on average, approximately \$30 million to bring a new insect repellent to market (Gupta and Bhattacharjee, 2007). Based on Environmental Protection Agency (EPA) information, more than 38% of the U.S. population and more than 200,000,000 people around the world still use DEET-based repellents (Gupta and Bhattacharjee, 2007).

2.5.2. Enhancement of efficacy of repellents

There is a large volume of published studies to enhance the protection and longevity of repellents that eventually resulted in development of numerous controlled-release repellent formulations. Here we briefly review the approaches to increase the protection time of repellent formulations under three heading:

- (1) Attempts to control the evaporation rate or lowering the vapour pressure
- (2) Attempts to prevent skin penetration and dermal absorption
- (3) Attempts to enhance the resistance of repellent formulation against environmental abrasion and perspiration

Prevent dermal absorption

Several studies have endeavoured to reduce the skin penetration of repellents. Optimization of repellent formulations and selection of proper carriers in topical repellents is an effective approach to decrease dermal absorption (Proniuk *et al.*, 2002). Ethanol, which is the common solvent in DEET-based products, evaporates quickly resulting in an increased repellent concentration on the skin. Replacing ethanol with less volatile carriers or with cyclodextrins can retard the skin penetration and reduce the toxic effect of DEET (Proniuk *et al.*, 2002) (Burgess, 2000).

Selection of suitable polymeric vehicles for active ingredients provides a means to reduce dermal absorption. Milutinović *et al.* (Milutinović *et al.*, 1999) showed that polyvinylpyrrolidone hydrogel-based formulations act as effective vehicles that also significantly reduce dermal absorption of DEET.

Solid lipid particles also provide carrier systems with controlled release properties. Iscan *et al.* (Iscan *et al.*, 2006) incorporated DEET into the solid lipid particles to reduce the percutaneous permeation and avoid toxic side effects (Iscan *et al.*, 2006).

Increased water resistance

Several reports considered enhancement of repellent resistance to water, rain, sweat and humidity. For example, Reifenrath *et al.* (Reifenrath *et al.*, 1990) reported that mixing DEET with polymers enhances the water-resistance significantly. Application of creams, polymer mixtures or microcapsules also can improve the water-resistance and increase efficacy (Nentwig, 2003).

Lowering the vapour pressure

One approach to control the release of repellents is to use “physical barriers” as obstacles. Repellent-loaded polymeric patches are an example (Chattopadhyay *et al.*, 2013, Chattopadhyay *et al.*, 2015). They effectively prolong the repellent activity of synthetic and natural repellents since the polymers retard the release of the repellents (Chattopadhyay *et al.*, 2015). Micro-encapsulation of volatiles in shells or walled materials have been widely investigated to control the release rate of repellents (Solomon *et al.*, 2012, Massey and Langley, 2015). In micro-encapsulation, the active ingredients are enclosed in tiny capsules produced by coacervation, interfacial polymerization, extrusion, and other processes. The release rate depends on the size and number of the microcapsules, the composition and thickness of the microcapsule walls, the concentration and properties of the excipient, and other additives used (Moore *et al.*, 2007). Microporous polymers (Tang *et al.*, 2016) and layered materials (Esposito *et al.*, 2015) were reported as volatile active carriers that successfully controlled the release of repellents.

Despite their relative simplicity, physical barriers suffer from several inherent drawbacks. For instance, encapsulation of actives occurs in a limited range of pH, electrolyte and colloid concentrations (Comunian *et al.*, 2013). The main disadvantage of trapping repellents inside a polymer matrix is the varying release rate of the actives (Akhtar, 2014). Industrial manufacturing of these system is also considerably constrained by the limited solubility of liquid repellents in polymers. In cases where the repellent dissolves in the polymer matrix, the polymer will progressively shrink as the repellent is released (Akhtar, 2014).

An alternative approach to lower the evaporation rate of active ingredients is utilizing “chemical barriers”, which comprise addition of chemicals to the repellent formulation. For instance, application of non-volatile solute such as olive oil or mineral oil (Weaving *et al.*, 1967) to prolong the effect of repellents has been investigated for many years. They increase the length of stay of active ingredient by lowering the vapour pressure of repellent formulation. Effect of perfume fixatives on evaporation rate of repellents also been studied (Khan *et al.*, 1975a, Khan *et al.*, 1975b). Perfume fixatives are bulky branching molecules which lower the vapour pressure. Some of the recommended perfume fixatives to improve the repellent longevity include 2,6-dinitro-3,4,5-triethyl-*t*-butyl benzene, 2,4-dinitr-*o*-3-methyl-6-*t*-butyl anisole, 2,4-di-*t*-butyl-5-methoxybenzaldehyde, 5-*t*-butyl-2,4,6-dinitro-*m*-xylene), tibetene and vanillin.

2.6. Synergy, magic of mixing

Mixing of ingredients to formulate repellent mixtures may result in three different types of behavioural interactions among the components namely additive effects, synergistic interactions, and antagonistic interactions (Akhtar and Isman, 2013).

Synergistic interactions occur when the response of sensory neurons to the mixture surpass the summation of responses to the individual components. On the other hand, antagonistic interactions take place when sensory neurons response to the mixture become less than the summation of responses to the components (Kang and Caprio, 1991).

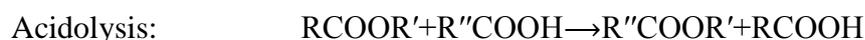
For instance, tamanu oil synergizes the repellent effect and increases the protection time of DEET and a range of plant-based repellents (Hieu *et al.*, 2010). The enhanced protection level

and time is attributed to lower vapour pressure and skin penetration of the mixture than the pure components (Akhtar and Isman, 2013). Vanillin also is known to synergize the repellent activity of a wide range of repellents (Tuetun *et al.*, 2005, Choochote *et al.*, 2007, Tawatsin *et al.*, 2001).

Deletre *et al.* (Deletre *et al.*, 2013) hypothesized that different modes of action in repellents function independently. In other word, resistance to one mode of action might not cause resistance to the other modes of action. If this theory be correct, proper selection of synergists based on evaluations of mode of action of repellents and synergists could be useful in reducing the risk of development of resistance in mosquitoes (Deletre *et al.*, 2013). However, since the mode of action of a wide range of repellents is unknown, searching for the perfect synergist is not a straight forward task (Rattan, 2010).

2.7. Transesterification

Simple mixing of ingredients may lead to substantial changes in their structure. Particularly, transesterification may play a key role in alteration of the backbone structure of compounds containing ester groups. Transesterification is an organic interaction where an ester group is transformed into another through exchange of the alkoxy moiety. This reaction can be accelerated by acid or base catalysts (Reid, 1937, Otera, 1993). The main transesterification reactions are as follow:



Note that vibrational spectroscopy techniques can be used to determine whether such reactions have occurred in the mixtures. This is due to the fact that the structural features of the molecules produce reproducible characteristics in the vibrational spectra and significant

changes in the structure of the molecules can be followed in the vibrational spectrum (Coates, 2000).

2.8. Azeotropes and pseudo-azeotropes

The definition of an azeotrope (from American Heritage Dictionary) is: “A liquid mixture of two or more substances that retains the same composition in the vapour state as in the liquid state when distilled or partially evaporated under a certain pressure.” Presence of such property is manifested by an extreme in either a pressure-composition or temperature-composition diagram (Claxton *et al.*, 1958, Nutting and Horsley, 1973).

The intersection of dew and bubble curves at an intermediate composition, in which the coexisting phase have the same composition, is the typical sign of azeotropy in pressure-composition and temperature-composition diagrams (Al-Jiboury, 2007).

The boiling point of an azeotrope is either greater than the boiling point of pure components (Higher boiling azeotrope) or less than them (Lower boiling azeotrope).

Azeotrope mixtures do not undergo separation by evaporation, condensation or distillation, only if these processes are completely equilibrium controlled (Schlünder, 1989). If diffusion plays a role in controlling the rate, the vapour-liquid phase change at constant composition may shift to other compositions. For instance, during non-equilibrium evaporation, interactions of evaporation and diffusion fluxes may cause concentration gradients (Toikka, 2006). Therefore, in absence of phase change resistance, equilibrium will be established only at the interface, whereas the bulk may remain apart from equilibrium.

Even in this case, it is possible that vapour has the same composition as the evaporating liquid, depending on the evaporation circumstances and transport properties. Such mixtures in which non-equilibrium evaporation does not alter the concentration either in the vapour or liquid, are called pseudo-azeotropes (Schlünder, 1989).

Based on the knowledge that a pseudo-azeotrope poses limits to separation performed by evaporation, and also the fact that negative pseudo-azeotrope evaporates slower than the pure

compounds, it can be concluded that negative pseudo-azeotrope mixtures of repellents guarantee a constant reduced release rate of the formulation.

2.8.1. Thermodynamics of azeotropes

The tendency of mixtures to form azeotropes depends on two main factors. They are: a) boiling points of the pure compounds, and b) the degree of non-ideal behaviour of the mixture (Al-Jiboury, 2007). The smaller the difference of boiling points of pure components and the more non-ideal the mixture is, the greater the likelihood of azeotrope formation (Al-Jiboury, 2007)

Mixing of miscible liquids containing molecules with the same size and equal intermolecular forces form a homogeneous ideal solution. In this case the properties of the mixtures depend only on the properties of the pure components (Smith, 2003). Ideal liquids obey Raoult's law:

$$y_i P = x_i P_i^{sat}(T), \quad i = 1, 2, \dots, n \quad (2.1)$$

Where x_i and y_i are the liquid and vapour composition of component i , T and P are the temperature and the pressure of the system and P_i^{sat} is the saturated vapour pressure of component i .

Raoult's law states that the partial vapour pressure of each component of an ideal mixture of liquids is equal to the vapour pressure of the pure component multiplied by its mole fraction in the mixture. Ideal liquid mixtures can easily be separated by evaporation since the vapour is richer in the compound with higher vapour pressure and does not have the same composition as the liquid. On the other hand, real liquid mixture may exhibit deviations from Raoult's law due to changes in the intermolecular forces.

Deviations from ideal behaviour in the liquid phase are considered by introducing liquid phase activity coefficient, γ_i . Assuming an ideal vapour, equation (2.1) becomes:

$$y_i P = x_i \gamma_i(T, x) P_i^{sat}(T), \quad i = 1, 2, \dots, n \quad (2.2)$$

where γ_i is the activity coefficient of component i in the liquid phase.

Positive deviations from Raoult's law ($\gamma_i > 1$) usually occur when the interactions among unlike molecules are weaker than the interactions among like molecules. In this case the mixture exhibits a higher vapour pressure than the corresponding ideal mixture.

Negative deviations ($\gamma_i < 1$) usually occur when the interactions among unlike molecules are stronger than the interactions among like molecules. In this case the mixture represents a lower vapour pressure than the corresponding ideal mixture.

The root cause for deviations from Raoult's law is the difference in the strength of intermolecular forces. For instance, the condition for the formation of higher boiling and lower boiling azeotropes in binary mixtures may be expressed as:

$$\begin{cases} \varepsilon_{AA} > \varepsilon_{AB} & \text{and} & \varepsilon_{BB} > \varepsilon_{AB} & \text{Lower boiling azeotrope} \\ \varepsilon_{AA} < \varepsilon_{AB} & \text{and} & \varepsilon_{BB} < \varepsilon_{AB} & \text{Higher boiling azeotrope} \end{cases} \quad (2.3)$$

Where ε_{ij} is the intermolecular interaction energy between molecules of types i and j .

Lee *et al.* (Lee 2002) showed that an azeotrope occurs when the departure from ideal behaviour in the mixture is large enough to overcome the vapour pressure difference of the components. In this case, extremal points appear in either pressure-composition at constant temperature or temperature-composition at constant pressure (Claxton *et al.*, 1958, Nutting and Horsley, 1973).

Based on Gibbs-Konovalov theorem (Toikka and Jenkins, 2002), the necessary and sufficient condition for existence of such extremal points is identical composition of the coexisting phases. In other words, the mixture exhibits maximum or minimum azeotrope behaviours, if and only if the following conditions are satisfied:

$$y_i = x_i \quad i = 1, 2, \dots, N \quad (2.4)$$

$$\left(\frac{\partial T}{\partial x_i}\right)_P = 0 \quad i = 1, 2, \dots, N - 1 \quad (2.5)$$

$$\left(\frac{\partial P}{\partial x_i}\right)_T = 0 \quad i = 1, 2, \dots, N - 1 \quad (2.6)$$

Where the boiling mixture exhibits either a minimum or a maximum vapour pressure at a constant temperature, or correspondingly, has a maximum or a minimum boiling temperature at a constant pressure.

2.9. Repellent selection rules for formation of pseudo-azeotrope mixtures

Wise selection of repellents and azeotrope formers can lead to negative pseudo-azeotrope formulations. This is the desired goal for a reduced, constant release rate. Management of the intermolecular interactions requires extensive knowledge of the chemical structure of repellents and their possible interaction sites.

In this section, some of the known repellents are classified based on their chemical structures. Their boiling points are also presented. The probable interactions among repellents, which can lead to pseudo-azeotrope formation are investigated.

2.9.1. Chemical structure of repellents

Several attempts have been made to investigate the basic molecular attributes of repellents. The molecular structure of known repellents and the structural classes of repellents which can play a vital role in the repellent activity are investigated.

Amides

The amides represent the most commercially popular class of modern insect repellents. N, N-Diethyl-*m*-toluamide (DEET), the most widely used mosquito repellent, is the main member of this group. The repellence of amides has been widely investigated (Suryanarayana *et al.*, 1991c). For centuries attempts have been made to obtain better repellents based on changing the substituents on the amide functional group and through optimising the length of the carbon chains (McCabe *et al.*, 1954, Gilbert *et al.*, 1955). Researchers are still interested in identifying the actual properties responsible for the repellent activity of amides.

Van der Waals surface, dipole moments, electrostatic potential and charge of the amide nitrogen, and the electrostatic potential of the amide oxygen are reportedly the influential

factors for repellence of the compound containing the amide group (Ma *et al.*, 1999, Apurba and Raj, 2006).

It also has been revealed that lipophilicity or hydrophobicity and the negative charge on the amide nitrogen atom may be key factors for the activity of this class of repellents (Apurba and Raj, 2006).

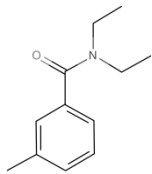
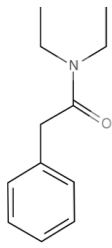
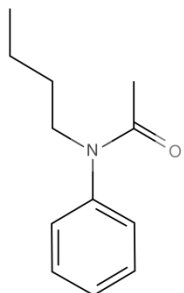
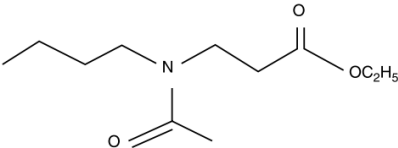
The structure and boiling point of DEET as well as a few other promising repellents containing amide functional group such as DEPA (N, N-diethyl phenylacetamide) and IR3535 (ethyl N-acetyl-N-butyl-3-aminopropionate) are presented in Table 1.

Piperidines

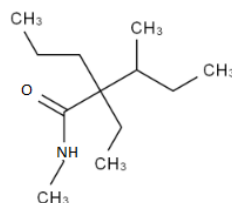
Piperidine is a heterocyclic compound that has been used as building block for the synthesis of repellents. For instance, discovery of effective repellents such as picaridin (Boeckh *et al.*, 1996), SS220 (Klun *et al.*, 2001) and AI3-35765 (Debboun *et al.*, 1999) has been initiated based on piperidine chemical structure.

Several molecular models, based on the stereo-chemical structure and the topological pattern of the molecules, have been developed in an attempt to predict the repellent activity of compounds such as SS220 and picaridin (Katritzky *et al.*, 2008). Chemical structures and boiling point of some of the most well-known piperidine-based repellents are presented in Table 2.

Table 1. Chemical structure and boiling point and boiling points of some of the known insect repellents, containing amide group.

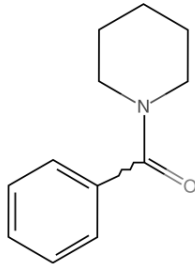
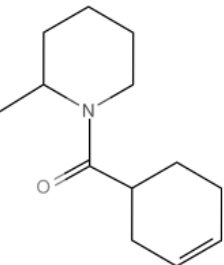
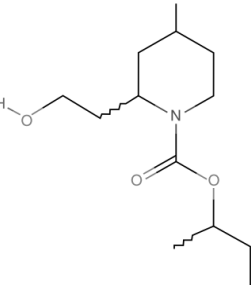
Common name	Formula name	Structural formula	Boiling point (°C)
DEET	N,N-Diethyl-meta-toluamide		288
DEPA	N,N-Diethyl-2-phenylacetamide		170
N-butyl acetanilide	N-butyl-N-phenyl-ethanamide		281
IR3535	Ethyl butylacetylaminopropionate		292

MNDA N-methylneodecanamide



258

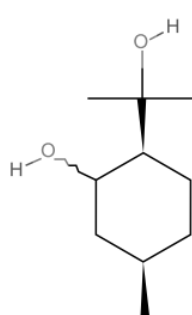
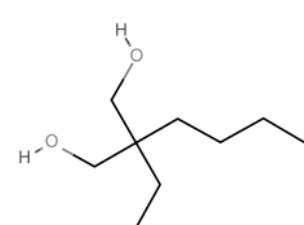
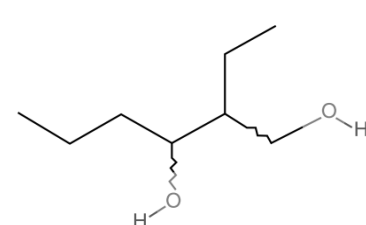
Table 2. Structure and boiling point of some of the known insect repellents, containing piperidine functional group.

Common name	Formula name	Structural formula	Boiling point (°C)
AI3-35765	1-[3-cyclohexen-1-ylcarbonyl] piperidine		332
AI3-37220 (SS220)	1-[3-cyclohexen-1-ylcarbonyl]-2-methylpiperidine		338.4
Picaridin	1-piperidinecarboxylic acid 2-(2-hydroxyethyl)-1-methylpropylester		296

Diols

The repellence of certain diols was reported by McCabe *et al.* (McCabe *et al.*, 1954). *p*-Menthane-3,8-diol (PMD) is one of the most effective commercial diol-based repellents. It is the main component of oil of lemon eucalyptus. This compound was developed in 1990 (Curtis *et al.*, 1990). The chemical structure and boiling point of some well-known diol-based repellents are given in Table 3.

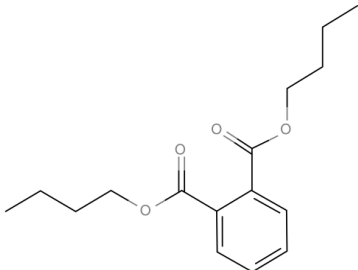
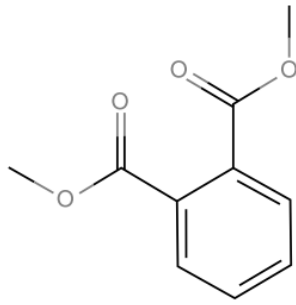
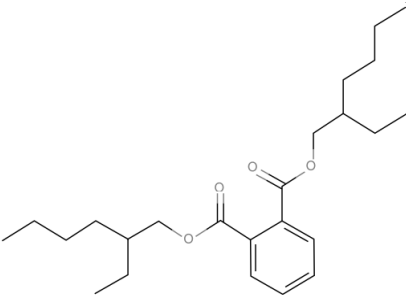
Table 3. Structure and boiling point of some of the known insect repellents, containing diol functional group.

Common name	Formula name	Structural formula	Boiling point (°C)
PMD	2-(1-Hydroxy-1-methylethyl)-5-methylcyclohexanol		266
BEPG	2-butyl-2-ethyl-1,3-propanediol		264
Rutgers 612	2-ethyl-1,3-hexanediol		244

Phthalates

Buc and Warren (Buc and Warren 1929) reported the repellent activity of phthalate-based compounds such as the dibutyl- and dimethyl esters of phthalic acid. Chemical structures and boiling points of some phthalates are presented in Table 4.

Table 4. Structure and boiling point of some of the known insect repellents, containing phthalate ester moiety.

Common name	Formula name	Structural formula	Boiling point (°C)
DBP	benzene-1,2-dicarboxylate		340
DMP	Dimethyl 1,2-benzenedicarboxylate		283
Diocetyl phthalate	bis(2-ethylhexyl) benzene-1,2-dicarboxylate		385

Carboxylic acids

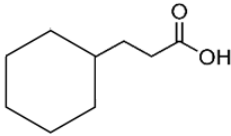
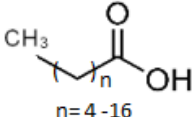
The repellent activity of a number of carboxylic acids such as hexanoic, heptanoic and nonanoic acid was first reported by Skinner *et al.* (Skinner *et al.*, 1970). Later, the repellent activity of acetic, pentanoic and hexanoic acids against both biting and non-biting tsetse flies were reported (Vale, 1980). More recent investigations, revealed the repellent activity of carboxylic acids with 6 to 12 carbons (Reifenrath, 2005).

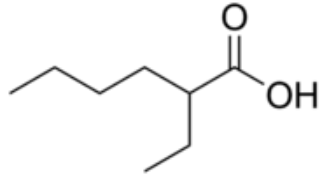
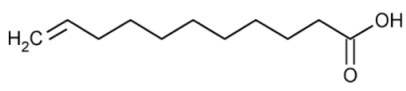
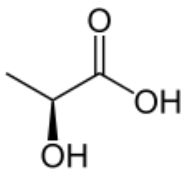
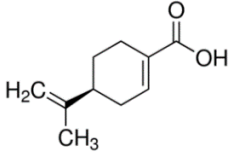
Combination of carboxylic acids as a repellent mixture has also been investigated. Binary mixture of octanoic and nonanoic acid as well as the ternary combinations of C8–C10 have been reported as effective repellents (Reifenrath, 2005).

Generally, the repellent activity of short chain carboxylic acids (C1-C9) is higher at higher concentrations, while the longer chain fatty acids (C13-C18) shows better repellence at lower concentrations (Bosch *et al.*, 2000).

The chemical structure of some of the reported repellent compounds containing carboxylic acid functional group are presented in Table 5.

Table 5. Structure and boiling point of some of the known insect repellents, containing carboxylic acid functional group.

Common name	Formula name	Structural formula	Boiling point (°C)
Cyclohexanepropionic acid	Cyclohexanepropionic acid		276
Fatty acids	Fatty acids		205- 361

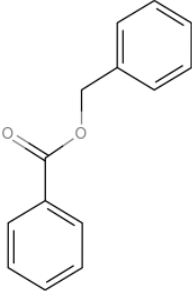
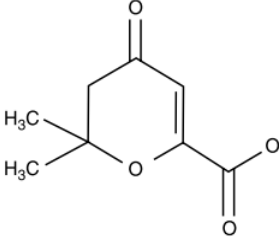
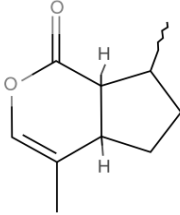
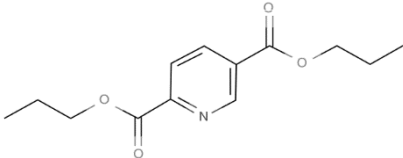
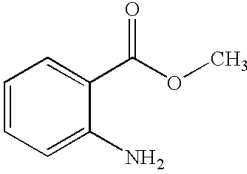
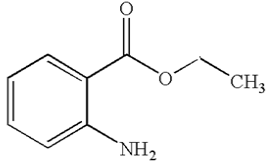
2-ethylhexanoic acid	2-ethylhexanoic acid		228
Undecylenic acid	Undecylenic acid		275
L-lactic acid	L-lactic acid		122
Perillic Acid	Perillic Acid		284.94

Esters

Repellent activity of ester functional group was first reported by Moore (Moore, 1934). He reported that unsaturated, cyclic esters are the best candidates in this group. This discovery was the prologue of identification of a large set of repellents containing ester functional groups.

The importance of oxygen atoms in the repellent activity of molecules is well-known (Nerio *et al.*, 2010). However, Samarasekera *et al.* (Samarasekera *et al.*, 2008) claim that the presence of an ester group in the repellent structures, enhances the repellent activity more than any other oxygenated functional group, e.g. hydroxyl, ether or carbonyl. Chemical structures of some repellents containing ester functional group are presented in Table 6.

Table 6. Structure and boiling point of some of the known insect repellents, containing ester functional group.

Common name	Formula name	Structural formula	Boiling point (°C)
Benzyl benzoate	Phenylmethyl benzoate		323
Indalone	Butyl-3,3-dihydro-2,2-dimethyl-4-oxo-2H-pyran-6-carboxylate, 2,2-dimethyl-6-carbobutoxy-2,3-dihydro-4-pyrone		270
Nepetalactone	2,7-dimethyl-4-oxabicyclo[4.3.0]non-2-en-5-one		270
MGK Repellent 326	di-n-propyl isocinchomeronate		175 (5 mmHg)
Methyl anthranilate	Methyl 2-aminobenzoate		256
Ethyl anthranilate	Ethyl 2-aminobenzoate		268

Other repellents

Other structural groups may show repellence effects in some molecules. However, due to the lack of general applicability they were not been deeply investigated. Phenols, monoalcohols, hydroxyketones and glycols are of this type.

Moreover, various structural classes such as alkaloids, phenols and terpenes have been identified as the active ingredients in plant-based repellents (Debboun *et al.*, 2015).

2.10. **Possible intermolecular interactions**

The structural studies of repellents reveal that most repellents have the potential of forming hydrogen bonds (HB) owing to presence of either a hydrogen acceptor (HBA) or hydrogen donor (HBD) group in the molecules. Hydrogen bonding is a key factor in enhancing the non-ideal behaviour of molecular systems and therefore the formation of azeotropes and pseudo-azeotropes (Eduljee and Tiwari, 1976, Ewell *et al.*, 1944).

The hydrogen bond (HB) was defined for the first time by Pauling (Pauling, 1939): “Under certain conditions a hydrogen atom is attracted by rather strong forces to two atoms, instead of only one, so that it may be considered to be acting as a bond between them.”

HB may happen in the same molecule, called intramolecular HB, or between different molecules, called intermolecular HB. HBD is an electronegative atom such as nitrogen, oxygen or fluorine while HBA is an electron-rich atom (Laurence and Berthelot, 2000).

Although hydrogen bonding is a well-known concept, finding proper ways to define and detect HBs is still of interest (Weinhold and Klein, 2014). Due to the difficulties in detecting and measuring the strength of HB through direct methods, such as measuring the binding energy,

it is a common practice to investigate the influence of HB formation via measurable parameters. For instance, the effect of HB on NMR (da Silva *et al.*, 2013), UV, Raman and FTIR spectra (Alex *et al.*, 1992, Bondesson *et al.*, 2007) were studied. Moreover geometrical, electrostatic and thermodynamic parameters such as hydrogen bond length, electrostatic potential near the HBA lone pair, and enthalpy of HB formation (Le Questel *et al.*, 1997) may provide valuable information for studying HB formation.

Considering the chemical structure of repellents in 2.9.1, it may be possible to design negative pseudo-azeotrope mixtures of repellents. This can lead to extend the residual effect of parent compounds and as a consequence to improve the efficiency of repellent formulations.

2.11. Prediction of pseudo-azeotrope formation

Towards the goal of evidence-based selection of repellents and azeotrope formers, there is a need to adapt a simple approach to make judgements about the feasibility of pseudo-azeotrope formation. Such an approach may evaluate whether selection of a specific repellent and azeotrope former is justified.

Simple thermodynamic models such as equation-of-state (EOS) models and the Gibbs energy (GE) models are used to predict the properties of mixtures (Breil and Kontogeorgis, 2009, Maia *et al.*, 2012, Papari *et al.*, 2012, Subramoney *et al.*, 2015, Wang *et al.*, 2015). However, they suffer from several imperfections, including poor accuracy and the need for numerous compound-specific parameters.

Activity coefficient models such as the non-random two-liquid (NRTL) and universal quasi-chemical (UNIQUAC) models are capable of prediction of phase behaviour of highly non-ideal VLE system (Reyes Labarta *et al.*, 2014, Haghtalab and Yousefi Seyf, 2015), provided sufficient data of the system are available .

Ab initio approaches were proposed to estimate the vapour-liquid and liquid-liquid behaviour of mixtures based on quantum mechanical calculations (Eckl *et al.*, 2008, Raabe and Koehler, 2002). Molecular simulations techniques have also been suggested to evaluate azeotrope points of a system through different methods such as Gibbs ensemble Monte Carlo (GEMC) (Li *et al.*, 2010), Gibbs-Duhem integration (GDI) (Kofke, 1993), VLE calculation

(Theodorou, 2010), and histogram-reweighting Monte Carlo simulation (Pandit and Kofke, 1999). However, computational approaches are time consuming and their accuracy depends on the approximations made.

Quantitative structure–property relationship (QSPR) modelling is capable of providing informative estimation of some desired properties of mixtures based on chemical structures of the parent compounds. Although QSPR modelling can provide a handy and cost effective approach for selection of proper repellents and azeotrope former, performance of QSPR models strongly depends on the numerical descriptor selection step (Zare-Shahabadi *et al.*, 2013). There are two simple types of approximation that have successfully been used for calculation of mixture descriptors. However, they are not practical with respect to the prediction of azeotrope formation. Centroid approximations, in which the mixture’s descriptor is calculated based on the ingredients’ descriptor, do not account for the nonlinear behaviour of a non-ideal mixture. On the other hand, weighted-contribution-factor approximations, in which weighing factors proportional to molar fraction of compounds are applied, are not of interest. Its main limitation is the requirement of experimental measurement of the mixture compositions at the azeotrope point (Zare-Shahabadi *et al.*, 2013).

In this work, a simple approach to get a quick idea of the feasibility of pseudo-azeotrope formation is developed. Here the possibility of pseudo-azeotrope formation is investigated by exploring the deviation of a mixture from ideal behaviour as caused by hydrogen bonding.

Hydrogen bonding is reported as the most important single cause of non-ideal behaviour of mixtures that results in azeotrope formation (Eduljee and Tiwari, 1976). Ewell *et al.* (Ewell *et al.*, 1944) used hydrogen bonding capability of liquids to predict non-ideal behaviour and azeotrope formation.

Spectroscopic methods can provide evidence of intermolecular interactions and specifically hydrogen bonding. In fact most types of hydrogen bonds were discovered by vibrational spectroscopy (Desiraju and Steiner, 1999). Other spectroscopic methods such as UV spectroscopy (Nunes *et al.*, 2014, Sancho *et al.*, 2011) and nuclear magnetic resonance (NMR) spectroscopy (Anderson *et al.*, 2007, Del Bene *et al.*, 1999) have also been studied to visualize hydrogen bonds.

2.11.1. Vibrational spectroscopy

Vibrational spectroscopy is a key component in study of interaction strength and geometries of hydrogen bonds. It can provide information through investigating the couplings between normal modes which are controlled by the potential energy surfaces of hydrogen bonds (Nibbering *et al.*, 2007).

The main informative vibrational motions in hydrogen-bonded systems is briefly described in the following.

Vibrational modes of hydrogen-bonded molecular systems

Generally, all the modes which may be affected by the motion of heavy atoms, can be identified in hydrogen bonded systems. In case of forming a typical X–H···Y hydrogen bond, in which X and Y are electronegative atoms, the stretching mode of the X–H bond (ν_{XH}), undergo major changes. Usually the absorption of the stretching mode of X–H display a red shift, peak broadening and increase in the intensity (Nibbering *et al.*, 2007).

Moving the absorption peak to lower frequencies is attributed to the reduction in the force constant of the oscillator. It also may reflect an increase of diagonal anharmonicity, i.e. anharmonicity of the vibrational potential along the X–H stretching coordinate (Nibbering *et al.*, 2007).

The red shift of the absorption band of the stretching mode of X–H is a typical measure of the strength of hydrogen bonds (Novak, 1974, Mikenda, 1986, Mikenda and Steinböck, 1996). Peak broadening may stem from an extensive range of interactions such as coupling of the high-frequency and low-frequency modes of X–H stretching coordinate, vibrational dephasing, Fermi resonances with overtones and combination tones of the original peaks, and presence of various hydrogen bonding geometries in the system intensity (Nibbering *et al.*, 2007).

The increase in the absorption intensity of X–H stretching mode has been ascribed to an electronic structural amendment.

The other perceptible vibrational modes are in-plane bending modes of X–H (δ_{XH}), which usually display slight blue shifts (Schuster *et al.*, 1976).

Formation of intermolecular dimers through hydrogen bonds usually generates six new vibrational modes including dimer hydrogen bond stretching (ν_{dimer}) and bending (δ_{dimer}) modes (Nibbering *et al.*, 2007).

2.11.2. Ultraviolet–visible (UV-Vis) spectroscopy

UV-Vis spectroscopy is the study of interaction between light and material. Material response to the light through reflection, scattering, absorbance, fluorescence/phosphorescence, and photochemical reaction (Skoog *et al.*, 2014).

In general UV-Vis spectroscopy measures the absorbance of the radiated light in the UV-Vis range (190–800 nm) of the electromagnetic spectrum (Skoog *et al.*, 2014).

UV spectroscopy provides information about various electronic transitions. UV-Vis spectroscopy is considered a successful technique to study the molecular structure of association effects among molecules. The association behaviour and hydrogen bonding interactions can be quantified by analysing band shifts and changes in band shapes (Zhang *et al.*, 2008). The impact of hydrogen bonding on UV-Vis spectra of compounds has been studied (Baba and Suzuki, 1961, Suzuki and Baba, 1967, Magnes *et al.*, 2004, Homocianu, 2011).

Beer-Lambert Law, Limitations and Deviations

The Beer-Lambert law as the basic principle of absorption analysis demonstrates a linear correlation between absorbance (A) to the concentration (c) and the path length (l) of the sample as presented in equation (2.7):

$$A = \epsilon lc \quad (2.7)$$

In equation (2.7) ϵ is the molar absorptivity or molar extinction coefficient which is a constant for each molecule for each wavelength (Denney, 1982).

According to Beer-Lambert law, provided the path length in a certain experiment is kept constant, absorbance should be directly proportional to the concentration.

Under certain circumstances the Beer-Lambert law is not obeyed and the relationship between absorbance and concentration is nonlinear. Most often deviations from Beer-Lambert law occur when the underlining assumptions are not satisfied. However, in very rare cases the Beer-Lambert law becomes invalid, a so-called real deviation. Extracting information of the UV-Vis spectra is only possible by proper study of the sources of deviation. Some of the main sources of deviation of Beer-Lambert's law are reviewed in the following.

Real Deviations

By increasing the concentration of the analyte in the solution the interaction of analyte with other analyte molecules also increases. The charge distribution of analyte will change at high concentrations. This will possibly result in changing the interaction of solvent-analyte, analyte-other solute or even forming hydrogen bonds. These new interactions probably cause a shift in the absorption wavelength of the analyte (Horvath, 1988).

Moreover, high concentrations of analyte may alter the refractive index of the solutions and in consequence cause deviation of the Beer-Lambert law. When significant changes in the refractive index (n) of the solution occur, a correction to Beer-Lambert formula must be applied as follows (Ohannesian and Streeter, 2001):

$$A = \epsilon lc (n^2 + 2)^2 \quad (2.8)$$

Although the real deviation changes from one compound to the other, generally one can say that in solutions the Beer-Lambert law is satisfied at concentration less than 10 mM without requiring corrections.

Chemical deviation

UV spectroscopy is an electron-related phenomenon. As a result, any change in the electronic structure of the analyte such as association, dissociation, dimerization and hydrogen bonding

may lead to changes in the absorption spectra. This causes deviation from Beer-Lambert law (Ohannesian and Streeter, 2001).

Instrumental deviation

Limitations in the instrument performance are other sources leading to the breakdown of the law. The greatest contributors to instrumental deviations are the polychromaticity of the source and stray radiation.

Monochromatic radiation is one of the assumptions used to drive Beer-Lambert Law. However, using such a radiation, restricted to a single wavelength, is not practical. Even the best wavelength selectors transmit a narrow band of light instead of a single wavelength. In order to minimize the polychromatic deviation, measurement should be done at the wavelength band in which the molar absorptivity does not change significantly. Due to this fact, absorption is reported at λ_{\max} (Upstone, 2000). Moreover, if the effective band width of the source is less than one-tenth of the natural bandwidth of the absorbing species, deviation from Beer-Lambert law is negligible. As a rule of thumb, a spectral band pass of 5 nm (or less) is satisfactory.

The presence of the stray radiation is another potential source of instrumental deviation. Stray light is unwanted detected light. In other word, stray light is the light in the system which is outside the bandwidth of the desired wavelength. The source of this light may be the monochromator or even it may come from the instrument. Fortunately this source of deviation may be diminishing by improving the instrument design (Upstone, 2000).

Deviations related to the nature of the sample

Sometimes the nature of the studied samples causes deviation of Beer-Lambert law. For instance, sample fluorescence may cause negative deviation of the law. This fact is due to detection of a combination of the transmitted light and the fluorescence emission.

In some samples the absorption of the chromophores is pH dependent. In other words, change in the pH will shift the wavelength and affect the linearity of the law.

Turbidity of the samples is another source of deviation. In this case the radiated light will be scattered and less light will be detected which cause a positive deviation of the Beer-Lambert law.

Some methods have been suggested to reduce this type of deviations such as inserting cut-off filters.

Other reported sources of deviation are of lesser importance because they can be avoided by improving the experimental set up. Unequal path length, non-homogeneity of the mixture and extremely high intensity of the radiated light are examples of this category (Upstone, 2000).

2.12. **Review of azeotrope determination methods**

Considering the necessary and sufficient condition for azeotrope formation, i.e. identical composition of vapour and liquid phase at equilibrium, azeotropic mixtures are best illustrated with compositional analysis of vapour and liquid equilibrium phase at constant temperature or pressure.

Thanks to the great advances in vapour-liquid equilibrium calculations and simulations (Li *et al.*, 2005, Kiva *et al.*, 2003a), the VLE of numerous systems have been determined either experimentally or by thermodynamic modelling. So far, however, there has been little discussion about confirmation of pseudo-azeotrope formation under non-equilibrium condition.

Among the non-equilibrium studies of azeotrope mixtures, the work of Barontini *et al.* (Barontini *et al.*, 2002) to identification of azeotropic mixtures based on thermogravimetry coupled with Fourier transform infrared spectrometry (TG-FTIR) is of interest.

Barontini *et al.* (Barontini *et al.*, 2002) suggested direct recording of the FTIR spectra of the released vapour that emanates from the evaporating mixture in a thermogravimetric analyser, and then to identify the vapour composition based on the Beer-Lambert law. In other words, they determined the vapour composition based on spectral absorbance.

However, the authors have mentioned that their technique is applicable only for binary mixtures in which separation of the component's contributions to the recorded FTIR spectra is possible.

It is noteworthy to mention that deviation from Beer-Lambert law, especially in case of presence of strong interactions and non-ideality, should be considered.

Assuming the absence of molecular interactions in the vapour phase of amine-carboxylic acid binary systems, Nhlapo *et al.* (Nhlapo *et al.*, 2012) and Focke *et al.* (Focke *et al.*, 2013) successfully applied online TG-FTIR technique to study the composition of the vapours released by some binary mixtures. The mixtures comprised amine and short-chain carboxylic acids, e.g. trimethylamine-acetic acid and trimethylamine-propanoic acid binary systems. However, they found the technique insufficient for binary systems containing amine and long-length carboxylic acid such as hexanoic acid and octanoic acid. In this case the amount of the released vapour was insufficient to allow accurate detection by the coupled FTIR instrument (Nhlapo, 2013). Nonetheless, Nhlapo suggested that future researchers should use an indirect approach to track the composition of evaporating mixtures (Nhlapo, 2013).

Indirect approaches attempt to analysis the released vapour off-line. Off-line evolved gas analysis is based on trapping the released vapour and applying a quantitative or qualitative identification methods such as gas chromatography, mass spectrometry, IR spectroscopy or other analytical techniques for successive characterization (Materazzi, 1997).

The Off-line approach has its limitations since the experiment is not completely under control. Since the vapour is collected over an extended period of evaporation time, the off-line approach does not provide accurate instantaneous profiles of the evaporation process (Materazzi, 1997).

An alternative approach is to analyse the residual liquid to study the evaporation process and indirectly the evolved gas. The variation in composition of vapour may be followed via mass balances considering the changes in the liquid composition. However, molecular interactions become significant in the liquid phase. In this case, deviations from the Beer-Lambert law should be considered in all spectroscopic interpretations.

Inverse analysis techniques may provide a quick and convenient way to determine the composition of the evaporating liquid based on the FTIR spectra.

2.12.1. Inverse analysis technique

Often a system contains parameters that cannot be measured directly. However, these parameters do affect some of the measurable system outputs. In the forward approach the measurable system outputs are obtained from the system parameters. The inverse problem estimates the unknown system parameters from their influence on the measurable system outputs. Two methods are known for solving an inverse problem namely inverse mapping and the forward inverse identification method. The latter adjusts the system parameters in a formal numerical way until the error between the predicted output and the system output of interest is minimized. The resulting parameters are the best estimates for the system output of interest.

On the other hand, inverse mapping (the backward inverse identification method) is based on constructing a surrogate model that directly maps the system output to the system parameters. Therefore, there is no longer a need for an optimization step.

In order to construct the surrogate model, a set of the system outputs for known system parameters are obtained and split into a training set and a validation set. The surrogate model uses the information provided through the training set to infer the system parameter from the system output which is not seen in the training set.

Constructing the surrogate model also comprises identifying the parameters of the surrogate. To this end, the accuracy of the surrogate model to estimate the system parameters of the validation set must be maximized. In other words, the prediction error of the estimated system parameters of surrogate model must be minimized. Partial Least Squared Regression (PLSR) is a well-known surrogate model used to solve an inverse problem in chemometrics. Construction of PLSR is fairly easy and it provides acceptable estimation accuracy. Moreover, it can handle co-linearity of the PLSR inputs (system outputs) and the PLSR outputs, noise problem, and the problems may cause in an inverse problem due to large number of variables (Andrade-Garda, 2009).

In this study PLSR was used to map the spectral variables (**X**-block) to the composition of the mixture (**Y**-block). To this end PLSR compresses the information in the **X**-block and **Y**-block by projecting the information onto PLSR directions in such a way that most of the variance in the input (**X**-block) and the output (**Y**-block) is explained. Therefore, training the PLSR means identifying the PLSR directions, and the PLSR prediction means projecting a known spectral input onto the PLSR direction as follows:

$$\mathbf{X} = \mathbf{TP}^T \quad \mathbf{Y} = \mathbf{UQ}^T, \quad (2.9)$$

in which **T** and **U** are the scores of the **X**-block and **Y**-block, while **P** and **Q** are projection directions of **X** and **Y** spaces respectively.

The only tuning parameter of a PLSR is the number of projection directions, which is determined in a validation process with the objective of minimizing the validation loss. In this study we used a leave-one-out cross validation (LOO-CV) technique. From total n spectra of n known mixture, we leave one spectrum out as a validation point while we construct the PLSR with the rest on $(n-1)$ training points. This process is repeated n times and the validation error in each iteration is added to form the total validation error. The LOO-CV is repeated while the number of PLSR directions is increased. Finally, the PLSR with the lowest validation error is selected to estimate the unknown mixture composition from known spectral data.

2.12.2. Differential scanning calorimetry

Differential scanning calorimetry (DSC) is a thermal analysis technique in which the heat effects related to a phase transitions or chemical reactions are monitored as a function of temperature (Bershtein and Egorov, 1994). DSC is widely used to investigate an extensive range of thermal properties of materials such as heat capacity, crystallization, melting, glass transition, etc. (Bershtein and Egorov, 1994, Liao, 1991, Buera *et al.*, 1998).

Due to extensive vaporization of volatile specimens, application of DSC for measuring vapour pressure or boiling point should be done under specific setups. In open pans, quick vaporization of the volatiles leads to broad endotherms, while closed pans suffer from the problem of self-pressurization and cause broad and multiple endotherms. Addition of a

pinhole of 25 to 125 μm in the lid of a hermetically sealed pan results in the reduction of specimen depletion and sharper boiling endotherms (Buera *et al.*, 1998).

There are a few studies that investigated the application of DSC to azeotrope formation. For instance, Jouhara *et al.* (Jouhara *et al.*, 2013) confirmed formation of a water-ethanol azeotrope mixture based on the peak shape of the DSC curve.

Direct investigation of boiling peaks to confirm azeotrope formations was not reported, since DSC measurement do not fulfil the equilibrium criteria necessary to study azeotropes.

The position of a boiling peak can provide an indication of the presence of a pseudo-azeotrope mixture under non-equilibrium conditions. This was investigated in this study.

2.13. Molecular simulation techniques

Molecular simulation techniques were used to gain insight into the nature of intermolecular interactions in the repellent mixtures. In this section the molecular simulation concepts and methods are briefly reviewed.

2.13.1. Introduction to molecular simulation

Molecular simulations are computational techniques which consider molecular structures in the simulations. The scale of molecular simulations vary from less than a nanometre to a few micrometres depending on the resolution of the molecular structure being studied (Ungerer, 2005).

Simulations of molecular interactions provides insight into bulk thermodynamic properties of a mixture, e.g. vapour pressure and evaporation rate.

Depending on the expected simulation outputs, molecular structure may be considered at very high resolution, i.e. taking every single electron in account, or at coarser levels.

The first category of molecular simulation techniques is known as quantum chemistry which considers the electronic level of molecular structures. This approach is based on solving the

Schrödinger's equation through numerical techniques in order to address some of the properties of the molecular system (Levine, 1991).

Quantum chemistry techniques are computationally expensive which limit its application to small systems, containing few atoms or molecules. Subsequently, alternative approaches are needed to tackle transport phenomena and thermodynamic properties of larger systems.

The second category of molecular simulation techniques considers molecular structure at a coarser level. Molecular dynamics (Frenkel and Smit, 2002b) and Monte Carlo simulation (Frenkel and Smit, 2002a) are the best known techniques. They can even deal with systems comprising tens of thousands of atoms. Molecular dynamics solves the equations of motion in order to analyse dynamic properties. This technique has been successfully applied to a large number of liquid systems to address dynamic properties such as viscosity and diffusion coefficients (Ungerer *et al.*, 2006).

On the other hand, Monte Carlo simulations adopt statistical methods to address equilibrium properties of molecular systems (Frenkel and Smit, 2002a).

Selection between molecular dynamics and Monte Carlo simulation to study a molecular system depends on the characteristics of the system and the desired properties. For instance, in systems with high relaxation times such as polymer melts and dense liquids, Monte Carlo simulations are more efficient than molecular dynamics. They are also more efficient for the simulation of fluid phase equilibria and adsorption in microporous solids (Ungerer *et al.*, 2006).

However, Monte Carlo methods cannot address the dynamic behaviours of molecular systems. The dynamics behaviour of molecular systems, particularly their transport properties are best treated by molecular dynamics.

In some specific problems such as protein folding and self-assembly of polymers in solution, a large number of atoms are involved which cannot be handled by the second category. Therefore, a third category of molecular simulation techniques, namely dissipative particle dynamics, has recently emerged (Hoogerbrugge and Koelman, 1992). This category decreases the resolution of the molecular structure at the expense of increasing the computation time.

The smallest unit considered in dissipative particle dynamics, is a set of molecules rather than single electron, atom, or molecule. This make these methods less quantitative in comparison with the first and second categories of molecular simulation techniques.

Considering the efficiency of Monte Carlo methods for addressing the thermodynamic properties of dense liquids, this technique was adopted to study the liquid repellent mixture.

2.13.2. Monte Carlo method

Monte Carlo methods are based on sampling techniques. These are generally used to solve mathematical problems in which direct calculation is not a straight forward task. They are particularly useful to solve problems comprising many (correlated) parameters. While different methods were suggested for solving a Monte Carlo problem, methods based on Markov Chain Monte Carlo (MCMC) have received most of the attention in molecular simulations (Geyer, 2011).

MCMC methods are designed such that the probability of the transition from the current state of the Markov Chain to the next step is independent of the history of the chain. Gibbs, Importance Sampling, and Metropolis are the best known MCMC sampling techniques (Geyer, 2011). In this study the Metropolis algorithm, designed by Metropolis (Metropolis *et al.*, 1953), was adopted to simulate equilibrium of a liquid with its vapour phase.

Implementing the Metropolis sampling method in molecular simulation comprises two steps. At each iteration of the algorithm, a new molecular system configuration is proposed. This can be done through, e.g. generating a random translation or random rotation. This configuration can be accepted or rejected according to an acceptance criterion designed on the basis of a desired probability distribution. The acceptance criterion, the probability of accepting the new configuration, is given by:

$$P_{accept} = \min\left(\frac{p_{proposed\ config}}{p_{old\ config}}, 1\right), \quad (2.10)$$

in which $p_{proposed\ config}$ and $p_{old\ config}$ are probability distributions of the proposed configuration and probability distributions of the old configuration.

A stationary state of the chain is obtained after drawing a sufficient numbers of samples. The chain visits a representative subset of the statistical ensemble, and the collection of the visited system configurations are used to infer the probability distributions of the molecular system configurations. Statistical summary of the obtained distributions is used for further calculation of the thermodynamic properties of the system. For instance, the most expected value set of the obtained probability distributions corresponds to the most expected molecular system configuration. For more details see (Ungerer *et al.*, 2006).

Macroscopic properties such as the potential energy, pressure and volume can be calculated according to standard averaging formulae after the generation of a sufficient number of configurations.

Molecular dynamics solves the equation of motion for every single atom, in every molecule, while considering all intramolecular and intermolecular interactions inside the system. It is noteworthy that MCMC nevertheless yields identical average values.

2.13.3. Practical implementation

The present study employed the Gibbs code that was introduced in 1997 for the computation of the fluid phase (Mackie *et al.*, 1997) and has been improved since. The Gibbs Code is included as a user-friendly engine in the MedeA[®] software. MedeA[®]-GIBBS is able to calculate thermo-chemical properties of single and multi-phase liquids based on Monte Carlo methods, while the intermolecular interactions are described by force fields.

In order to formulate the simulation algorithm, a basic knowledge of the relevant concepts and selection rules for the required parameters is a prerequisite. The theory behind the selection of parameters is briefly reviewed in the following Sections.

Ensembles

In statistical thermodynamics, it is a common practice to use a collection of snapshots of microscopic properties, called “statistical ensembles”, to calculate a meaningful average of the desired macroscopic properties. A statistical ensemble is a collection of several states of the system with different positions and velocities of the molecules (Ungerer, 2005). Several types of ensembles with particular statistical characteristic have been developed. One should adopt the correct ensemble on the basis of the macroscopic constraints that hold for the problem being addressed.

In the present study, MedeA[®]-GIBBS was performed in the isothermal–isobaric (NPT) ensemble. In the NPT ensemble, the number of molecules, the pressure and the temperature are kept constant while the density of the system is allowed to fluctuate. Thus, the NPT statistical ensemble is useful for systems with an imposed pressure and unknown density (Yiannourakou *et al.*, 2013).

Cut-off of Intermolecular Interactions

To reduce the computation time, the potential energy corresponding to separation distances greater than some threshold level were ignored. The threshold level is known as the cut-off distance. This concept can be applied for moderately polar and quadrupolar molecules, in which the electrostatic energy does not make a major contribution to the attractive interactions.

The validity of implementing a cut-off distance depends on the type and range of interactions. For instance, short range interactions such as repulsive interactions can be curtailed at a cut-off of 8-10 Å. However, ignoring long range interactions beyond 10 Å, e.g. those generated by dispersion forces, can cause major distortion of the final results (Ungerer, 2005).

The typical value of 10 Å, for the cut-off distance was adopted in this study, while the part of dispersion interactions that were ignored were accounted for by a long range correction term in the Lenard-Jones energy term.

Degree of flexibility of the molecular model

Depending on the type of molecule and the level of approximation, rigid, flexible and semi-flexible molecular models can be selected to describe the molecular structure. For instance,

noble gases and small poly-atomic molecules can be described as rigid molecules. This also means that their intramolecular interaction energy is constant. Flexible molecular models considerable additional degrees of freedom to describe all possible conformations (Ungerer, 2005).

In the current study, a semi-flexible model was used for the molecular structures since it can successfully address the required degrees of freedom while keeping the computation time under control.

2.13.4. Force field

Force fields are predefined mathematical functions and parameters, used to quantify the molecular interactions. In ‘all atoms’ force fields each atom is modelled and all the direct interaction with all atoms in its vicinity are taken into account (Yiannourakou *et al.*, 2013).

Although the ‘all atoms’ force fields provide an accurate account for molecular geometry and structure, the huge number of force centres in large systems makes this computationally inefficient. In order to speed up calculations, groups of atoms can be lumped together to represent a single force centre. So, in this alternative class of ‘united atoms’ force fields, a force centre is allocated to a cluster of atoms. Depending on the location of the force centres, the united atoms approach is either classified as a classical united atoms (UA) or anisotropic united atoms (AUA). UA potentials disregard hydrogen atoms and assign separate force centres to other atoms. The impact of hydrogen atoms is accounted for through additional parameters in the potential terms (Frenkel and Smit, 2002c).

In anisotropic united atoms potentials, the force centres are shifted to an intermediate position between the main atoms and the associated hydrogen atoms in order to reflect the impact of hydrogens on the potential terms more effectively (Toxvaerd, 1997).

AUA force fields face major limitations but calibrated united atoms potentials have successfully modelled complex molecules (Ungerer, 2005). However, well-calibrated united atoms potentials are not yet available for some polar functional groups. For instance, the tertiary amide functional group, which is present in a main class of repellents, was not available in UA force fields up to now. Thus, in this study, tertiary amide anisotropic united

atom (AUA) force field parameters were established and validated. The potential functions in AUA force field are reviewed in 2.13.5.

2.13.5. Introduction of molecular potentials to AUA force field

The total energy (E), is the sum of the potential energies and kinetic energies of the system. Due to the stochastic nature of the Monte Carlo methods, the influence of the kinetic energy must be accounted for by a proper analytical integration (Ungerer, 2005).

The potential energy of the many molecule system needs to be determined in the course of Monte Carlo simulations. The molecular potentials determine the potential energy of the system from known positions of all the atoms in the system. To a good approximation, this potential energy is the same as the output obtained by solving Schrödinger's equation for the multi-atom system (with given fixed positions of the nuclei and considering all the electrons present).

The total potential energy is the sum of two main contributions, i.e. the energies assigned to intermolecular and intramolecular interaction respectively:

$$U_{tot} = U_{intermolecular} + U_{intramolecular} \quad (2.11)$$

Intermolecular energy

The intermolecular energy has four main components:

$$U_{intermolecular} = U_{el} + U_{pol} + U_{disp} + U_{rep} \quad (2.12)$$

In (2.11), U_{el} represents the electrostatic potential energy due to the Coulombic forces between the permanent electronic charge distributions;

U_{pol} is the polarization energy which arises from the Coulombic forces between the induced charge distributions by the surrounding molecules and the permanent charge distribution of the nearby interacting molecules;

U_{disp} is an attractive force between all atoms, due to the coulombic interaction between the fluctuating dipoles, quadrupoles and higher moments of charge distribution; and

U_{rep} represents the repulsive energy, which prevents the molecules from approaching too close to each other as a result of the basic principles of quantum chemistry. According to the Fermi exclusion principle it is not possible for filled electron orbitals to overlap.

In the following Sections, the method for determining the various contributions to the intermolecular energy are explained.

i. Electrostatic Energy

In order to account for the permanent electronic charge distribution in a molecule it is a common practice to place several partial charges at preferred sites in the molecule. The location of the charges is mainly on the atomic nuclei however; additional charges may also be used to adjust the model (Ungerer, 2005).

Several methods have been reported in the literature to determine the location and amplitudes of the electric charges. For instance, the electronegativity equalization method (Freeman) is one of the key approaches for charge calculation. Using density function theory (DFT) effective electronegativity of the atom i in a molecule can be calculated by equation (2.13) :

$$X_i = A_i + B_i \cdot q_i + k \sum_{j=1(j \neq i)}^N q_j / R_{i,j} \quad (2.13)$$

Where N is the number of atoms in the molecule, q_i and q_j are the charges distributed on the atoms i and j respectively and $R_{i,j}$ is the distance between atoms i and j (Mortier *et al.*, 1985, Van Genechten *et al.*, 1987, Mortier *et al.*, 1986). The coefficients A_i , B_i and k are empirical parameters, which should be obtained via EEM parameterization (Varekova *et al.*, 2007). The parameters which have been used in this study are reported in Appendix A.

ii. Polarization energy

The electrostatic field of surrounding molecules (E), influence the internal charge distribution of each molecule which result in creation of induced dipole moment (μ_p) as indicated in:

$$\mu_p = \alpha_p E \quad (2.14)$$

Where α_p is the polarizability of the molecule, μ_p is the induced dipole moment and E is the electric field.

Polarisation energy refers to the interaction energy of the induced dipole moment in the electrostatic field and expressed as:

$$U_{Pol} = -\frac{1}{2}\alpha_p E^2 \quad (2.15)$$

Since taking the polarisation in account significantly affects computation times, the polarisation energy is ignored in low polarity systems. For moderately polar systems, the impact of the polarisation energy is considered through adjustment of the Lennard-Jones potential parameters. However, the polarisation energy should be considered in polar systems (Ungerer, 2005).

iii. Dispersion and repulsive energy

Dispersion energy includes the interactions between the fluctuating components of the charge distribution, e.g. fluctuating dipoles and quadrupoles. Although dispersion energy includes three body interactions (i.e. between three nuclei), due to their small contribution in comparison with pairwise interactions, they are not explicitly taken into account. To compensate, the neglected terms are considered implicitly through calibration of effective dispersion parameters.

Since there is no explicit theoretical expression for repulsion energy several empirical potentials have been proposed. The Lennard-Jones potential was used in this study. Lennard-Jones potential is the most widely used term to treat dispersion-repulsion energy and is expressed as:

$$U_{Lj} = U_{rep} + U_{disp} = 4\epsilon_{ij} \left[\left(\frac{\sigma_{ij}}{r_{ij}} \right)^{12} - \left(\frac{\sigma_{ij}}{r_{ij}} \right)^6 \right] \quad (2.16)$$

In equation (2.16) σ_{ij} is the separation distance¹ and ε_{ij} is the depth of the minimum interaction energy².

Lorentz-Berthelot combining rules were applied to express the cross parameters σ_{ij} and ε_{ij} from σ_i and ε_j as shown below:

$$\sigma_{ij} = \frac{\sigma_{ii} + \sigma_{jj}}{2} \quad (2.17)$$

$$\varepsilon_{ij} = \sqrt{\varepsilon_{ii} + \varepsilon_{jj}} \quad (2.18)$$

Intramolecular energy

The intramolecular energy is split up in to a sum of the following terms (Ungerer, 2005):

$$U_{intramolecular} = U_{str} + U_{bend} + U_{tors} + U_{dn} \quad (2.19)$$

In equation (2.19) U_{str} is the stretching energy, arising from the variations in the bond lengths;

U_{bend} is the bending energy, associated with the variations in the bond angles. It accounts for the deviations from the preferred hybridization geometry;

U_{tors} is the torsion energy which accounts for the energy of rotations along four successive atoms in the chain, and

U_{dn} is the distant neighbour internal energy to address the pair interactions between atoms separated by more than three bonds. In the following subsections, the method of determination of various contributions to the intramolecular energy are explained.

¹ The separation distance is the position where the magnitude of attractive and repulsive terms are exactly the same and the Lenard-jones interaction energy is zero.

² The depth of minimum interaction energy, ε_{ij} , corresponds to $r_{min} = 2^{1/6}\sigma_{ij}$.

i. Stretching energy

In general stretching energy is characterized by a harmonic potential to address the variation of bond length around its mean value:

$$E = \frac{1}{2} k_{str}(L - L_0)^2 \quad (2.20)$$

Where k_{str} represents the stiffness of the bond, L is the bond length and L_0 is its mean value. In some force fields like UA-TraPPE and AUA, the stretching term of energy is neglected, because at normal temperatures the amplitude of the vibrations is negligible. In this work the bond length was set to the mean value of L_0 and the contribution of the contribution of bond stretching to internal energy was neglected.

ii. Bending energy

Bending energy generally is treated by a harmonic potential. In AUA force field the bending energy is defined as:

$$E = k_2(\theta - \theta_0)^2 \quad (2.21)$$

Where θ_0 is the mean value of the angle, k_2 is the product of a rigidity constant and the Boltzmann constant. Both parameters are obtained from molecular structure and infrared spectroscopy (Ryckaert *et al.*, 1989).

iii. Torsion Energy

There are a few expressions for treating the torsion energy. AUA force field uses the term proposed by (Toxvaerd, 1997):

$$E = \sum_{n=0}^p a(n)\cos^n \chi \quad (2.22)$$

In (2.22) the torsion angle χ is defined as:

$$\chi = \varphi + 180^\circ \quad (2.23)$$

Where φ is dihedral angle which is defined from the coordinates of four successive atoms.

iv. Distant neighbour intermolecular energy

The distant neighbour intramolecular interaction (also known as non-bonded interactions) corresponds to interactions between atoms separated by more than three bonds. Non-bonded interactions may comprise dispersion, repulsion, polarization and electrostatic components.

2.14. Evaluation of repellence

Mosquito repellence tests were performed through biological assessments (bioassay for short) procedures. Bioassays are used to assess the effective dose of a repellent and to estimate the total protection time that repellent can provide after application on the skin.

Generally, there are two main types of bioassays namely *in vitro* and *in vivo* systems. *In vitro* systems evaluate mosquito reaction to repellent on an inanimate surface such as treated filter paper, leather, clothes (Debboun *et al.*, 2006). Olfactometers are also *in vitro* evaluation systems for airborne repellents (Hao *et al.*, 2012, Omrani *et al.*, 2010).

In vivo repellent bioassays study the effect of repellents on the behaviour of mosquitoes through direct observation of repellent-treated animals and humans (Debboun *et al.*, 2006).

The *in vivo* efficacy of repellents can be studied in the field or in the laboratory. Detailed descriptions of these approaches are provided in the standard procedures published by the American Society for Testing and Materials (ASTM), The U.S. Environmental Protection Agency (EPA), and the World Health Organization (WHO).

World Health Organization (WHO) recommends evaluating repellents on human subjects as the end-user (WHO, 2009) via standard arm-in-cage procedures.

2.14.1. Arm-in-cage test

Arm-in-cage test provides two specific outputs: First, the relation between the applied dose of the repellent and the mosquito's response can be investigated. This is used to determine the effective dose (EDs) of a repellent. To this end, sequential repellent mixtures, diluted with a proper diluent to various concentrations, should be tested to find the effective dose range.

Second, the complete protection time of repellents (CPT), a major criterion for efficacy, can be determined. Here, 1 mL of a standard solution should be compared with the same amount of the candidate repellent. The standard procedure employs 200-250 non-blood-fed active female mosquitoes. They are placed in two standard cages. Before testing commences, the readiness of the mosquitoes should be assessed by checking the level of their response to the presence of an untreated hand. The hands are protected by nitrile gloves to prevent the mosquito bites during the test. Next 1 mL of a standard solution is applied to a certain exposed area of the forearm skin, while the same amount of repellent is applied on same area of the other arm.

The treated arm is inserted to the cage and exposed for 3 minutes and the number of mosquitoes that landing and/or probing are counted. Then, the standard-applied arm is inserted into the cage and the number of landings and/or probings is counted in the same way. This process should be repeated at 30 or 60 minutes intervals throughout the experiment, which usually lasts no longer than eight hours (WHO, 2009).

Observations of this test are quantified in terms of complete protection time (CPT) and percent repellence (R). The CPT is express as the time from repellent application to the occurrence of the first bite. The repellence is expressed as a ratio of the number of mosquitoes landing and/or probing on the repellent-treated arm (T) to the number of them landing and/or probing on the standard-treated arm (C) expressed as a percentage (Debboun *et al.*, 2006).

$$R = 1 - (T/C)$$

In order to minimize variation of responses and generate precise and repeatable measures, special care over physical and biological factors affecting the test outcome should be taken. For instance, the selection of mosquito specimens, the human test subjects and laboratory testing conditions need to be considered carefully. For more information about the standardized test procedures see (WHO, 2009). Note that modified versions of the arm-in-cage test have been proposed (Maharaj *et al.*, 2010).

2.14.2. Ethical considerations

It is an ethical imperative to fully inform volunteers about all the relevant aspects of the research, before they agree to participate. A full description of the nature and purpose of the experiments, materials, methodology and all the possible consequences should be provided to volunteers before starting the bioassay. The participants should be aware of their right to withdraw at any stage of the test. The participants also should be aware of the scope and the privacy of the data, and of the anonymity of the contributors (Govere *et al.*, 2007). The informed consent forms, used in this study, are presented in Appendix B.

It is important to ensure the mosquitoes are not infected. Moreover, in case of working with test compound with poorly established toxicity profiles, the toxicokinetics of the compound should first be determined in animal models (Govere *et al.*, 2007).

Chapter 3

EXPERIMENTAL

3. Experimental

3.1. Reagent and suppliers

IR3535 and nonanoic acid were selected as model compounds. IR3535 is an effective and safe mosquito repellent (WHO, 2006b, WHO, 2016). It includes an ester and a tertiary amide functional group, both of which can act as hydrogen bond acceptors.

A range of carboxylic acids, as molecules capable of forming strong interactions with IR3535, were reviewed. Nonanoic acid was selected as the azeotrope former based on safety considerations (WHO, 2012), pH value, and as a consequence, skin irritation potential, in addition to its inherent repellence effect (Reifenrath, 2005).

IR3535, DEET and acetone were supplied by Merck chemicals. Nonanoic acid was supplied by Sigma Aldrich. The reagents were used as received without further purification.

3.2. Instrumentation

3.2.1. FTIR spectroscopy

Liquid phase FTIR data were collected using a Perkin-Elmer Spectrum RX 100 spectrometer. Background was corrected and spectra were recorded at room temperature in the wavenumber range 4000 to 600 cm^{-1} at a resolution of 2 cm^{-1} .

3.2.2. Raman spectroscopy

Raman spectra were recorded in the macro sample chamber of a HORIBA Scientific, Jobin Yvon Technology T64000 Raman spectrometer in the backscattering configuration. The excitation source was a 514.6 nm Krypton-Argon laser. The recorded Raman spectra represent an average over 7228 samplings with an acquisition time of 120 ms.

3.2.3. UV-Vis spectroscopy

The UV spectra of the mixtures were recorded using a double beam Cary Bio UV-Vis spectrometer. The spectra were recorded at room temperature over the wavelength range 200-800 nm. No solvent was used.

A fixed amount of nonanoic acid (1.5 mL) was titrated by step-wise adding 1 mL IR3535. At each step the mixture was homogenized and a spectrum was recorded. The same procedure was used in reverse starting with 5 mL IR3535 and titrating with nonanoic acid. The sample cell contained the mixture of IR3535 and nonanoic acid while the reference cell contained nonanoic acid. The reason was that nonanoic acid and IR3535 absorb at the similar wavelengths and this approach made it easier to interpret the information.

In mixtures, the total absorbance is the sum of the individual component absorbances. The Beer-Lambert absorbance law was used to quantify the interaction between nonanoic acid and IR3535. It also applies for mixtures containing more than one absorbing species. ΔAbs was defined as the difference in the measured absorbance and the associated theoretical absorbance (Thakkar *et al.*, 2012).

Usually the molar absorptivity varies as a function of wavelength. So it is not constant over the whole range of the spectrum. The molar absorptivity of pure nonanoic acid and IR3535 were determined at each wavelength. The problem of varying molar absorptivity can be side-stepped by considering only a single wavelength, i.e. λ_{max} . This is justified as the deviation in the molar absorptivity near λ_{max} is minimal. This approach was also explored in this study.

3.2.4. TGA

The thermogravimetric measurements were performed using a Perkin-Elmer TGA 4000 thermogravimetric analyser. A 180 μ L open alumina pan was partially filled with 85 ± 5 mg of sample. The sample was kept isothermal at 50 °C for the duration of the test period. The high test temperature of 50 °C was selected to maximise volatility and because it corresponds to the highest temperature at which repellents are probably expected to function in actual use. The data were collected under nitrogen (N_2) at a flow rate of 50 mL min^{-1} to prevent oxidation.

3.2.5. DSC

Differential scanning calorimetry (DSC) was performed on a Mettler Toledo DSC 4000 heat flux instrument. Approximately 15 to 20 mg of each sample was placed in a 40 μL aluminium pan with a pinhole and heated from $-40\text{ }^{\circ}\text{C}$ to $400\text{ }^{\circ}\text{C}$ at a heating rate of $10\text{ }^{\circ}\text{C min}^{-1}$ in nitrogen flowing at 50 mL min^{-1} .

3.2.6. Density

Density measurements of IR3535 were carried out with an automated SVM 3000 Anton Paar rotational Stabinger viscometer. The measurements were performed at atmospheric pressure and in the temperature range of 293.15-373.15 K. The SVM 3000 is equipped with Peltier elements for efficient thermostability. The absolute uncertainty of the temperature was 0.02 K. The viscometer was rinsed with ethanol 3 times. Then it was kept at 373 K for 20 minutes to ensure that the cell was cleaned and dried before each measurement.

3.3. Method development: Part 1- Oven test

The typical sign for the presence of an azeotropic mixture is an invariant composition of the vapour during equilibrium distillation. However, the process involved in the application of repellents is an open evaporation situation that is very different from distillation (Schlünder, 1989). So the pseudo-azeotrope composition should be substantiated by investigating the stability of the vapour composition near a pseudo-azeotrope composition during evaporation.

Evolved gas analysis, e.g. TG-FTIR, can be used to investigate the evaporation behaviour of liquids. However, due to the very low volatility of mixtures at the measurement temperature considered presently, it was not possible to adequately detect and quantify the composition of the vapour released in these experiment. Too little vapour was released to allow sensing by the FTIR.

Instead a pragmatic oven test was developed to study the behaviour of evaporating mixtures. It was used to follow the temporal change in mass and composition of the remaining liquid. This allowed assessment of a constant release behaviour, i.e. to confirm the presence of a pseudo-azeotropic mixture and to locate its composition.

Fourteen binary mixtures of IR3535 and nonanoic acid with different compositions were prepared. The initial compositions of mixtures are presented in Appendix C. The samples were transferred into evaporation dishes. The volume of the mixture in each evaporation dish was 13.5 ± 0.1 mL.

All the samples were placed in evaporation dishes and allowed to evaporate in a temperature-controlled convection oven. They were placed on a slowly rotating platform to ensure that, on average, they experienced similar conditions with respect to convection effects caused by the air flow patterns in the oven. In addition, a wire mesh was also installed at the air inlet to diffuse and homogenize the flow inside the oven. The test was conducted at 50 ± 1 °C.

The samples were removed regularly after a few days have passed and the masses of the remaining mixtures were determined using an electronic balance (XPS360 model with 0.001g accuracy). At each mass measurement, 10 μ L of each mixture was sampled and immediately subjected to FTIR analysis. The remaining mass was re-determined to correct for this sample loss. The evaporation dishes were then returned to the convection oven in order to continue the experiment.

The liquid phase FTIR spectra were recorded at room temperature in the wavenumber range 4000 to 600 cm^{-1} at a resolution of 2 cm^{-1} .

The tests were carried out over 33 days (i.e. 785 h). The FTIR spectra were used to determine the composition of the samples. Inverse identification method was adopted to determine the composition of the unknown compositions from their known FTIR spectra.

3.3.1. The inverse composition identification method

The inverse mapping approach, in which the surrogate model of the system inverse is constructed to directly map the measured system response to the system parameters, was adopted (Andrade-Garda, 2009). In order to construct the inverse map, the partial least square regression (PLSR) method was adopted to map the FTIR spectra to the corresponding compositions (Asaadi *et al.*, 2016). In order to construct the PLSR to estimate the unknown compositions from the known spectra, a set of spectra from known mixture compositions were first recorded and they represented the training set.

The training set comprised 24 different known mixtures of IR3535 and nonanoic acid in such a way that the composition of each component is roughly uniformly distributed from 0% to 100% as shown in Appendix D. The tuning parameter of the PLSR is the number of PLSR scores. The equivalent term in principal component regression method is the number of principal components. In order to determine the optimum number of PLSR scores, cross validation tests were conducted. One out of the 24 training points was taken out of the training set, and used as the validation point. The PLSR was constructed with the rest of the 23 training points to estimate composition of the validation point by introducing the spectrum of the validation point. This process was repeated, in turn, for each of the 24 training points. The optimum number of the PLSR scores to construct the inverse map was found to be three.

3.4. Method development: Part 2 - Repellence test

3.4.1. Animal preparation

Full ethical approval was obtained from Health Ethics Committee of the South African Medical Research Council.

Adult *Anopheles arabiensis* were collected from a stock population cage in which both sexes have been maintained. The mosquitoes were maintained at 27 °C and a relative humidity of 70% under a 12/12-hour light/dark photo period. Adults were provided with 10% sucrose solution and were periodically blood fed on restrained pigs.

Repellence assays were performed with 3-5-day old female *An. arabiensis* that had previously fed on a 10% sucrose solution and then starved for 6 h.

3.4.2. Test Repellents

Five repellent formulations were investigated: (1) Pure IR3535; (2) Pure nonanoic acid; (3) Pure DEET; (4) Negative pseudo-azeotrope containing 75% of IR3535 and 25% of nonanoic acid; (5) Positive pseudo-azeotrope containing 10% of IR3535 and 90% of nonanoic acid.

Acetone was used as negative control.

3.4.3. Test Procedure

The standard WHO guidelines were adapted for use in the repellent activity trials (WHO, 2009).

Repellence was assessed for topical application of the test substance on the human's arm skin followed by subsequent exposure of the treated area to the unfed female mosquitoes. The number of landing relative to the untreated negative control was recorded, and the repellence percentage determined. This was done over extended periods of time following the initial topical application. Details were as follows:

Paper cups (500 mL) were modified by replacing the base of the cup with mosquito netting held in place with a rubber band and covering the mouth of the cup with transparent plastic film. Twenty, unfed 5-day old, active host-seeking female *An. arabiensis* selected from the test mosquitoes using an aspirator were introduced to the cup.

All the samples were tested on two male and two female volunteers. The test area of the volunteers' skin was washed with scent-free soap and rinsed with water. An aliquot of 0.2 mL of acetone (for the control hand) or the prepared repellent formulations (for the test hand) was applied evenly to 5 cm² length of the forearm skin and allowed to dry.

Initially, the readiness of mosquitoes to probe was assessed by keeping an untreated arm in contact with the cup for 30 seconds. Mosquito activity was observed through the transparent plastic film. In the next step the cup was placed in contact with the treated forearm of volunteers. During the three-minute exposure period the number of mosquitoes probing (attempting to feed on the volunteers, through the netting) was recorded. The repellence effect was determined hourly for up to six hours post application for the samples with promising results. For each measurement a new batch of mosquitoes was introduced to the same cup.

According to the WHO guide protection (P) is stated as the number of mosquitoes probing on the treated arm (T) relative to the number of probing on the control arm (C).

$$P = 1 - (T / C) \quad (3.1)$$

Chapter 4

RESULTS

4. Results

4.1. Vibrational spectroscopy

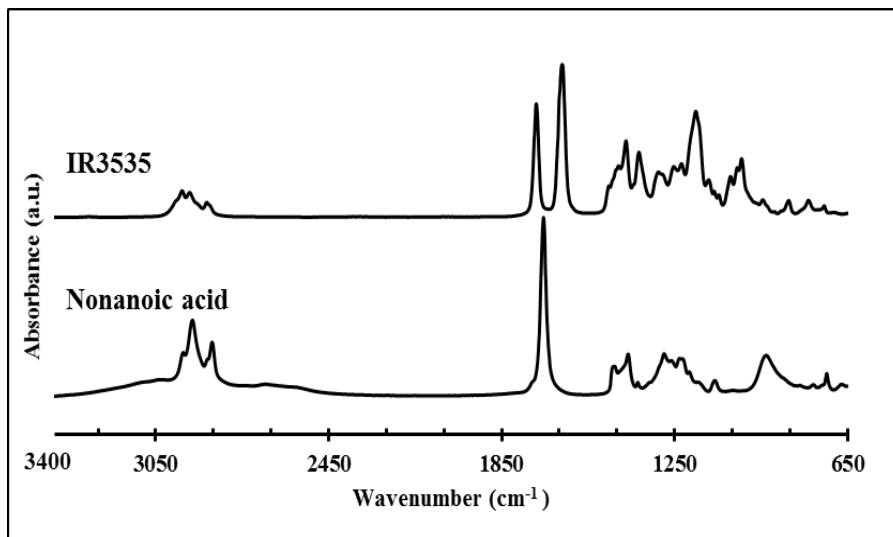


Figure 1. FTIR spectra of nonanoic acid and IR3535

Liquid phase FTIR and Raman spectra of the pure nonanoic acid and neat IR3535 are shown in Figure 1 and Figure 2 respectively.

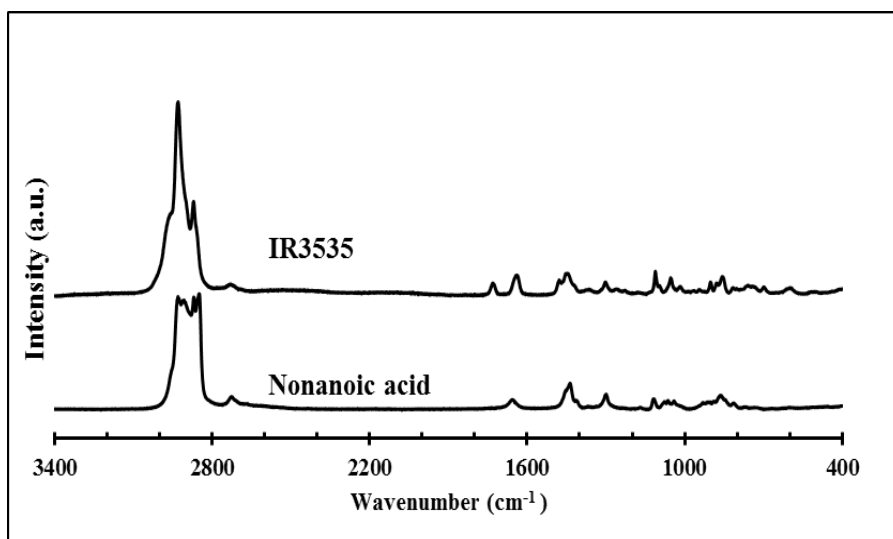


Figure 2. Raman spectra of nonanoic acid and IR3535

Figure 1 shows a broad peak around 3000 cm^{-1} in the FTIR spectra of nonanoic acid. However, the breadth and shape of the peak differs from the usual OH stretching band (Bratož *et al.*, 1956).

Figure 1 also shows a relatively broad peak at 932 cm^{-1} in the FTIR spectra of nonanoic acid. This peak is assigned to the out of phase OH...O wag (Hadzi and Sheppard, 1953).

The sharp intense peak around 1705 cm^{-1} in the FTIR spectra of nonanoic acid is related to the carbonyl stretching absorption (Colthup, 2012). There are two strong peak in the same vicinity in the FTIR spectra of IR3535. The strong peaks around 1730 cm^{-1} and 1640 cm^{-1} in the FTIR spectra of IR3535 are assigned to the carbonyl stretching absorption of ester (Dollish *et al.*, 1974) and amide (Lin-Vien *et al.*, 1991) functional groups respectively.

Figure 3 shows the FTIR spectra of the binary IR3535-nonanoic acid mixtures at various concentrations.

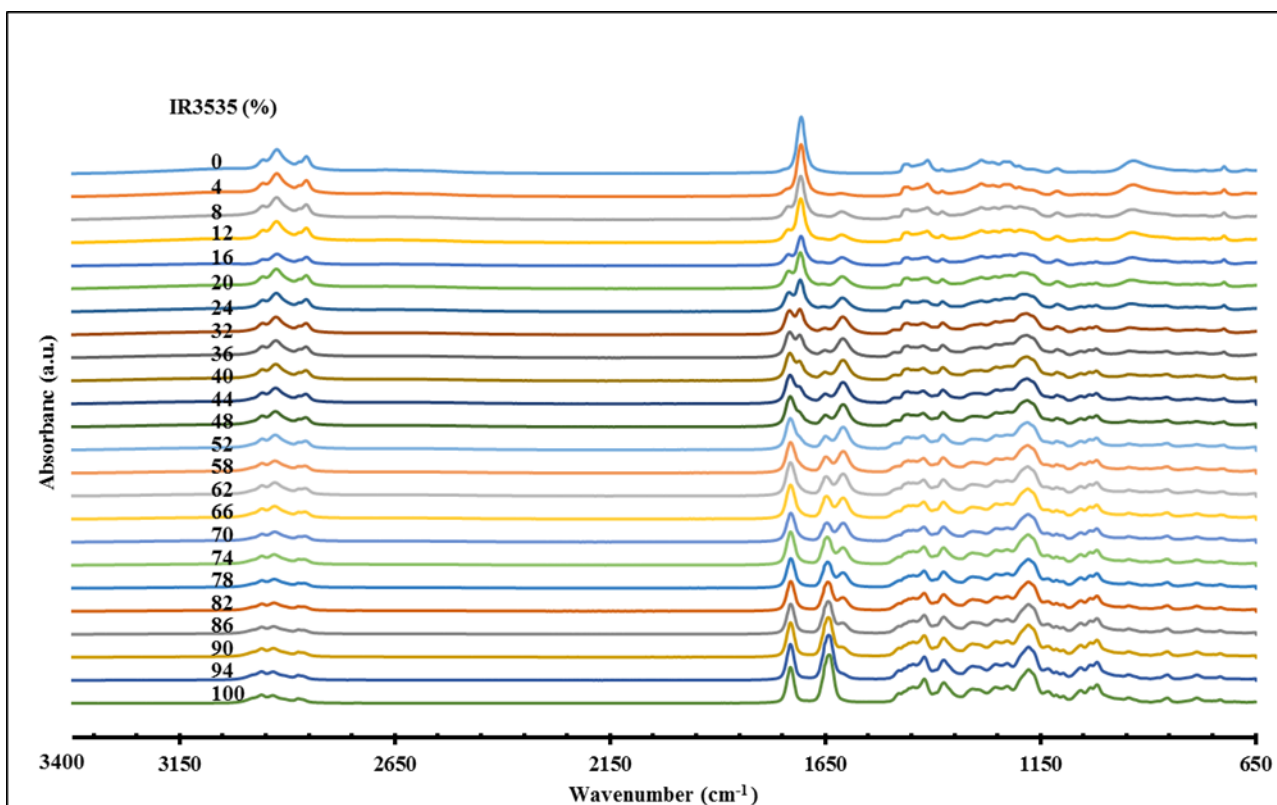


Figure 3. FTIR spectra of binary mixtures of nonanoic acid and IR3535 at various concentrations. The indicated IR3535 concentrations refer to the IR3535 content of the liquid phase.

Figure 4 shows the Raman spectra of the binary IR3535-nonanoic acid mixtures at various concentrations.

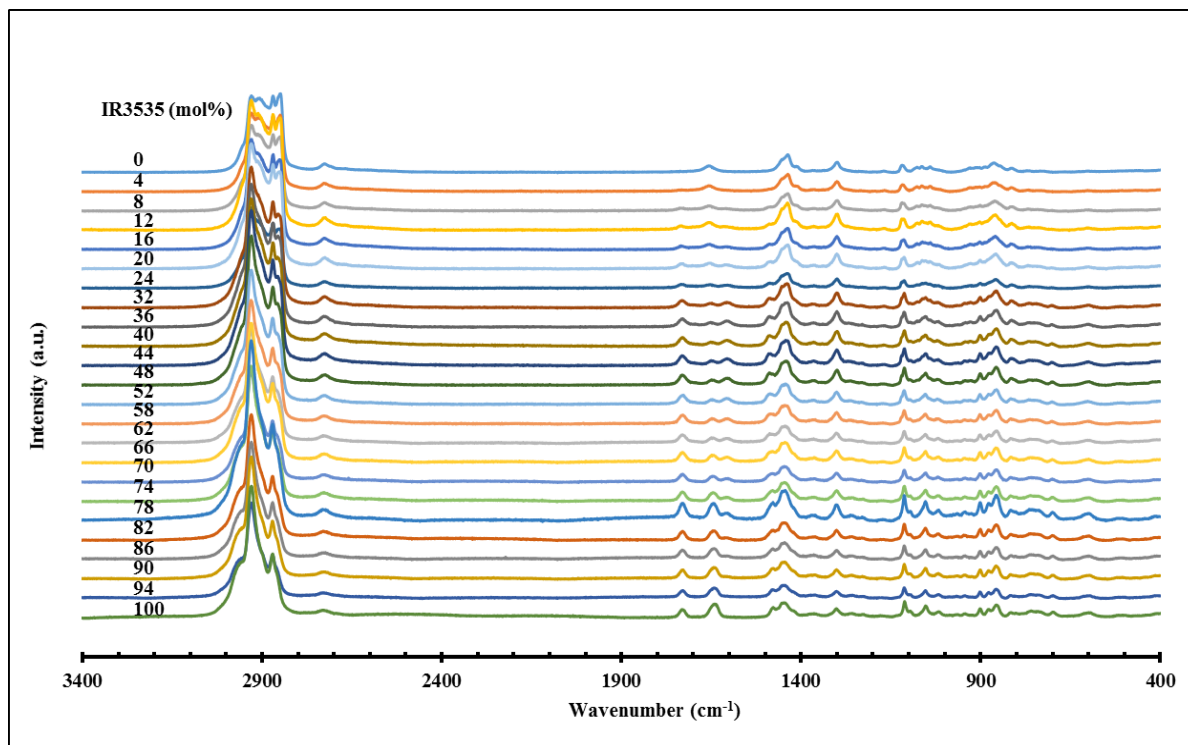


Figure 4. Raman spectra of binary mixtures of nonanoic acid and IR3535 at various concentrations. The indicated IR3535 concentrations refer to the IR3535 content of the liquid phase.

Figure 3 and Figure 4 show that addition of IR3535 to nonanoic acid causes alteration in the shape and position of some of the main peaks. Tracking the changes in the position and intensity of special peaks may provide valuable information about intermolecular interactions such as hydrogen bonding.

Figure 5 represents the position of the carbonyl peak in the FTIR spectrum of nonanoic acid. The frequency of this peak is almost constant upon IR3535 addition.

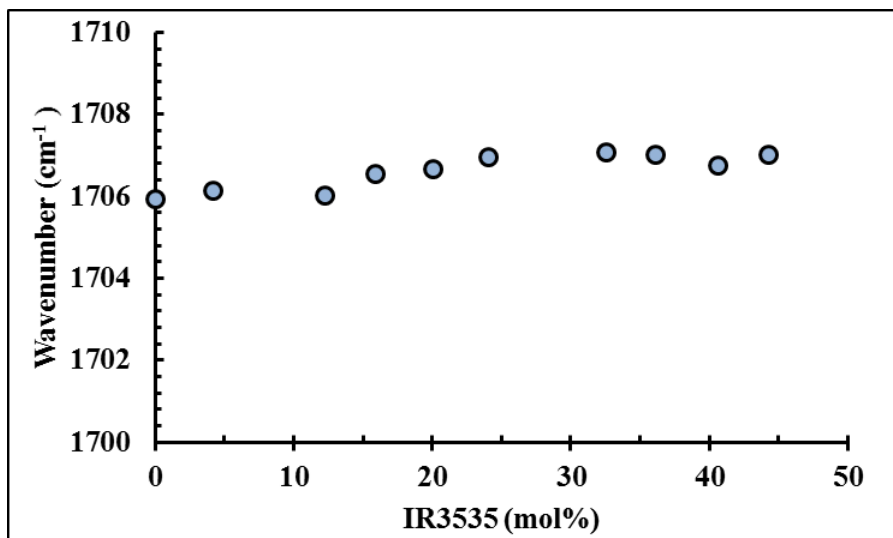


Figure 5. The position of the peak assigned to carbonyl bond in cyclic dimer structure as a function of IR3535 molar concentration in the FTIR spectra

Figure 3 illustrates formation of a new peak around 1610 cm^{-1} in the FTIR spectrum of binary mixtures. Figure 4 also shows formation of a weak Raman band around 1606 cm^{-1} .

Figure 6 shows the variation of the position of the new peak in the FTIR spectra. The position of this peak is almost constant, around 1610 cm^{-1} , at various concentrations of IR3535.

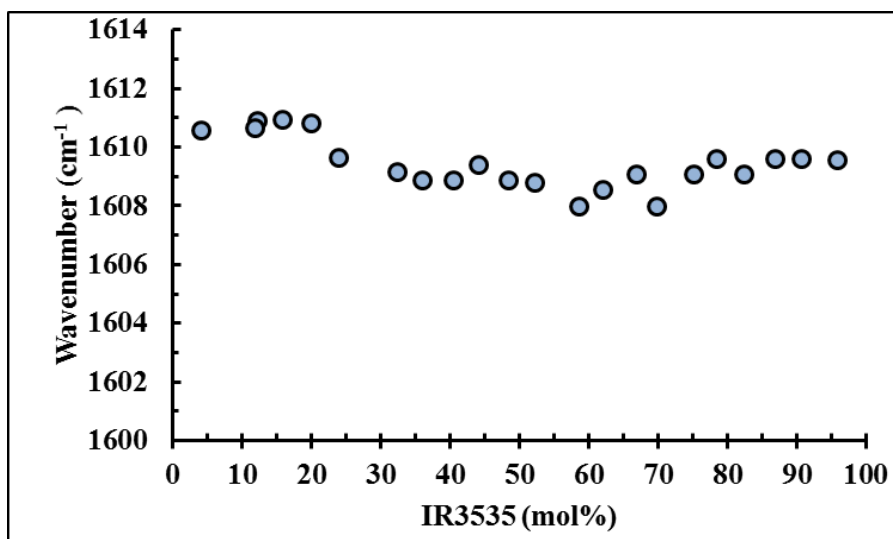


Figure 6. Frequency new-formed peak as a function of IR3535 molar ratio in the FTIR spectra

4.2. UV-Vis spectroscopy

Figure 7 and Figure 8 present the UV-Vis spectrum of nonanoic acid and IR3535 respectively.

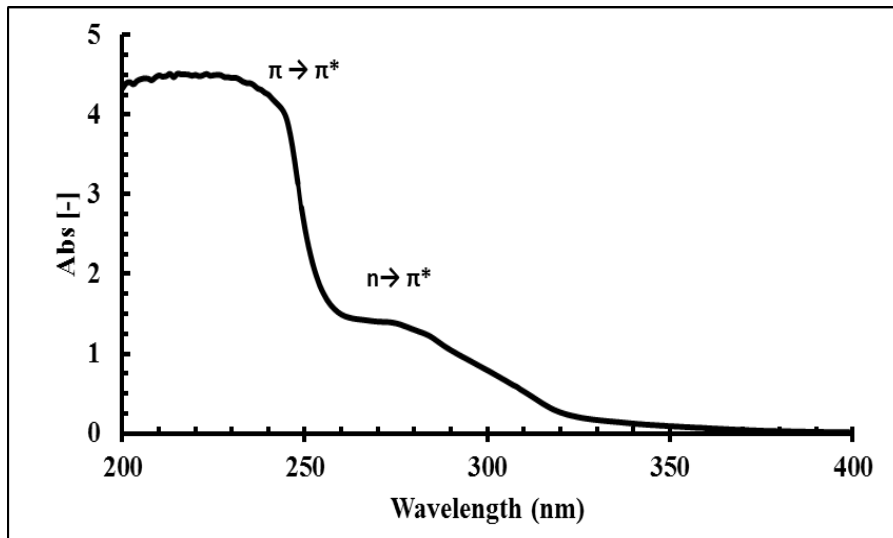


Figure 7. UV-Vis spectrum of nonanoic acid

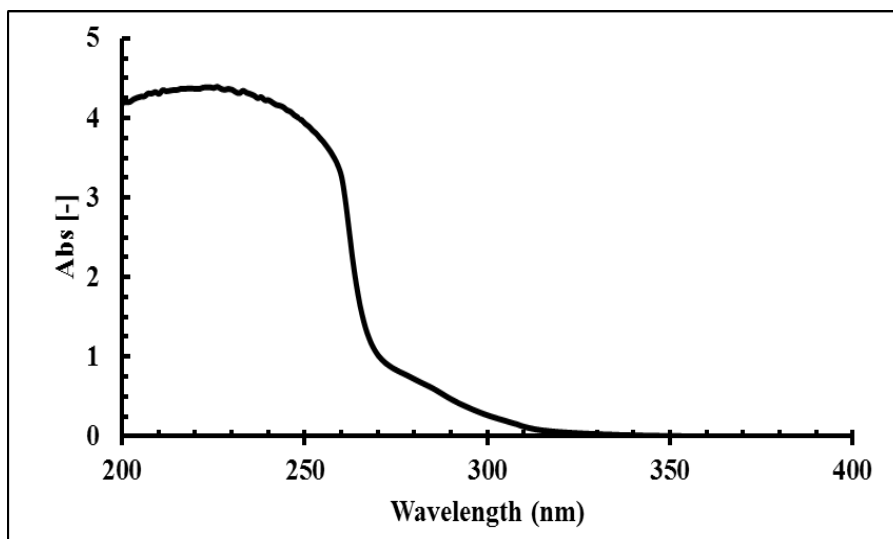


Figure 8. UV-Vis spectrum of IR3535

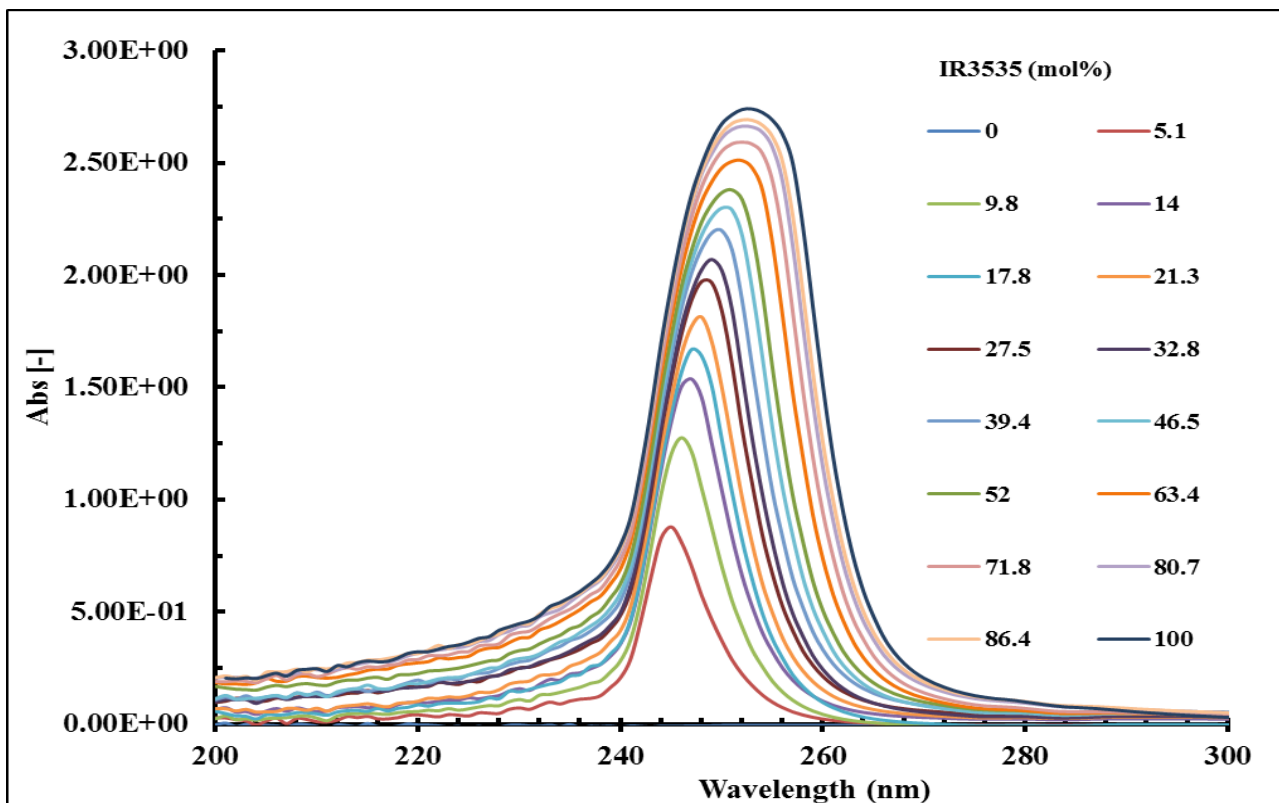


Figure 9. UV-Vis spectra of nonanoic acid-IR3535 mixtures (with nonanoic acid as reference) at various compositions. The indicated IR3535 concentrations refer to the IR3535 content of the mixtures.

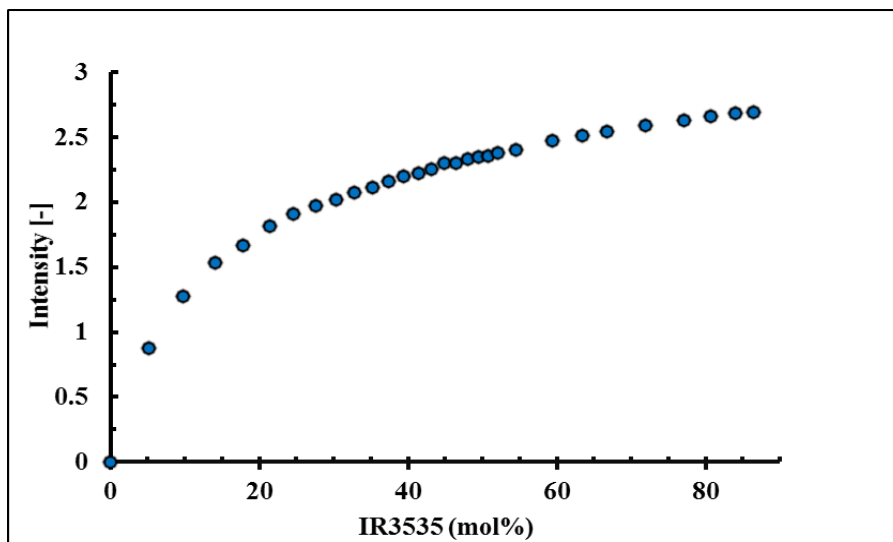


Figure 10. Intensity of the main peak of figure 9 at its maxima versus IR3535 molar concentration

Figure 10 shows that addition of IR3535 primarily causes a sharp increase in the intensity of the absorption peak. Above 20 mol% IR3535 the increase in the peak height becomes less pronounced.

ΔAbs is shown for different concentrations in Figure 11. The deviation of the Beer-Lambert law at λ_{max} ($\lambda_{1max} = 247 \text{ nm}$ and $\lambda_{2max} = 253 \text{ nm}$) are shown in Figure 12.

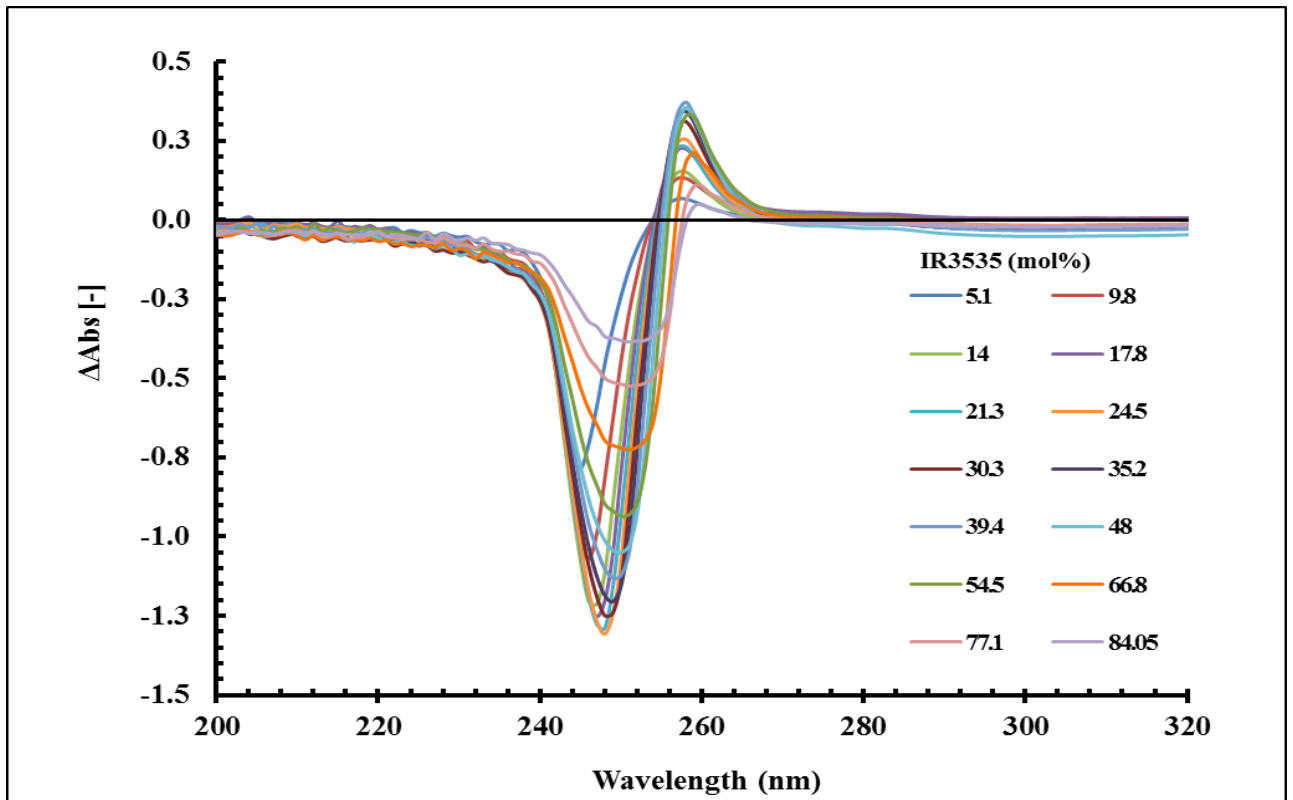


Figure 11. Δ Abs of IR3535-nonanoic acid mixtures at different concentrations

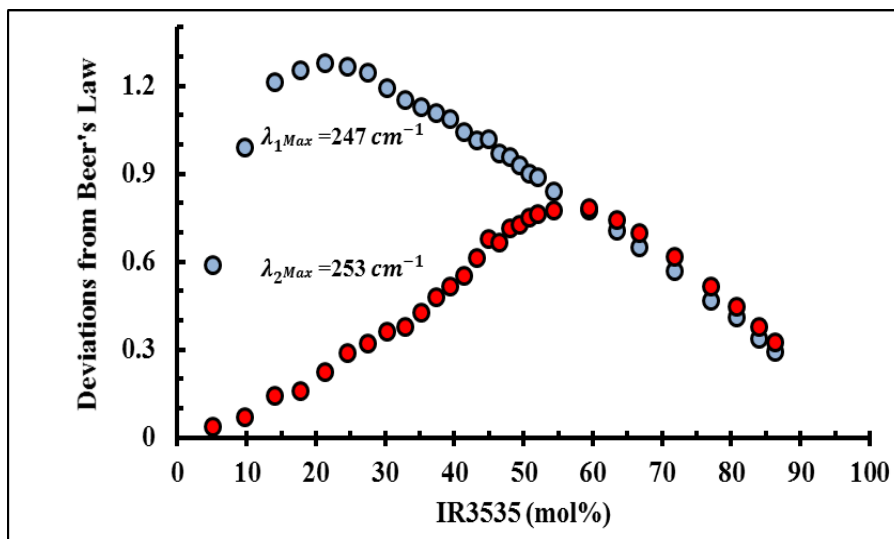


Figure 12. Deviation from Beer-Lambert law at $\lambda_{1max} = 247$ nm and $\lambda_{2max} = 253$ nm

4.3. Oven test

The weight-loss graphs of the binary IR3535-nonanoic acid mixtures are presented in Figure 13.

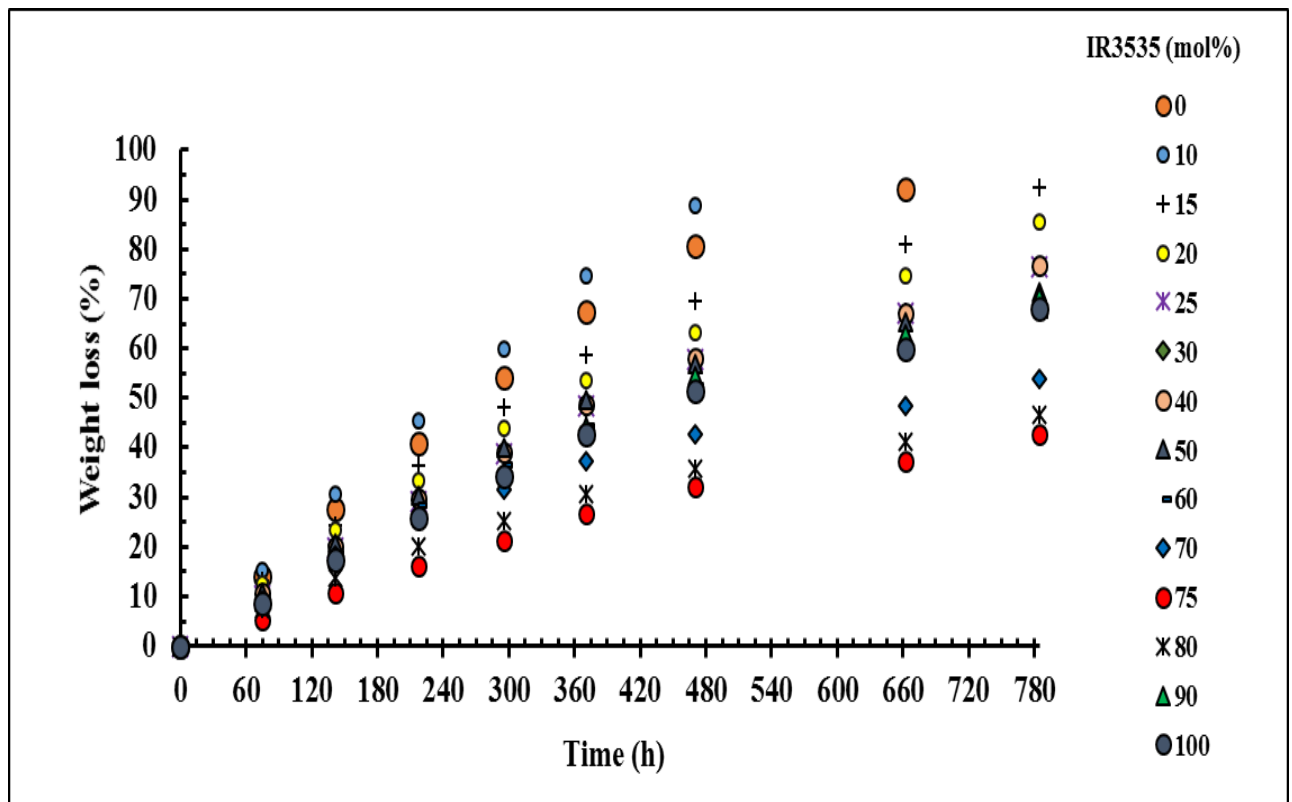


Figure 13. Evaporation profile of IR3535 and nonanoic acid binary mixtures obtained in oven test. The indicated concentrations refer to the primary IR3535 content of the liquid phase.

Figure 13 reveals that evaporation rate is the fastest when the initial concentration of IR3535 is 10% whereas the slowest evaporation rate is observed for a mixture with an initial concentration of 75% IR3535.

The composition of the residual liquid was determined by inverse analysis technique. The IR3535 mole fraction in the remaining liquid were then plotted against released mole fraction in Figure 14 and against time in Figure 15.

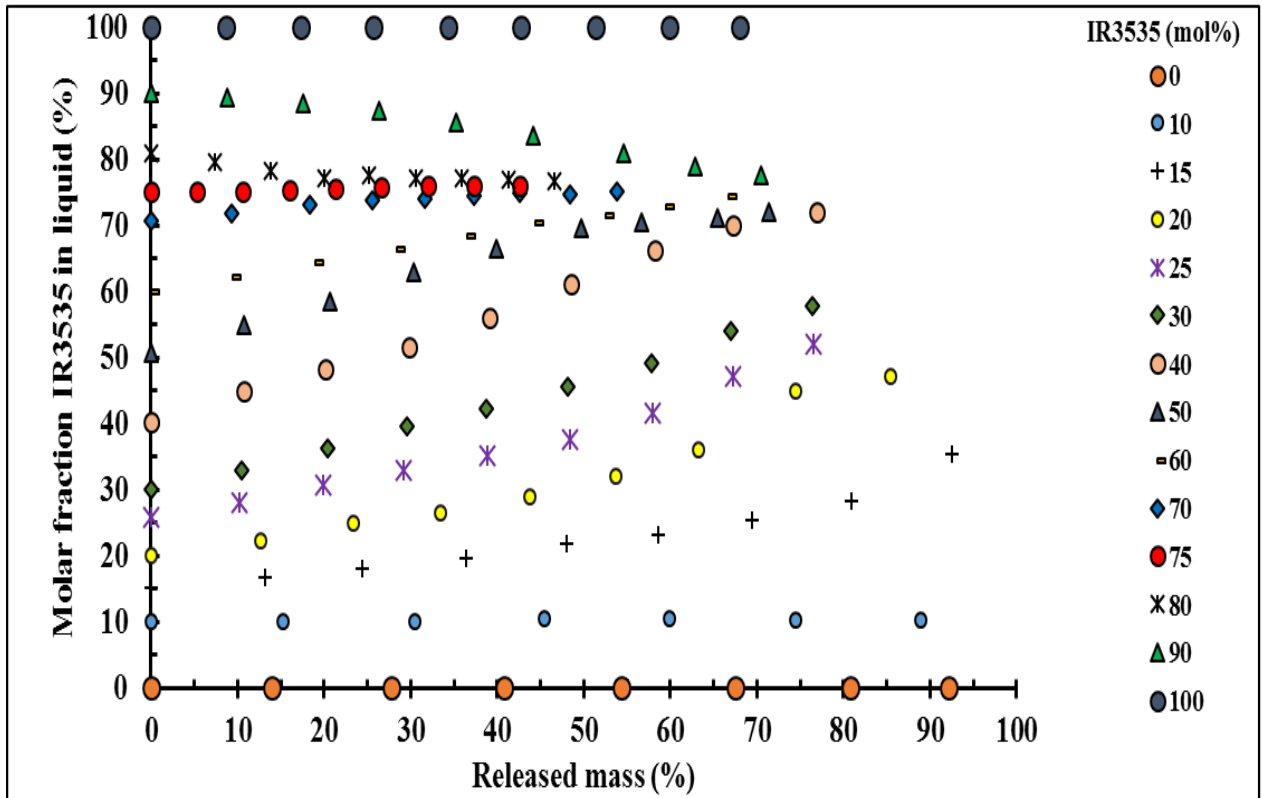


Figure 14. Mole fraction of IR3535 remained in the liquid phase as a function of the fraction of mixture released. The indicated concentrations refer to the primary IR3535 content of the liquid phase.

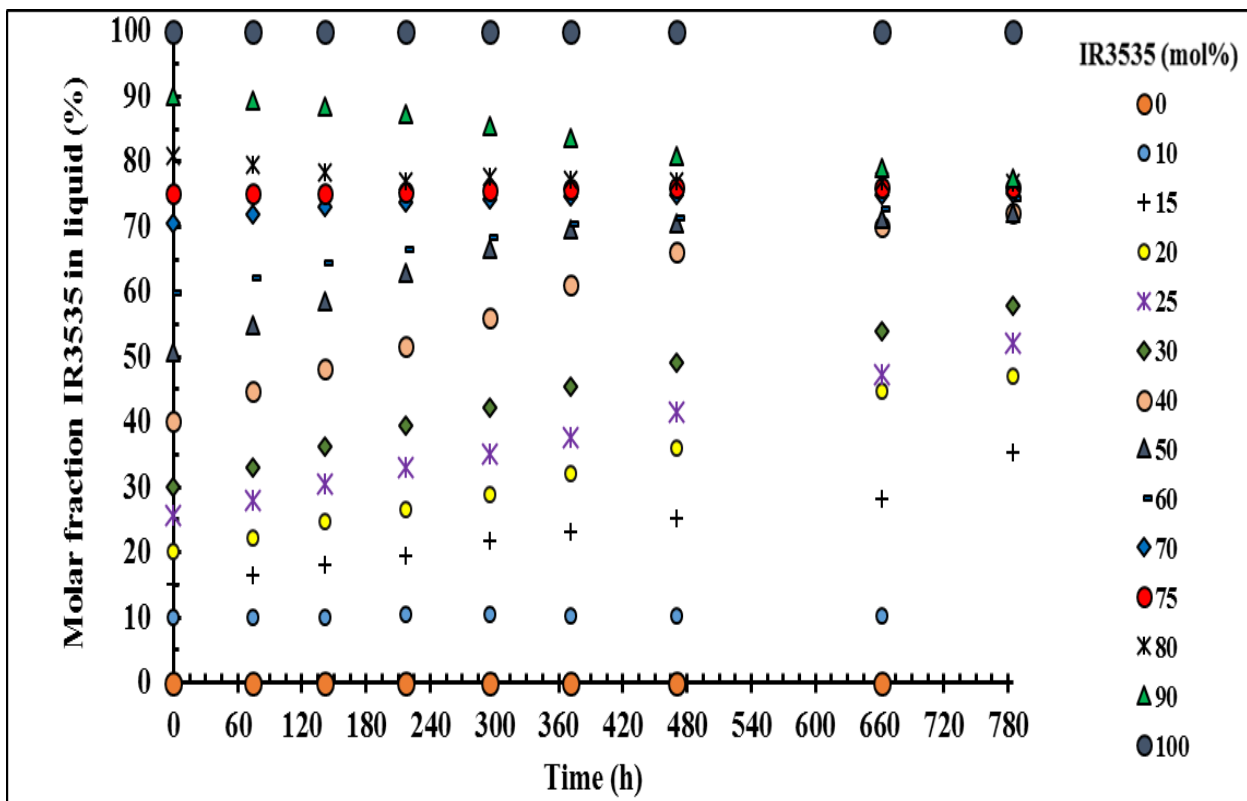


Figure 15. Mole fraction of IR3535 remained in the liquid phase as a function of time. The indicated concentrations refer to the primary IR3535 content of the liquid phase.

The vapour compositions of the mixtures obtained by performing a mass balance.

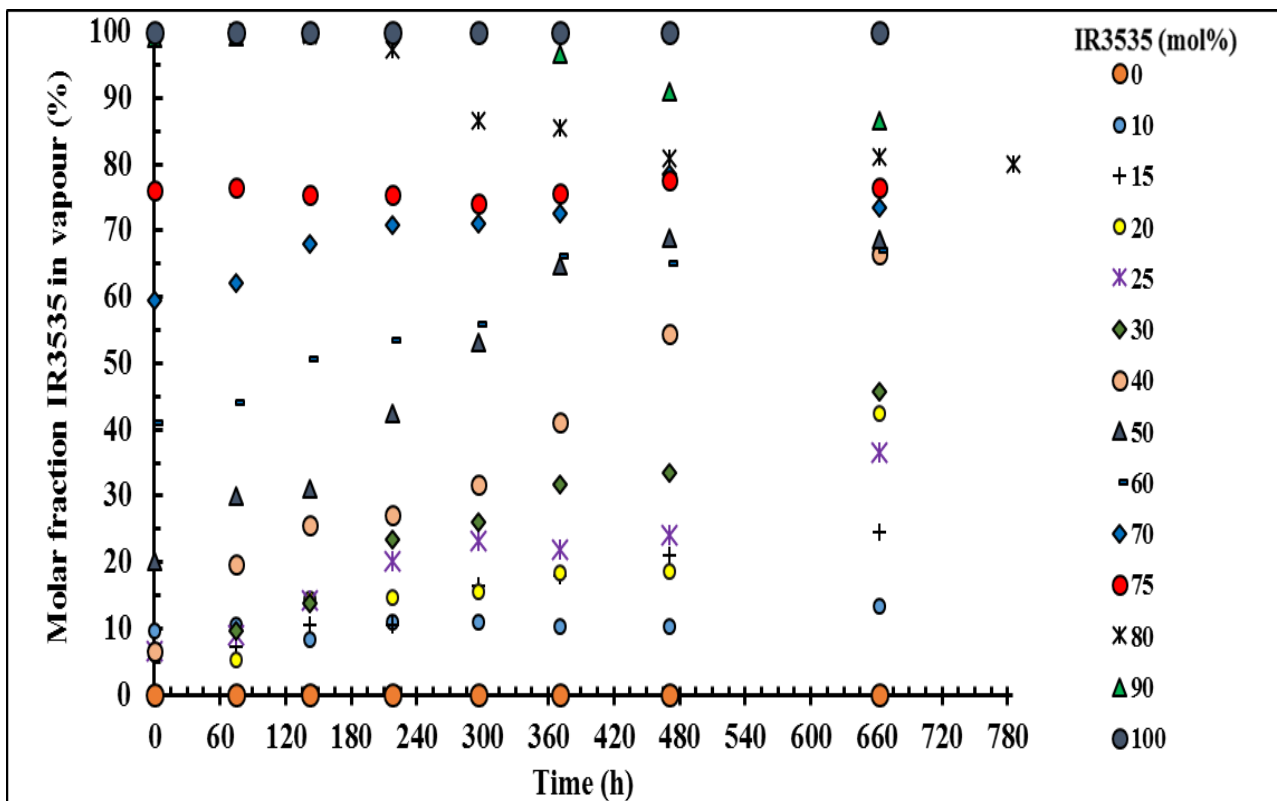


Figure 16. Mole fraction of IR3535 in the released vapour as a function of time. The indicated concentrations refer to the primary IR3535 content of the liquid phase.

4.4. TGA

Figure 17 shows the TGA mass loss curves for IR3535, nonanoic acid and the selected mixtures.

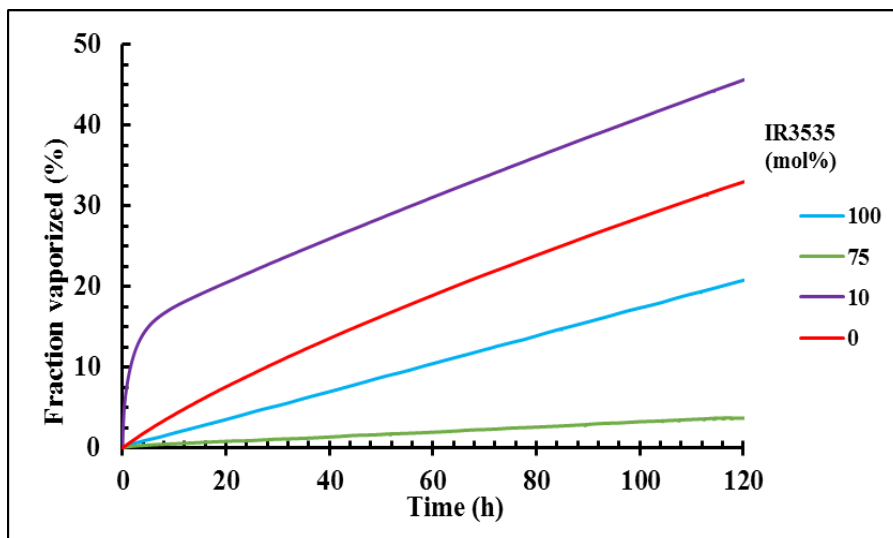


Figure 17. TGA evaporation profiles of selected binary mixtures compared with pure nonanoic acid and pure IR3535. The indicated concentrations refer to the initial IR3535 content of the liquid phase.

4.5. DSC

DSC profiles of IR3535, nonanoic acid and IR3535-nonanoic acid binary mixtures at various concentration are shown in Figure 18.

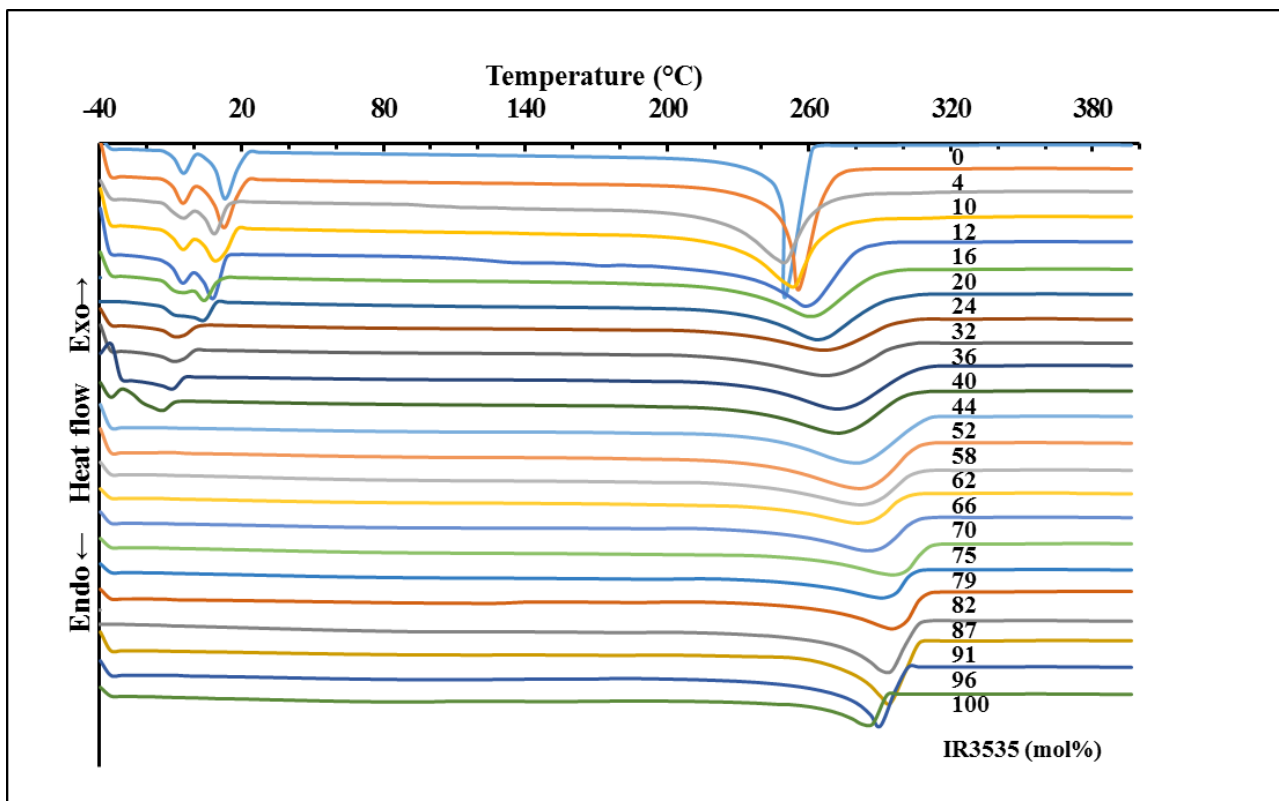


Figure 18. DSC profiles of IR3535-nonanoic acid binary mixtures in comparison with pure IR3535 and pure nonanoic acid. The indicated concentrations refer to the primary IR3535 content of the liquid phase.

4.6. Repellence test

Results of protection after the three-minute exposure period are presented in Table 7.

Table 7. Three-minute mosquito repellence screening results for DEET and binary mixtures of IR3535 and nonanoic acid. Protection was measured after a three-minute exposure period

Repellent / Test person	1	2	3	4
DEET	1.00	0.82	0.83	0.93
IR3535	0.86	0.94	0.83	0.79
Nonanoic acid	1.00	0.24	0.83	0.93
10% of IR3535	0.71	0.82	0.67	0.86
75% OF IR3535	1.00	0.94	1.00	1.00

The protection of 0.8 was considered significant for further investigation. All samples showed >0.8 protection in the initial study. However, testing of the pure nonanoic acid and the positive pseudo-azeotrope (containing 10% IR3535) was discontinued because of allergic responses during the initial evaluation.

In order to assess the total protection time, the other three samples were subjected to a time lag trial. The results of the time lag test over a period of six hours is presented in Table 8.

Table 8. Time lag repellence tests using DEET, IR3535 and negative pseudo-azeotrope containing 75% IR3535

Sample	Observer	3 minutes	30 minutes	1 hours	2 hours	3 hours	4 Hours	6 hours
DEET	1	0.92	0.67	1.00	1.00	0.25	0.00	---
	2	0.79	0.64	0.93	0.86	0.29	0.00	---
	3	0.86	0.64	0.93	0.93	0.14	0.00	---
	4	0.76	0.65	0.71	0.76	0.29	0.00	---
IR3535	1	0.67	0.67	0.42	0.42	0.33	0.58	0.33
	2	0.71	0.86	0.79	0.64	0.50	0.50	0.14
	3	0.64	0.71	1.00	0.79	0.79	0.79	0.79
	4	0.65	0.71	0.65	0.65	0.59	0.65	0.47
75% of IR3535	1	1.00	1.00	1.00	1.00		1.00	0.67
	2	1.00	1.00	1.00	1.00	1.00	1.00	0.64
	3	1.00	1.00	1.00	1.00	1.00	1.00	0.64
	4	1.00	1.00	1.00	1.00	1.00	1.00	1.00

To simplify the comparison, the average protection reported by all the volunteers for all three samples during the six hours' exposure time is shown in Figure 19.

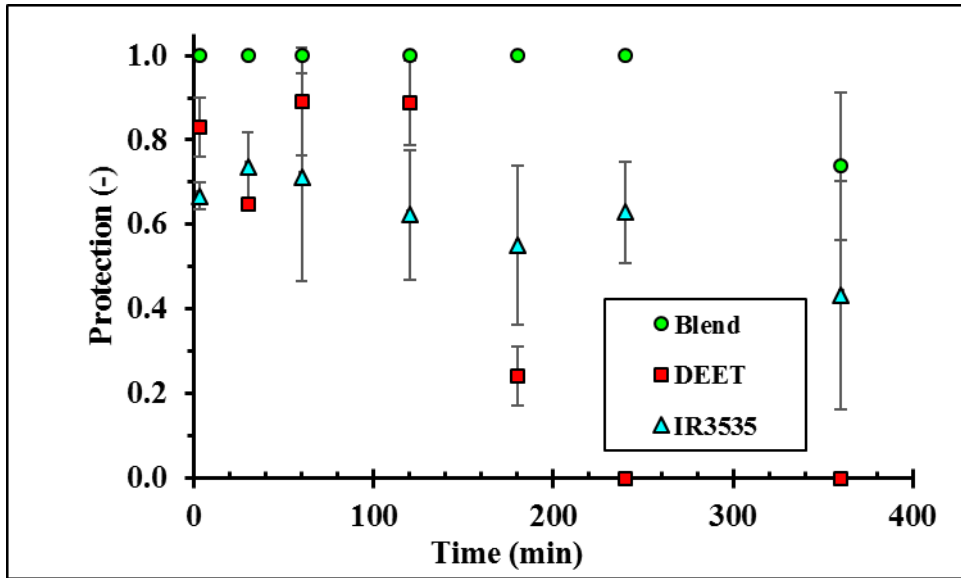


Figure 19. Protection of negative pseudo-azeotrope, IR3535 and DEET tested 3 to 360 minutes after application on skin

Chapter 5

DISCUSSION

5. Discussion

5.1. Vibrational spectroscopy

The O–H stretch band, the C=O stretch band, the C–O stretch band, the O–H in-plane bending band, and the O–H out-of-plane wagging bands are the most informative bands in nonanoic acid as they are all sensitive to hydrogen bonding.

As shown in Figure 1, nonanoic acid shows a broad O–H stretch band in the FTIR spectrum around 3000 cm^{-1} which is superimposed on the C–H stretch bands. This band is very broad, having a half intensity band width of 700 cm^{-1} (Bratož *et al.*, 1956). The unusual width and shape of the O–H stretching band of carboxylic acids arises, in part, from the presence of an equilibrium mixture of open chain and cyclic forms (Bellamy *et al.*, 1963). The shape and position of the O–H band in Figure 1 suggests the predominance of the dimer form. See the structure in Figure 9. The O–H stretching bands are weak in the Raman (Lin-Vien *et al.*, 1991). The out-of-phase OH··O wag at 932 cm^{-1} in the FTIR spectrum of nonanoic acid in Figure 1 confirms formation of hydrogen bonds among acid molecules and formation of cyclic dimer structures (Hadzi and Sheppard, 1953). This band is related to out-of-plane wagging of hydrogens involved in the dimer ring. Since this band occurs only for the dimer structures, it is known as the “dimer band” (Mayo *et al.*, 2004). The dimer band is only of medium intensity and it is noticeably broader than other bands in the vicinity.

These observations are in agreement with the reported liquid structure of other carboxylic acids. It is well known that carboxylic acids usually undergo dimerization (Allen and Caldin, 1953) and that the mixture consist of monomers, linear oligomers and dimer structures. The degree of dimerization increases with the chain length of the acid (Tanaka *et al.*, 1990).

Overtone and combination of bands near 1420 cm^{-1} and 1300 cm^{-1} , related to O–H bend and C–O stretch, are enhanced by Fermi resonance with the broad O–H stretch band and their contribution observed in the low frequency wing in the $2500\text{--}2700\text{ cm}^{-1}$ region as some weaker superimposed band shoulders (Bratož *et al.*, 1956).

The sharp and intense absorption band at 1705 cm^{-1} in the FTIR spectra is assigned to carbonyl bond of nonanoic acid, with the monomer contribution observed as a weak band at 1738 cm^{-1} (Mayo *et al.*, 2004).

There is a band cluster in the FTIR spectrum at 1320 to 1200 cm^{-1} . The narrow region on the 1315 - 1290 cm^{-1} , in the FTIR is also assigned to dimers (Hadzi and Sheppard, 1953). Two weak bands observed at 1287 and 1410 cm^{-1} both involve interacting C–O stretch and C–O–H in-plane bending (Hadzi and Sheppard, 1953).

Both functional groups present in the chemical structure of IR3535, i.e. ester and an amide functional groups, may involve in hydrogen bonding. The ester group presents a C=O band around 1730 cm^{-1} which is strong in FTIR but due to the relatively low depolarization ratio, about 0.09-0.12, weaker in Raman spectra (Dollish *et al.*, 1974, Freeman, 1974).

In addition, there is a band cluster in the 1300 - 1150 cm^{-1} region which is mainly related to C–O stretch in the ester group (Hadzi and Sheppard, 1953, Thompson and Torkington, 1945).

The ethyl ester group, i.e. O–CH₂–CH₃, can be observed in the FTIR through various vibrational bands such as the medium band near 2980 cm^{-1} attributed to CH₃ antisymmetric stretch, the weak band close to 1475 cm^{-1} related to CH₂ deformation, the weak band around 1455 cm^{-1} is ascribed to CH₃ antisymmetric deformation, the weak band around 1400 cm^{-1} related to O–CH₂ wag and the medium band around 1375 cm^{-1} assigned to CH₃ symmetric deformation (Thompson and Torkington, 1945).

The CH₂ deformation band in the CH₂ (C=O) group is observed in the FTIR near 1420 cm^{-1} (Alan R. Katritzky, 1960).

The amide functional group of IR3535 can be characterized by a carbonyl bond observed at 1640 cm^{-1} in both IR and Raman (Brown *et al.*, 1959). Additional bands include C–N stretch at 1420 cm^{-1} in the FTIR and in-plane NCO deformation around 600 cm^{-1} in the Raman. The vibration of R–C(=O)–NR₂ occurs at 740 cm^{-1} (Dollish *et al.*, 1974).

Figure 5 shows that addition of IR3535 does not change the position of the carbonyl bond of the nonanoic acid dimer. This constant position of this peak indicates that the hydrogen-bonded cyclic dimers do not necessarily dissociate on addition of IR3535.

As shown in Figure 3 and Figure 4, adding IR3535 to nonanoic acid causes formation of a new intermolecular interaction which results in formation of new peaks in the Raman and FTIR spectra. Figure 3 shows a new peak developing around 1610 cm^{-1} in binary mixtures of IR3535 and nonanoic acid. Figure 6 shows that the position of this peak is almost independent of mixture composition. Figure 4 also shows formation of a new low intensity peak in the Raman spectra in the same vicinity, around 1606 cm^{-1} . Although the frequency of this peak in Figure 6 is in the region of carboxylate ion (COO^-), other spectral features do not support the formation of an ionic complex between IR3535 and nonanoic acid. When a salt forms with a carboxylic acid, the $\text{C}=\text{O}$ and $\text{C}-\text{O}$ bonds of the acid are replaced by two equivalent $\text{C}\cdots\text{O}$ “bond-and-a-half” bonds. These CO_2^- bonds interact out-of-phase and in-phase to give two bonds. The antisymmetric CO_2^- stretch band is usually seen at $1650\text{-}1540\text{ cm}^{-1}$, strong in the IR and weak and depolarized in the Raman. The symmetric CO_2^- stretch band is usually seen at $1450\text{-}1360\text{ cm}^{-1}$, medium-weak in the IR and strong and polarized in the Raman. In this case the symmetric CO_2 is not visible in Raman and FTIR.

5.2. UV-Vis spectroscopy

Deviations from the Beer-Lambert law were taken in account so that only those deriving from chemical interactions were relevant. See Appendix E.

Absorption of energy in UV (190-400 nm) and VIS (400-800 nm) may change the electronic energy of molecules and cause transfer of the electron from occupied molecular orbital (usually a non-bonding n or bonding π orbital) to an unoccupied molecular orbital (an antibonding π^* or σ^*). The amide and ester functional groups in IR3535 and the acid functional group in nonanoic acid undergo electronic transitions in UV-Vis range of electromagnetic radiation. The electronic transitions of all three functional groups are due to the presence of the carbonyl bond. The electronic transitions of the carbonyl bond are represented in Figure 20.

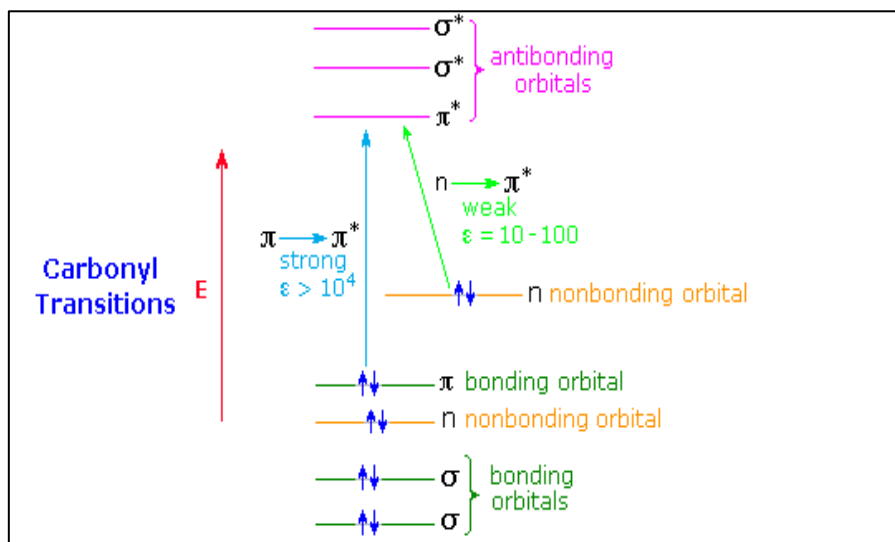


Figure 20. Two major electronic excitations of a carbonyl group (Reusch, June 2010)

Nitrogen and oxygen next to the carbonyl group in amide, acid and ester withdraw electrons from the carbonyl carbon and stabilize the oxygen lone pair in the carbonyl group. This inductive effect on the oxygen lone pairs shifts the $n \rightarrow \pi^*$ band to higher frequencies, i.e. a hypsochromic effect (Kumar, 2006). The position and intensity of $\pi \rightarrow \pi^*$ and $n \rightarrow \pi^*$ bands depends on the solvent as well as the substituents at the nitrogen and other carbon atoms. However, while the influence of these factors is complex, as a general rule there is usually a red shift in going from nonpolar solvent such as cyclohexane to polar solvent such as water (Nielsen and Schellman, 1967).

As shown in the UV-vis spectrum of nonanoic acid in Figure 7, the electronic transition behaviour and photochemistry of monomer and dimer forms are different. The absorption band of monomer forms are much broader, lower intensity and appears at a longer wavelength than that of dimer (Lourderaj *et al.*, 2006).

The hyperchromic effect, the blue shift of the absorption in the dimeric form, is due to the stabilization of the non-bonding orbital and as a consequence of the increasing the gap of $n \rightarrow \pi^*$ transition (Singleton *et al.*, 1987).

The electronic transition for the acid in the form of monomer appears below 200 nm which is beyond the scope of this study.

The longest-wavelength broad peak (280 nm) is characterized as an $n \rightarrow \pi^*$ transition. The band at immediately lower wavelength (~200-260 nm) has been suggested as a $\pi \rightarrow \pi^*$ transition (Singleton *et al.*, 1987).

As mentioned previously, both amide and ester functional groups in IR3535 are active in the UV-Vis spectrum. The amide group exhibits two main electronic transitions. The first one is the forbidden $n \rightarrow \pi^*$. This transition corresponds to the excitation of one of the lone pair electrons on the oxygen of the carbonyl group to the antibonding π^* orbital. Due to the mismatch between the n -orbitals and the π^* orbitals, the probability of such an excitation is very low. In other words the absorptivity of $n \rightarrow \pi^*$ is very low (10-100 $\text{L mol}^{-1}\text{cm}^{-1}$) and this transition is seen as a very weak peak (Robinson *et al.*, 2014). The shape, intensity and position of UV bands of the amide functional group varies based on factors such as solvent, number and nature of the substitution on the nitrogen and carbon atoms, etc. (Nielsen and Schellman, 1967).

Generally the $n \rightarrow \pi^*$ transition of amides in a non-polar solvent appears as a shoulder in the range of 225-235 nm (Nielsen and Schellman, 1967). In a polar solvent, e.g. in aqueous solutions, this excitation may not be perceivable. The reason is the blue shift of $n \rightarrow \pi^*$ coupled with the red shift of $\pi \rightarrow \pi^*$. The $n \rightarrow \pi^*$ transition undergoes a blue shift due to the interaction of the non-bonded electron with the polar solvent (Karelson and Zerner, 1990). On the other hand the $\pi \rightarrow \pi^*$ undergoes a red shift in polar solvents which is related to the decrease in the energy of the excited state and stabilization by the solvent (Chou *et al.*, 1993).

The $\pi \rightarrow \pi^*$ transitions in the UV spectra of amides has a long history of interest. Kaya *et al.* (Kaya and Nagakura, 1967) studied the effect of substitution on the nitrogen on the $\pi \rightarrow \pi^*$ band shift in the gas phase. Nielsen *et al.* compared $\pi \rightarrow \pi^*$ excitation in aqueous and cyclohexane solutions and reported red shift of the absorbance peak in the polar solvents (Nielsen and Schellman, 1967).

It is worth mentioning that although the major absorption in the 140-260 nm is attributed to the $\pi \rightarrow \pi^*$ transition, several types of Rydberg transitions such as n-Ryd. 3px, n-Ryd. 3py, π -Ryd. 3pz, and n-Ryd. 3s also are in its vicinity and interact with the $\pi \rightarrow \pi^*$ (Morisawa *et al.*, 2013).

The ester functional group in IR3535 also exhibits two absorption maxima. The allowed $\pi \rightarrow \pi^*$ and the forbidden $n \rightarrow \pi^*$. Since the nature of these transitions is the same with the amide's one, the peaks appear very close to each other and may completely overlap. As a matter of fact, transitions in both functional groups are related to the conjugated π bond of the carbonyl group. The nitrogen, in amide, and oxygen, in ester, show hypochromic effects particularly for the $n \rightarrow \pi^*$ transition. In other words, the substituents pull electrons from carbonyl carbon and increase the bond order of the C=O. This inductive effect shifts the $n \rightarrow \pi^*$ transition to higher frequencies.

As mentioned in Section 3.2.3, to simplify the interpretation, nonanoic acid was selected as the reference to study IR3535-nonanoic acid titration. As shown in Figure 9, addition of IR3535 to nonanoic acid results in a peak at 240 nm. This peak is the sum of ester and amide carbonyl absorption since both undergo $\pi \rightarrow \pi^*$ transitions in the UV-Vis region.

By increasing the concentration of IR3535, these two $\pi \rightarrow \pi^*$ transitions begin to separate. Broadening the peak provides evidence for this assertion. However, such a separation may be seen more clearly by following the maximum in the intensity versus the concentration as shown in Figure 10.

Since the ester and amide carbonyl $\pi \rightarrow \pi^*$ transitions separate after reaching the IR3535 molar concentration of 15%, the level of overlap of two peaks decreases, the intensity of the peak does not increase significantly and the peak width starts to increase.

Obviously if there is no interaction between IR3535 and nonanoic acid based on Beer-Lambert law one should expect a linear increase with addition of IR3535 due to the increase in the concentration. Deviation of the Beer-Lambert law may have different reasons as mentioned above. However, in this case the deviation is primarily due to the chemical interaction of the acid and IR3535 molecules since all other sources of deviation were offset.

Figure 11 shows that both positive and negative deviation of Beer-Lambert law are present in the mixtures. In other word, there are at least two types of strong molecular interactions in the system.

Figure 12 shows that the deviation from the Beer-Lambert law is at a maximum when the molar concentration of IR3535 in the mixture is around 20% or 60% for 247 and 253 nm respectively. Since deviation of Beer-Lambert was mostly limited to chemical deviation, it can be concluded that strongest interactions happen around 20% and 60% IR3535.

5.3. Oven test

According to Figure 13, on the experiment condition, i.e. at 50 °C and ambient pressure, 68% of the initial weight of pure IR3535 had evaporated after 780 hours. However, at the same period only 42% of the mixture with primary concentration of 75% IR3535 had evaporated.

On the other hand, 90% of mixture with primary composition of 10% IR3535 evaporated after 480 hours, while almost 80% of pure acid was vaporized at the same period of time.

These observations, i.e. occurrence of maximum and minimum of evaporation rate for binary mixtures rather than for pure IR3535 and nonanoic acid are typical signs for positive and negative pseudo-azeotropes respectively at the corresponded concentrations.

This test was intermittently stopped to collect samples for FTIR analysis. In doing this small samples were removed but this, in the end their total amounted to less than 1% of the initial mass. Nevertheless, it is prudent to seek independent substantiation. One possibility is to study the weight-loss with accurate isothermal thermo-gravimetric analysis.

Both Figure 14 and Figure 15 show that concentration of IR3535 in the remaining liquid initially either increases or decreases but then stabilises at a plateau value around the composition of 75% IR3535. Convergence of the compositions around the same value for all mixtures irrespective of their initial concentration is a typical sign for negative pseudo-azeotrope mixture.

It is also clear from Figure 15 that the initial composition around 10 mol% IR3535 is stable and the composition remained almost fixed at this level during the test, however other mixture compositions diverged from this plateau value. This observation indicates formation of a positive pseudo-azeotrope mixture at this concentration. Figure 16 reports the results of a mass balance and it confirms the fact that the emitted vapour compositions also approached the same plateau values as found for the liquid phase. This indicates that, over time, evaporation of an IR3535-nonanoic acid mixture at 50 °C will diverge from the positive pseudo-azeotrope or converge to the negative pseudo-azeotrope point. These points are azeotrope-like as the relative concentrations of the vapour and liquid phases become identical.

5.4. TGA

As expected the rate of evaporation correlated with the normal boiling point and nonanoic acid was more volatile than IR3535. As shown in Figure 17, 35 wt.% of the initial mass of nonanoic acid had evaporated after 115 h, whereas only about 20 wt.% of the IR3535 had evaporated during this period.

The mixture containing 75 mol% IR3535 was the least volatile as it showed the lowest mass loss rate. Only 5 wt.% of the initial mass of this mixture had evaporated after 115 h. The reduced volatility of the mixture at this composition in comparison with the pure compounds is attributed to formation of a negative pseudo-azeotrope. As expected from the stability of negative pseudo-azeotropes, the mass loss rate of this mixture is almost constant analogous to a pseudo-component.

The mass loss rate of the mixture containing 10 mol% IR3535 was initially the highest. The higher volatility of this composition, in comparison with the pure compounds, is attributed to formation of positive pseudo-azeotropes. As expected, positive pseudo-azeotropes are not stable. As a result, after about 10 h, the mass loss rate dramatically decreased and approached a slope similar that for the nonanoic acid. In other words, positive azeotrope featured the highest overall volatility. After a while the composition of the evaporating mixture had changed and the composition converged to the composition of pure nonanoic acid. In principle mixture with similar starting concentration can also approach the composition of the negative pseudo-azeotrope.

The reduced and enhanced volatility of the binary mixtures containing 75 mol% and 10 mol% IR3535 respectively are likely attributable to chemical interactions between the IR3535 and nonanoic acid.

5.5. DSC

As shown in Figure 18, the DSC data for nonanoic acid showed three thermal transitions. Two endothermic peaks are observed at $-8\text{ }^{\circ}\text{C}$ and $8\text{ }^{\circ}\text{C}$. Generally, fatty acids crystalize in different crystal forms or polymorphs. For more detail about polymorphism in fatty acids see references

(Schlenk, 1961). When the temperature increases, and just below the melting point, all the polymorphs transform irreversibly to the most stable one (Moreno et al., 2007, Gandolfo et al., 2003, Garti et al., 1980). This causes an endotherm peak, just before the melting peak.

Nonanoic acid showed a single boiling transition with a onset temperature of 229 °C which is attributed to boiling point and is in agreement with the literature (Bond, 2003).

IR3535 melts at -90 °C. Consequently, in the temperature range studied, IR3535 showed only a single thermal (boiling) transition with an onset temperature of 238°C.

According to Figure 18, IR3535-nonanoic acid binary mixtures in some molar ratios featured higher boiling transitions when evaporated into a stream of nitrogen gas. The highest apparent boiling point in Figure 18 is allocated to the sample with molar composition of about 75 mol% IR3535 with a transition boiling onset of 251 °C. This matches the negative pseudo-azeotrope composition.

On the other hand, IR3535-nonanoic acid binary mixtures in some molar ratios featured lower boiling transitions when evaporated into a stream of nitrogen gas. The lowest apparent boiling point in Figure 18 is allocated to the sample with molar composition of 10 mol% IR3535 with transition boiling onset of 220 °C. This composition was discovered as the positive pseudo-azeotrope mixture.

DSC results confirm that this system features two mixtures with respectively a higher and a lower apparent boiling point than the parent compounds. However, this need not necessarily imply that pseudo-azeotrope compositions would also exist at the much lower temperature of 50 °C. This is because azeotrope compositions usually shift with temperature. So the observed agreement can be regarded as serendipitous.

5.6. Repellence test

Figure 19 shows performance comparisons of the negative pseudo-azeotrope blend and the neat repellents DEET and IR3535 in a standard topical repellence test. During the first two hours of exposure, DEET and IR3535 showed a relatively high level of protection, however after the third hour the protection provided by DEET showed a sudden drop, whereas the

protection provided by IR3535 showed a more gradual decrease. DEET failed to show any protection four hours post application but IR3535 was still $0.63(\pm 0.12)$ effective relative to the negative control. In comparison to these two repellents, the IR3535-nonanoic acid negative pseudo-azeotrope (i.e. the mixture containing 75% IR3535) showed superior repellence and a longer lasting effect. It provided essentially full protection for up to four hours. After six-hours post application the protection level decreased to $0.74 (\pm 0.17)$ which is still much higher compared to IR3535 (with the protection of $0.43 (\pm 0.27)$) or DEET (with protection of zero).

Another observation reported by all four volunteers was that application of IR3535 and DEET just repelled the mosquitoes, whereas the mixture of IR3535 and nonanoic acid showed an additional mode of action beyond mere repellence. While the 75 mol% IR3535 mixture was repelling the mosquitoes, it also weakened the mosquitoes. They behaved as if they were disorientated or dizzy resulting in knock-down. Most mosquitoes exposed to this mixture also died.

Chapter 6

MOLECULAR SIMULATION

6. Molecular simulations

As shown in Chapter 4 and discussed in Chapter 5, IR3535 and nonanoic acid mixtures form a negative pseudo-azeotrope at 75 mol% IR3535 and a positive pseudo-azeotrope at 10 mol%. In this section molecular simulation results are presented. They were generated in an attempt to explore the origin of the double pseudo-azeotrope that was observed. The nature of the interactions and particularly hydrogen bond formation between nonanoic acid and IR3535 was studied.

6.1. Insertion of missing parameters to AUA

The anisotropic united atom (AUA) force field was used to describe the intermolecular potential energy. The Lorentz-Berthelot combining rules were applied for the parameters of the Lennard-Jones potentials, i.e. the separation distance (σ_{ij}) and the depth of the potential well correspond to the minimum of the potential energy (ϵ_{ij}).

In order to cover the tertiary amide functional group in AUA, new potentials were added to the force field database. They were based on reported parameters for amine and ketone functional groups. The supplementary parameters are listed in Table 9 to Table 12.

Table 9. Added stretching parameters of the anisotropic united atoms intermolecular potential for tertiary amides

	L₀	Ref.
N _{amide} – C _{sp2, amide}	1.3729 Å	(Aparicio-Martínez and Balbuena, 2007)

Table 10. Added bending parameters of the anisotropic united atoms intermolecular potential for tertiary amides

	K	θ	Ref.
C _{sp2, amide} – N _{amide} – CH ₃	57128.00	111.0	(Orozco <i>et al.</i> , 2012, Chen <i>et al.</i> , 2007)
C _{sp2, amide} – N _{amide} – CH ₂	57128.00	111.0	(Orozco <i>et al.</i> , 2012, Chen <i>et al.</i> , 2007)
N _{amide} – C _{sp2, amide} – O _{sp2, amide}	114288.00	122.9	(Boutard <i>et al.</i> , 2005, Jorgensen <i>et al.</i> , 1996)
N _{amide} – C _{sp2, amide} – CH ₂	80438.00	119.2	(Boutard <i>et al.</i> , 2005, Jorgensen <i>et al.</i> , 1996)
N _{amide} – C _{sp2, amide} – CH ₃	80438.00	119.2	(Boutard <i>et al.</i> , 2005, Jorgensen <i>et al.</i> , 1996)

$O_{sp^2, amide} - C_{sp^2, amide} - CH_2$	80438.00	120.4	(Boutard <i>et al.</i> , 2005, Kranias <i>et al.</i> , 2003)
$O_{sp^2, amide} - C_{sp^2, amide} - CH_3$	80438.00	120.4	(Boutard <i>et al.</i> , 2005, Kranias <i>et al.</i> , 2003)
$CH_3 - C_{sp^2, amide} - CH_3$	105822.00	119.2	(Ferrando <i>et al.</i> , 2010, Cornell <i>et al.</i> , 1995)
$CH_3 - C_{sp^2, amide} - CH_2$	105822.00	119.2	(Ferrando <i>et al.</i> , 2010, Cornell <i>et al.</i> , 1995)
$CH_2 - C_{sp^2, amide} - CH_2$	105822.00	119.2	(Ferrando <i>et al.</i> , 2010, Cornell <i>et al.</i> , 1995)
$CH_3 - CH_2 - C_{sp^2, amide}$	74900.00	114.0	(Ferrando <i>et al.</i> , 2010, Ungerer <i>et al.</i> , 2000)
$CH_2 - CH_2 - C_{sp^2, amide}$	74900.00	114.0	(Ungerer, Beauvais <i>et al.</i> 2000, Ferrando, Lachet <i>et al.</i> 2010)

Table 11. Added torsion parameters of the anisotropic united atoms intermolecular potential for tertiary amides (In units of K)

A0	A1	A2	A3	A4	A5	A6	A7	A8
$CH_3 - N_{amide} - C_{sp^2, amide} - CH_3$ (Orozco <i>et al.</i> , 2012)								
189.01	979.05	482.82	-1436.8	-1465.1	-1219.3	913.04	541.13	16.99
$CH_3 - N_{amide} - C_{sp^2, amide} - CH_2$ (Orozco <i>et al.</i> , 2012)								
189.01	979.05	1482.82	-1436.8	-1465.1	-1219.3	913.04	541.13	16.99
$CH_2 - N_{amide} - C_{sp^2, amide} - CH_3$ (Orozco <i>et al.</i> , 2012)								
189.01	979.05	1482.82	-1436.8	-1465.1	-1219.3	913.04	541.13	16.99
$CH_2 - N_{amide} - C_{sp^2, amide} - CH_2$ (Orozco <i>et al.</i> , 2012)								
189.01	979.05	1482.82	-1436.8	-1465.1	-1219.3	913.04	541.13	16.99
$O_{sp^2, amide} - C_{sp^2, amide} - N_{amide} - CH_3$ (Boutard <i>et al.</i> , 2005)								
468.4	-583.65	-210	842	0	0	0	0	0
$O_{sp^2, amide} - C_{sp^2, amide} - N_{amide} - CH_2$ (Boutard <i>et al.</i> , 2005)								
468.4	-583.65	-210	842	0	0	0	0	0
$C_{sp^2, amide} - CH_2 - CH_2 - N_{amide}$ (Orozco <i>et al.</i> , 2012)								
816.65	2509.94	9.01	-3609	-54.51	286.01	-104.22	-133.18	279.1
$CH_2 - CH_2 - N_{amide} - C_{sp^2, amide}$ (Orozco <i>et al.</i> , 2012)								
189.01	979.05	1482.82	-1436.8	-1465.1	-1219.3	913.04	541.13	16.99
A0	A1	A2	A3	A4	A5	A6	A7	A8

Table 12. Applied charges for tertiary amides

	Charge	Ref.
N _{amide}	-0.46	(Jorgensen and Swenson, 1985)
CH ₂ (-N)	0.275	(Jorgensen and Swenson, 1985)
CH ₃ (-N)	0.275	(Jorgensen and Swenson, 1985)
O _{sp2, amide}	-0.45	(Ferrando <i>et al.</i> , 2010)
C _{sp2, amide}	0.45	(Ferrando <i>et al.</i> , 2010)

6.2. Validation of the added parameters

The density of IR3535 was measured over a range of temperatures. The validity of the tertiary amide parameters for IR3535 were checked by comparing calculated densities with experimentally measured ones. The details of the procedure that was used and the parameters that were applied are described in the flowchart presented in Appendix F. The measured densities of IR3535 at various temperatures are presented in Appendix G. As shown in Figure 21, there is reasonably good agreement between the measured and calculated densities.

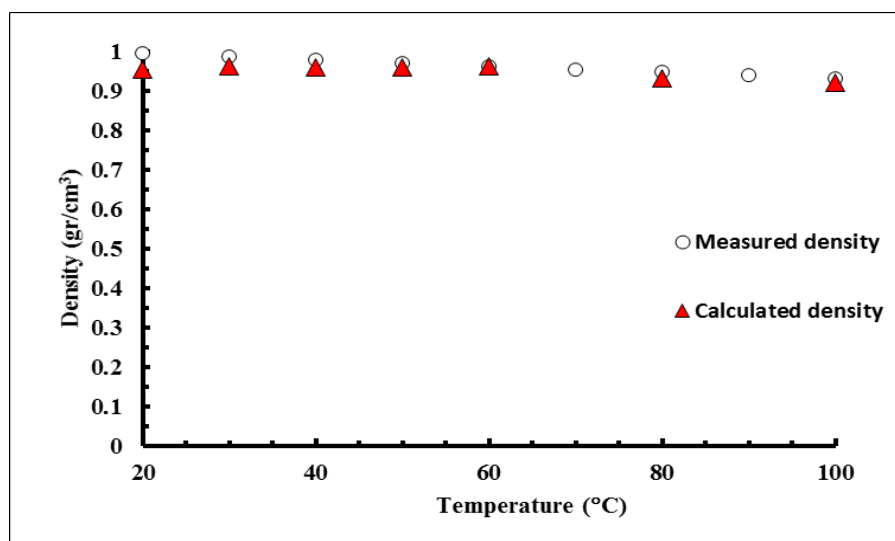


Figure 21. Comparing the measured (○) densities of IR3535 with values (▲) calculated using the AUA model

In addition, the validity of the modified AUA force field parameters were also checked against data for another tertiary amide, i.e. N,N-dimethylacetamide. Calculated results were compared with density data and experimental the radial distribution functions (RDF) determined over a range of temperatures. The correspondence between these data were acceptable. See Appendix H and Appendix I for more detail.

6.3. Ensemble

MC simulations are performed by MedeA[®]-GIBBS in the isothermal–isobaric ensemble (NPT). All simulations were performed using MedeA[®] software (MedeA[®]).

Throughout the simulations, the number of molecules, the temperature and the pressure kept constant at 250, 323 K and 1 bar respectively. However, the density of the system was allowed to vary. Both the nonanoic acid and IR3535 were treated as semi-flexible molecules.

The move probabilities that were implemented, took into account the type of ensemble (NPT) and the semi-flexible nature of the molecules. The simulations runs were performed in two stages. In the first stage the density was equilibrated. The details of this stage are presented in Figure 22. The second stage involved production runs during which the ensemble properties were calculated. The details of the production runs are presented in Figure 23. The molecular simulation flowchart is presented in Appendix J.

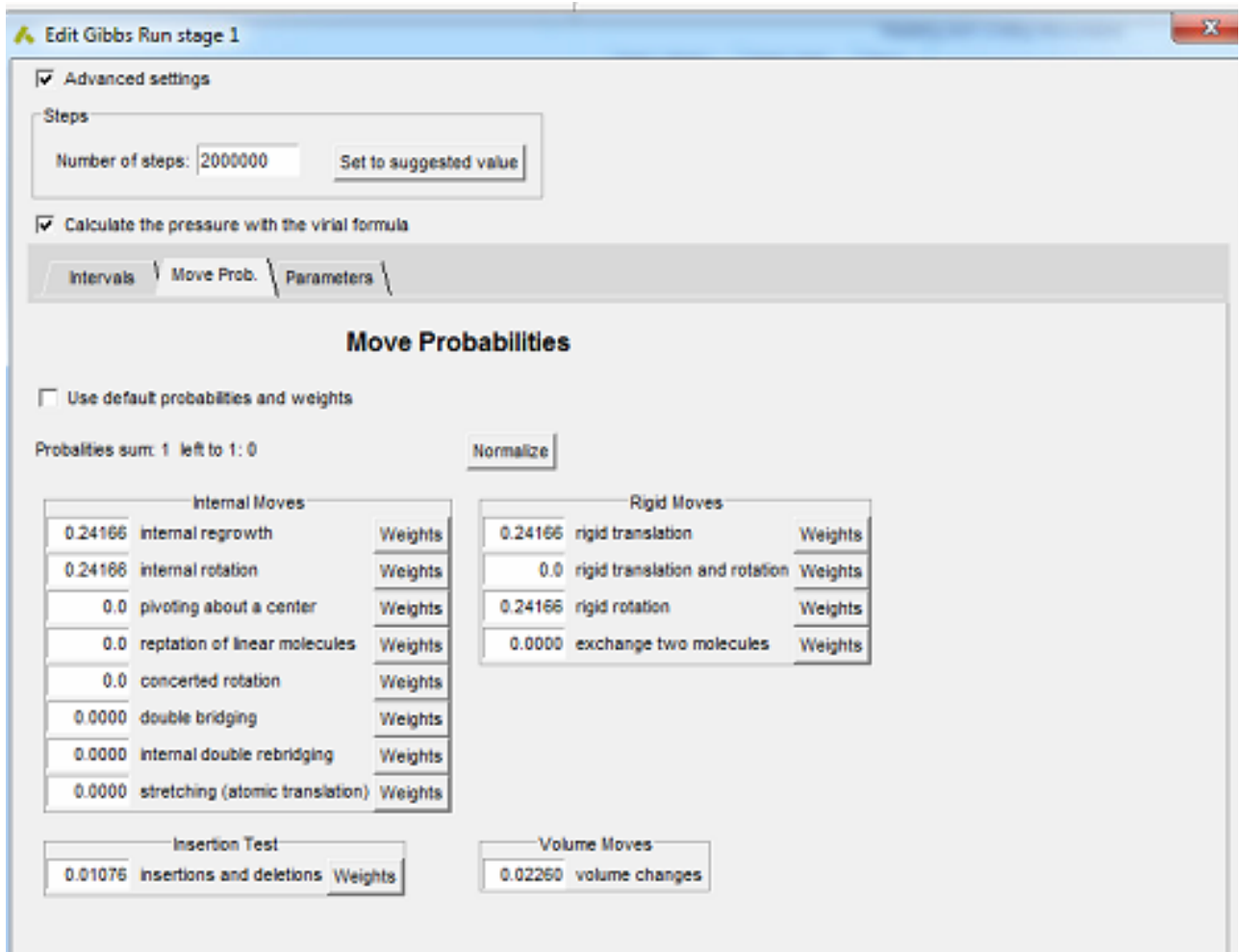


Figure 22. Adopted move attempts for internal and rigid moves, Insertion test and volume moves in the first stage run to equilibrate the density

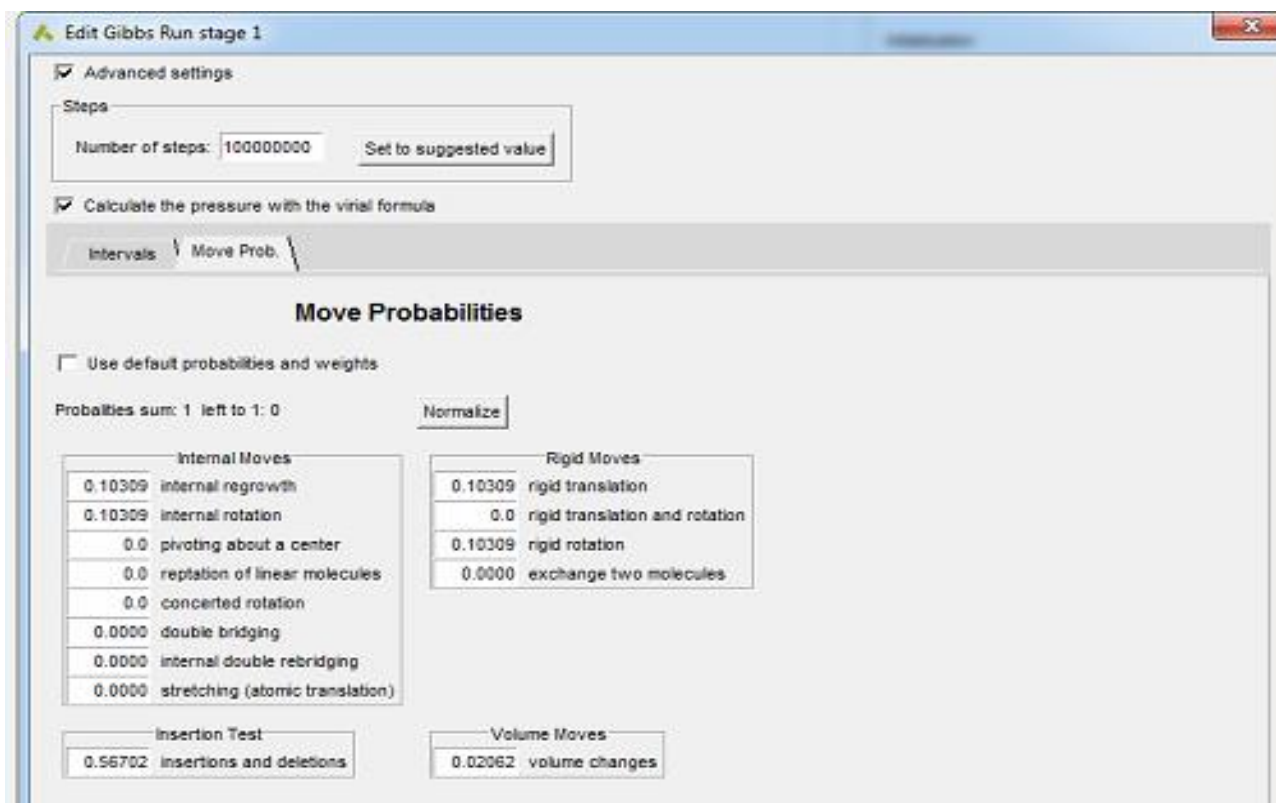


Figure 23. Adopted move attempts for internal and rigid moves, Insertion test and volume moves

In the production run

6.4. Radial distribution functions

6.4.1. Nonanoic acid

Several investigators studied the structure of carboxylic acids in the liquid state (Soffientini *et al.*, 2015, Lajovic *et al.*, 2012). The strong peak at 1.8 Å in the RDF of the pair carbonyl oxygen in nonanoic acid is attributed to hydrogen bond formation (Lajovic *et al.*, 2012). The formation of strong hydrogen bonded cyclic dimers is indicated by the expected orientation of the molecules in conjunction with the position of the other peaks (Lajovic *et al.*, 2012). The impact of the strong hydrogen bond is also reflected by the observation that the RDFs do not return to their average value of unity before a distance of ca. 10 Å (Lajovic *et al.*, 2012). Figure 25 shows the configuration of a dimer ring, which is the predominant configuration in pure nonanoic acid.

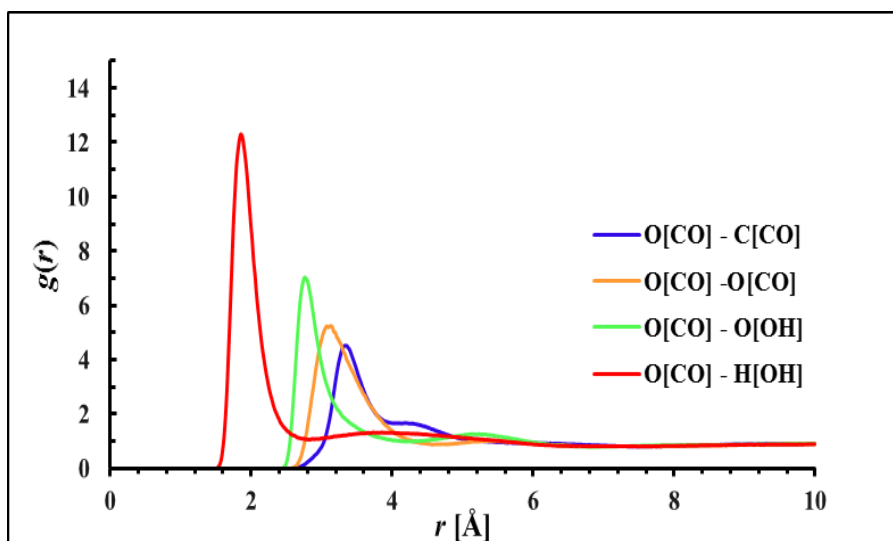


Figure 24. Partial radial distribution functions of the carbonyl oxygen atom in the nonanoic acid molecule

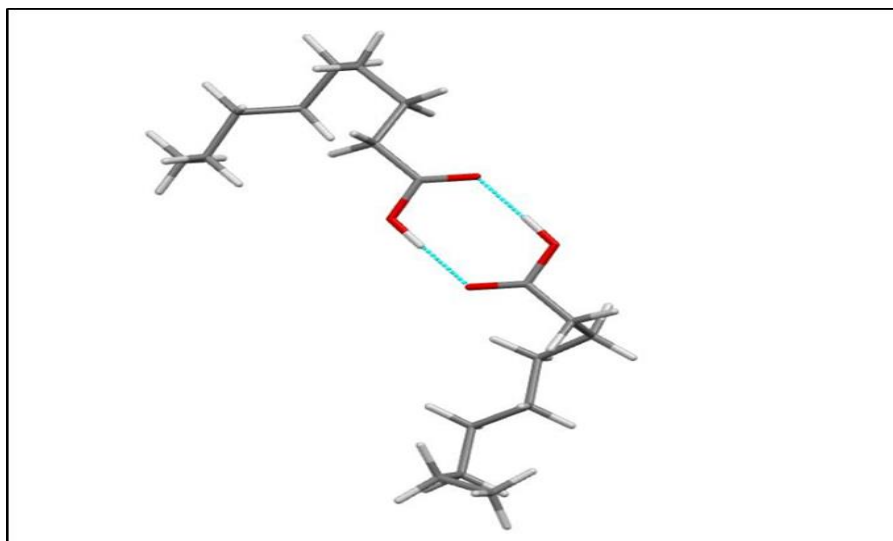


Figure 25. Snapshot of dimer ring configuration in nonanoic acid at P = 1 atm, T = 323 K. The short contacts are shown with dash blue lines

Partial radial distribution of H-O(OH) presented in Figure 24 reveals another interesting aspect of the hydrogen bonding in nonanoic acid. Although there are two oxygen atoms capable of forming hydrogen bonds in the nonanoic acid molecule (Xu and Yang, 2010), only the carbonyl oxygen is involved.

Deconvolution of the radial distribution function involving hydroxyl hydrogen and hydroxyl oxygen discloses three distinct peaks at around 3.3 Å, 3.9 Å and 4.6 Å. The first peak corresponds to the cyclic dimer while the second peak is attributed to the presence of higher order aggregates in the liquid (Xu and Yang, 2010).

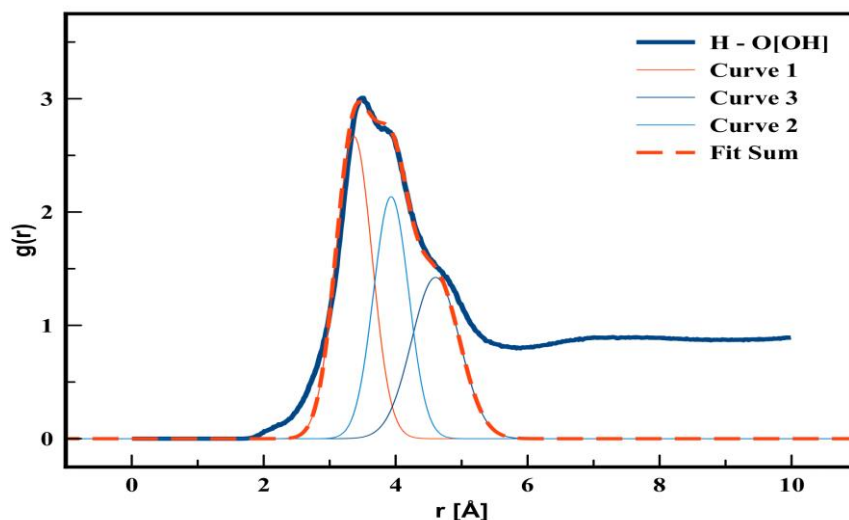


Figure 26. Deconvolution of the peak related to H(OH)-O(OH) in partial radial distribution function of nonanoic acid as calculated presently

6.4.2. IR3535

The presence of two different polar functional groups, i.e. an amide and an ester, in the chemical structure of IR3535 facilitates several complicated intramolecular as well as intermolecular interactions.

There are four possible hydrogen bonds that can form in IR3535: 1) a carbonyl oxygen of ester group and an aliphatic hydrogen, 2) a carbonyl oxygen of amide group and an aliphatic hydrogen, 3) a sp³ oxygen of ester group and an aliphatic hydrogen 4) a nitrogen and an aliphatic hydrogen. All these interactions can be either intra- or intermolecular. These multiple possibilities complicate the interpretation of the interactions in pure IR3535.

The partial radial distribution functions involving the methyl groups (and not other aliphatic carbons) and the hydrogen bond acceptors, either oxygens or nitrogen, in IR3535 are presented in Figure 27. Other plots, showing the correlation between hydrogen acceptors and donor, are not shown here in order to keep the number of graphical representations under the control.

Note that in this study the united atom approach was used. In this approach hydrogens are not considered explicitly in the course of the simulation. However, if required, their positions can be reconstructed from the positions of carbons. This is the reason why typical geometric criteria for characterizing hydrogen bonds, based on bond lengths and angles, would not apply.

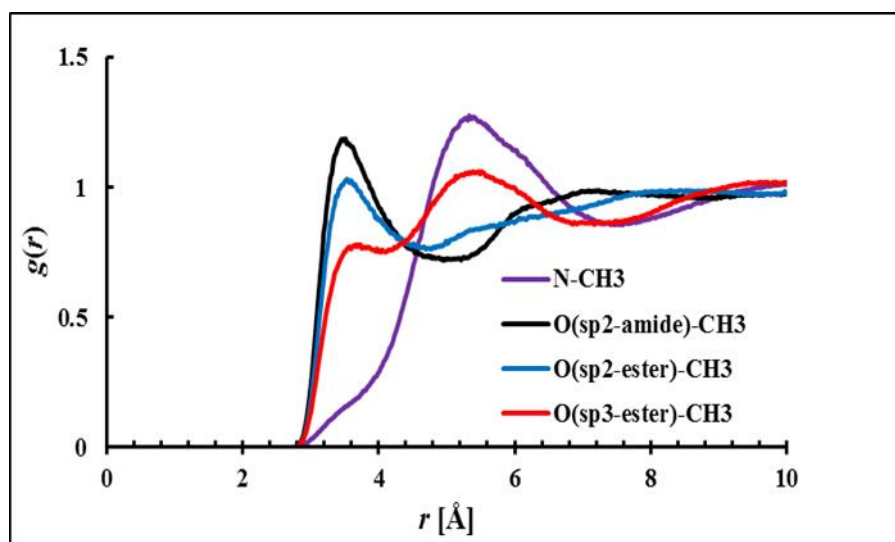


Figure 27. Partial radial distribution functions of either nitrogen or oxygen with methyl groups in IR3535

The presence of the two peaks in the O(sp³-ester)-CH₃ correlation is a clear indication of two different type of interaction between the mentioned groups (Cordeiro, 1997).

From Figure 27, it is clear that there is a weak correlation between all the acceptors with a portion of them hydrogen bonded to methyl groups. This specific type of hydrogen bonding interaction, which occur between strong acceptors and C–H, is known as “soft hydrogen bonding” (Park *et al.*, 2009). Although the soft hydrogen bond is considered to be a very weak intermolecular interaction, it plays a role in the fields of the supramolecular chemistry and macromolecules (Park *et al.*, 2009). Soft hydrogen bonding and other intermolecular nonbonding interactions, resulting from electrostatic or dipole/dipole interactions, lead to the clustering of IR3535 molecules. This is indicated by the snapshot of IR3535 aggregation is shown in Figure 28. The snapshot and the short contacts represented in Figure 28 provide a clear picture of the non-random distribution of IR3535. The short contacts are shown in dash

blue line. Noteworthy are the numerous short contacts defined by all intermolecular contacts shorter than the sum of the van der Waals Radii of the atoms involved.

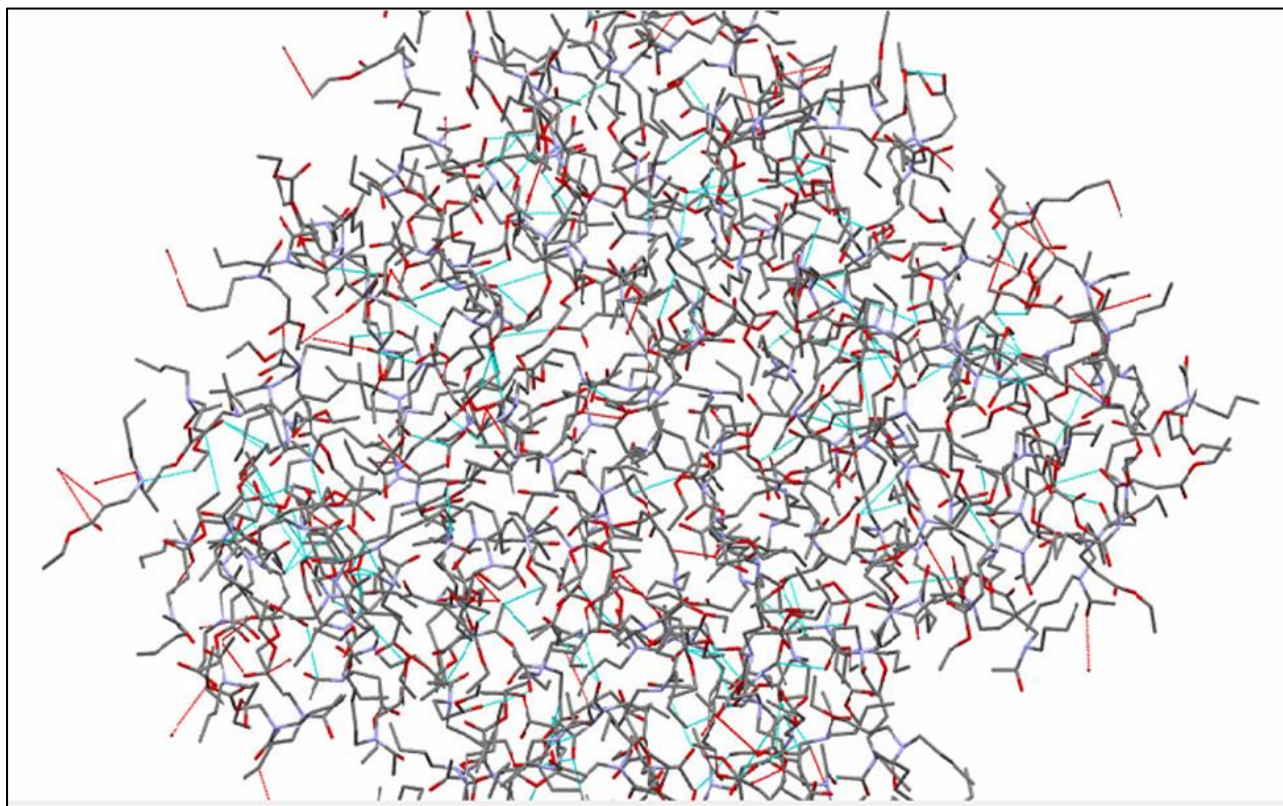


Figure 28. Snapshot of IR3535 aggregation in IR3535 at P = 1 atm, T = 323 K. IR3535 molecules are shown by red, blue, and grey lines for oxygen, nitrogen and carbon atoms, respectively. The short contacts are shown with dashed blue lines

Two typical molecular aggregates, in the pure form of IR3535, are presented in Figure 29. Typically, the IR3535 molecules aggregate as triplets.

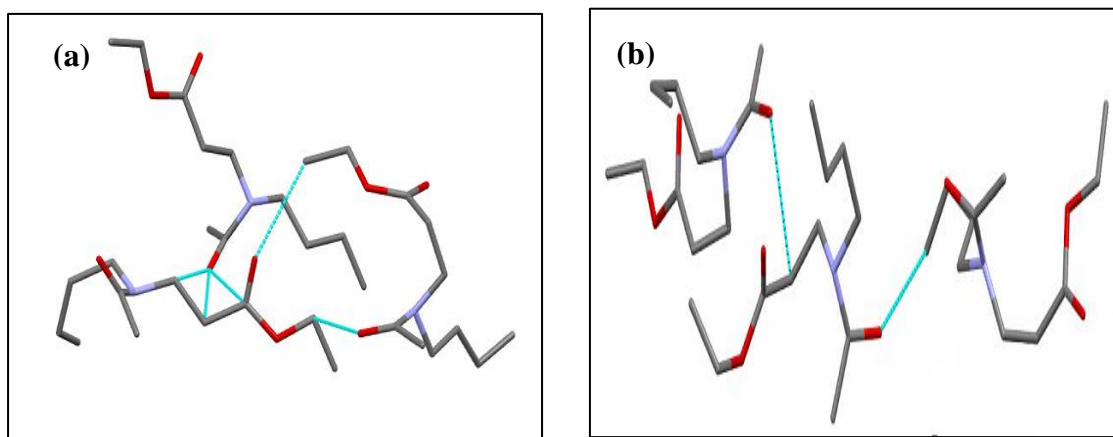


Figure 29. Two typical aggregations of IR3535 molecules. Red, blue, and grey lines represent oxygen, nitrogen and carbon atoms, respectively. The short contacts are shown with dash blue lines.

6.4.3. Mixtures

As described in sections 6.4.1 and 6.4.2, both nonanoic acid and IR3535 are strongly structured liquids in their pure form. Adding nonanoic acid to IR3535 brings about a rearrangement in the structure of both compounds due to formation of unlike intermolecular interactions. The modelling data indicates that the structuring of the liquid mixtures depends on the relative concentrations of the two components. The TGA and oven test data are consistent with weak structuring of the IR3535 components at high acid concentrations whereas enhanced structuring occurs at low acid concentrations.

The partial radial distribution functions involving the hydroxyl hydrogen and the carbonyl oxygen of nonanoic acid in a series of mixtures with various concentration are presented in Figure 30. The strong peak at 1.8 Å is taken as the sign of hydrogen bonding involving the hydroxyl hydrogen and the carbonyl oxygen (Lajovic *et al.*, 2012). Therefore, Figure 30 indicates that up to 70 mol%, the addition of IR3535 does not lead to a significant breakup of the hydrogen bonds between the acid molecules. However higher additions of IR3535 do not lead to such a breakup. This is supported by the invariant peak height in the concentration range 0 to 70 mol% IR3535, followed by a sudden decrease beyond this level.

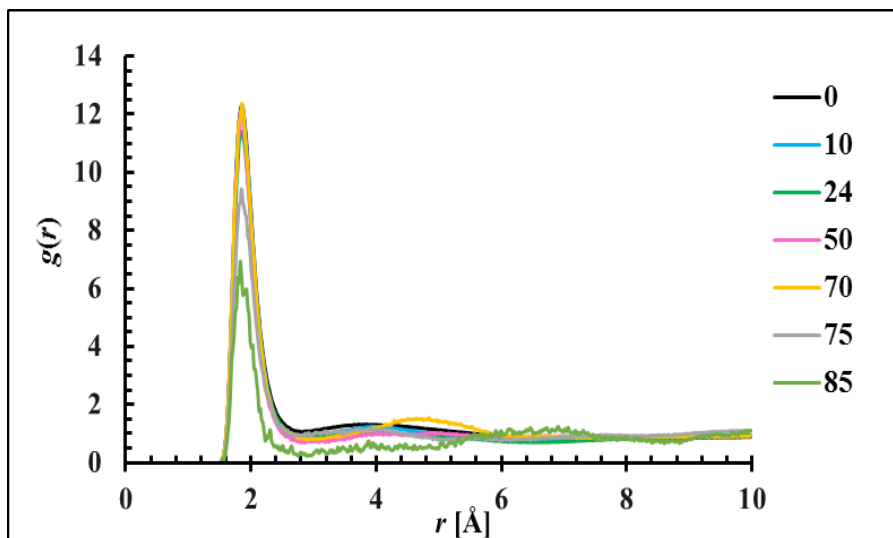


Figure 30. Partial radial distribution functions H(OH) - O(CO) in the nonanoic acid molecule at various concentrations of IR3535. The indicated concentrations refer to the IR3535 content of the liquid phase.

The radial distribution function involving the hydroxyl hydrogen and the hydroxyl oxygen is presented in Figure 31. As mentioned before, there is no indication that hydrogen bonds form between the hydrogen hydroxyl and the oxygen hydroxyl. This is attributed to preferential involvement of hydroxyl hydrogen in the hydrogen bonding with carbonyl oxygen. The presence of peaks around 3.3 Å and 3.9 Å is attributed to the cyclic dimers and larger aggregates (Xu and Yang, 2010). Figure 31 suggest that most nonanoic acid molecules stay in the form of dimers up to a loading of 50 mol% of IR3535. Adding more IR3535 leads to a dissociation of the cyclic dimers. Near and above 75 mol% IR3535, i.e. close to the negative pseudo-azeotrope composition, higher order aggregates predominate. This is indicated by the dominance of the peak located at 3.9 Å.

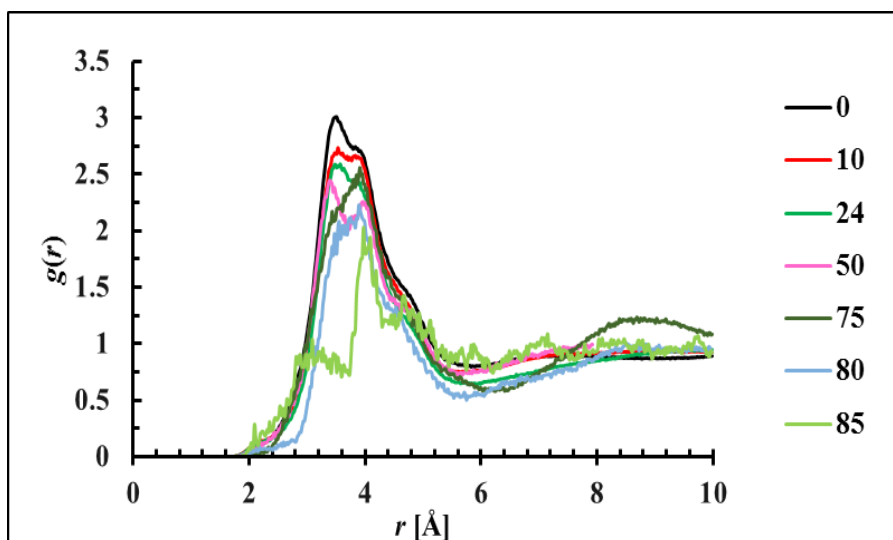


Figure 31. Partial radial distribution functions H(OH) - O(OH) in the nonanoic acid molecule at various concentrations of IR3535. The indicated concentrations refer to the IR3535 content of the liquid phase.

Additional support for this assertion is provided by considering the radial distribution functions involving the carbonyl carbon and the carbonyl oxygen of nonanoic acid at various concentration of IR3535. See Figure 32. The two peaks in the graphs are attributed to the dimer and larger aggregates. It is clear from Figure 32 that increasing the IR3535 up to 70% decreases both peaks slowly. However, at 75 mol% IR3535, the height of peak corresponding to larger aggregates (peak located at 4.5 Å), increases in intensity. This suggests that the acid molecules are forming bulkier aggregates.

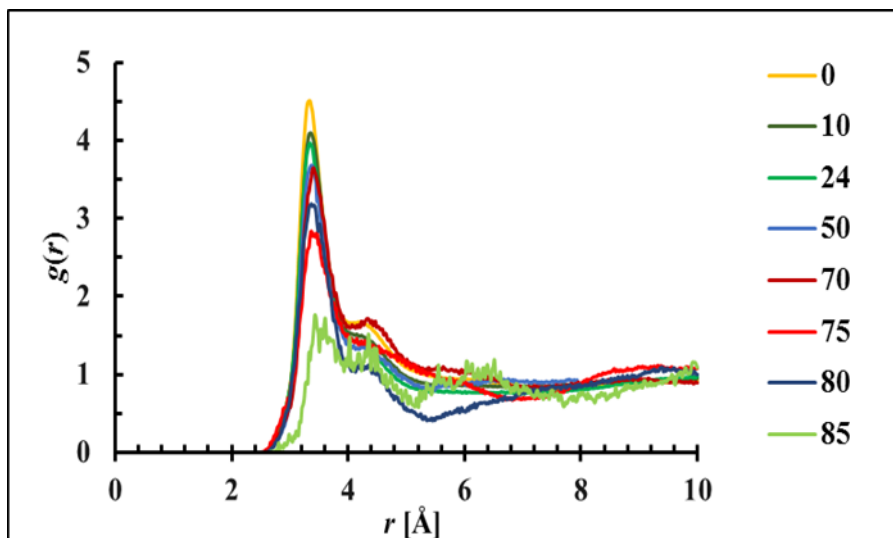


Figure 32. Partial radial distribution functions C(CO) - O(CO) in the nonanoic acid molecule at various concentrations of IR3535. The indicated concentrations refer to the IR3535 content of the liquid phase.

Dimerization is also indicated by a strong correlation between the carbonyl oxygens as it indicates carboxylic-carboxylic interactions (McCabe *et al.*, Vahid and Elliott, 2010). The radial distribution functions involving the carbonyl oxygens of nonanoic acid are shown in Figure 33. It is clear that increasing the molar concentration to 85 mol% IR3535 has resulted in a sudden shift of the peak to greater distances and also the emergence of a new peak. These observations support the notion that, at higher concentrations of IR3535, the dimers aggregate into higher order clusters.

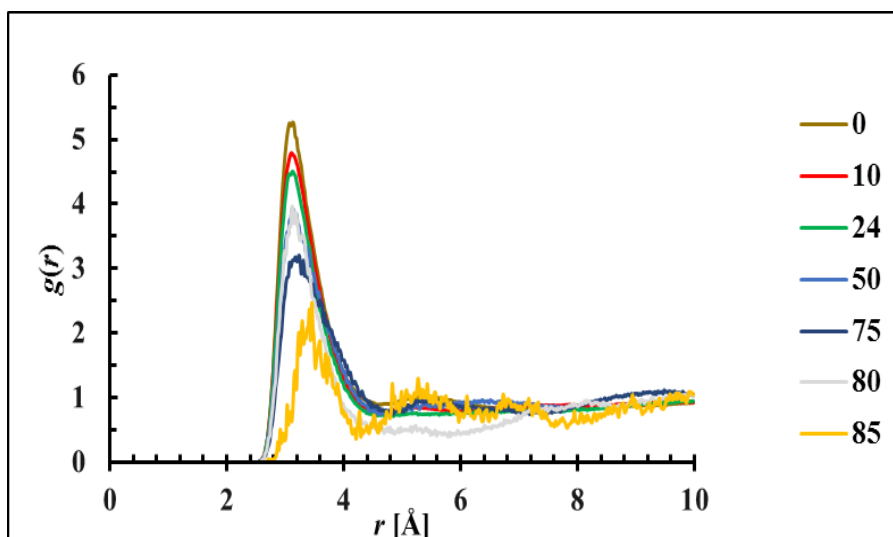


Figure 33. Partial radial distribution functions O(CO) - O(CO) in the nonanoic acid molecule at various concentrations of IR3535. The indicated concentrations refer to the IR3535 content of the liquid phase.

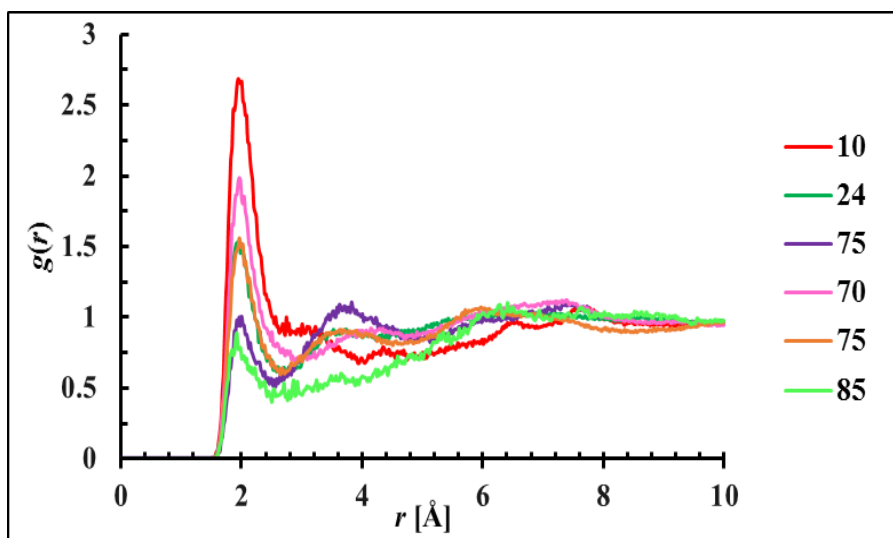


Figure 34. Partial radial distribution functions of H(OH) - O(sp²-ester) at various concentrations of IR3535. The indicated concentrations refer to the IR3535 content of the liquid phase.

Figure 34 shows the partial radial distribution functions for the hydroxyl hydrogen and the carbonyl oxygen of the ester group. The peak around 2 Å indicates the formation of a hydrogen bond between the hydroxyl hydrogen of the acid and the carbonyl oxygen of the ester group in IR3535. It is clear that at low concentrations of IR3535 the hydroxyl hydrogen forms hydrogen bonds with the ester carbonyl. This interaction weakens on adding IR3535 up to 50 mol%. After that the strength increases up to 70 mol% IR3535 before it decreases again.

The radial distribution functions for the carbonyl carbon in the acid and the carbonyl oxygen in the ester group is shown in Figure 35. The graphs show that the correlation between the ester and acid functional group is at its maximum around the positive pseudo-azeotrope composition and is effectively absent around the negative pseudo-azeotrope.

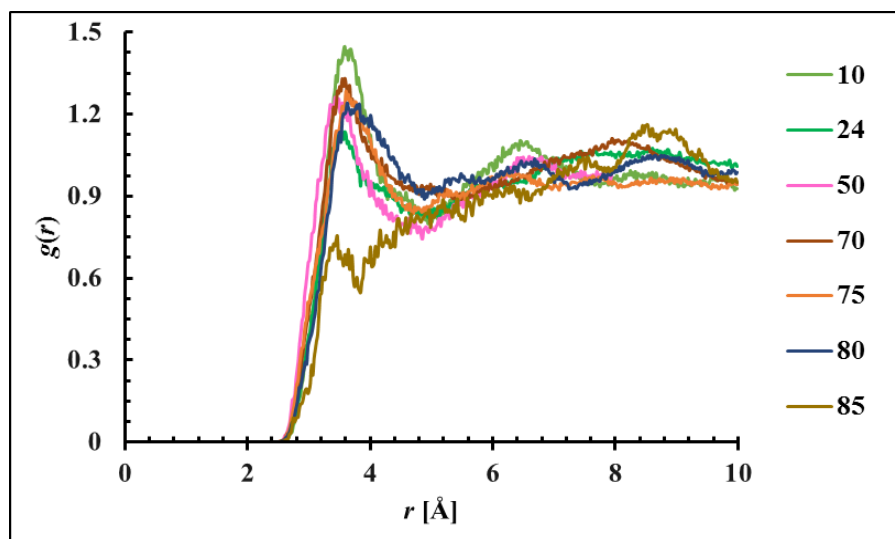


Figure 35. Partial radial distribution functions involving C(CO-acid) - O(sp²-ester) at various concentrations of IR3535. The indicated concentrations refer to the IR3535 content of the liquid phase

The sp³ oxygen in the ester group is also a possible site of hydrogen bond formation. The radial distribution functions involve the hydroxyl hydrogen in the acid and the sp³ oxygen of ester in IR3535 is shown in Figure 36. It appears that the sp³ hydrogen bonding is insignificant up to 80 mol% IR3535. However, some hydrogen bonding may be present beyond this concentration as evidenced by the emergence of a peak at 2 Å.

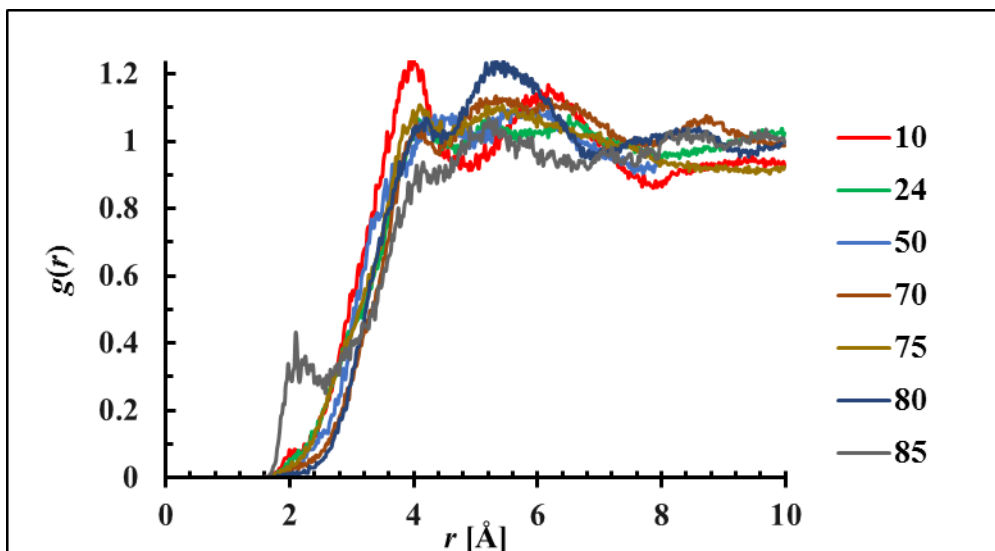


Figure 36. Partial radial distribution functions H (OH) - O(sp³-ester) at various concentrations of IR3535. The indicated concentrations refer to the IR3535 content of the liquid phase.

The snapshots generated by Medea[®] indicates that at high concentration of IR3535, most of the nonanoic acid molecules interact with the IR3535 present, aggregating to form larger clusters. A snapshot of IR3535-nonanoic acid aggregation at the molar ratio of 3:1 is shown in Figure 37. The formation of larger aggregates is likely to significantly reduce the volatility of the IR3535-nonanoic acid binary mixtures.

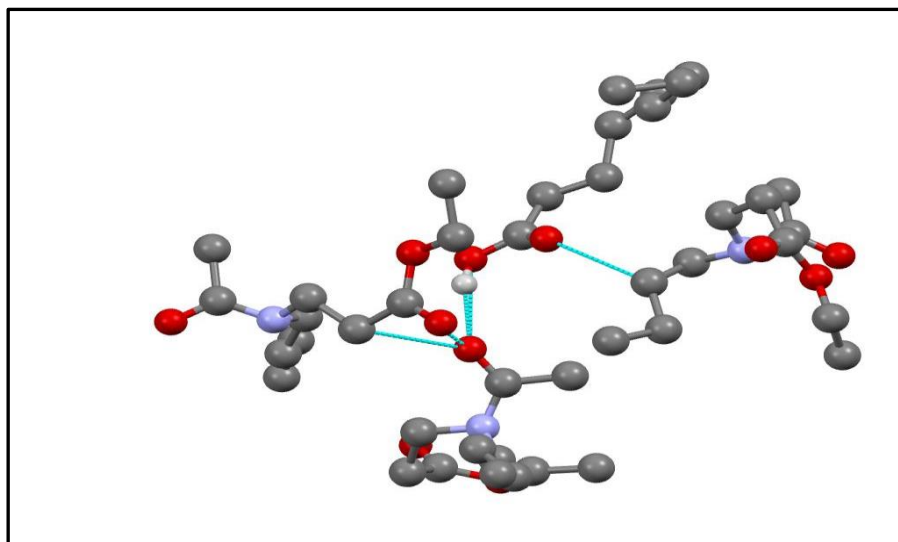


Figure 37. Snapshot of IR3535-nonanoic acid (3:1) aggregation at $P = 1$ atm, $T = 323$ K. Red, blue, and grey spheres represent oxygen, nitrogen and carbon atoms, respectively. The short contacts are shown with dash blue lines

Figure 38 shows the partial radial distribution functions for the hydroxyl hydrogen in nonanoic acid and the carbonyl oxygen of the amide group in IR3535. The considerable intensity and invariance of the peak indicates a very high propensity for hydrogen bond formation between the amide group and the hydroxyl hydrogen. This peak is much more pronounced than the peaks for any other group. The peak maximum is reached at ca. 75 mol% IR3535, i.e. near the negative pseudo-azeotrope composition.

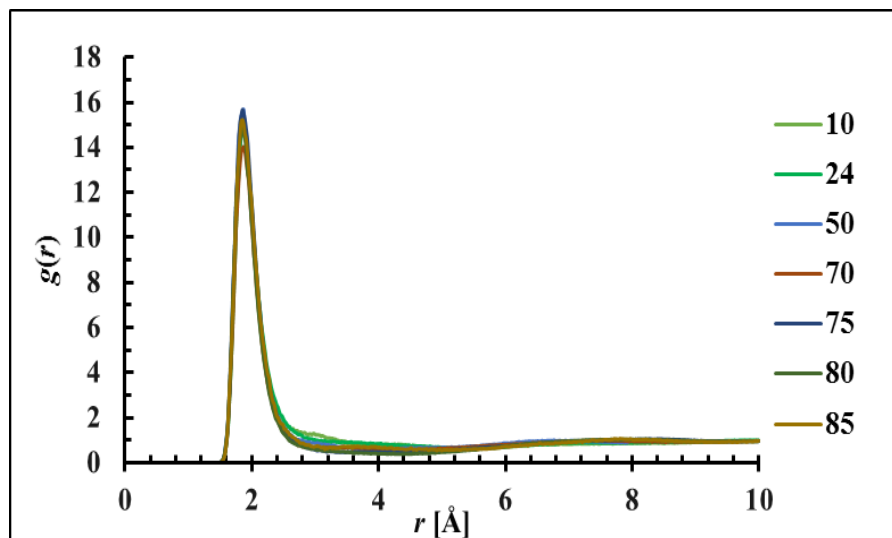


Figure 38. Partial radial distribution functions H(OH) - O(sp²-amide) at various concentrations of IR3535. The indicated concentrations refer to the IR3535 content of the liquid phase

Figure 39 shows the correlation between the nitrogen atoms of IR3535 in a series of mixtures. The structure between the IR3535 molecules only breaks at very high concentration of acid molecules and a new structure starts to form. This is reflected by the disappearance of the peak at 6.5 Å and the development of a new peak at 7.6 Å. This suggests that IR3535 molecules tend to become separated from each other. This can be seen in Figure 40 where the distance between the ester carbonyl oxygen and nitrogen increases with increasing acid content. This is more clearly shown in Figure 41 where an increase in the distance between ester and amide functional group is evident. The loss of aggregation between IR3535 molecules in the presence of larger amounts of nonanoic acid, is probably the causing the enhanced volatility of the positive pseudo-azeotrope IR3535-nonanoic acid binary mixture.

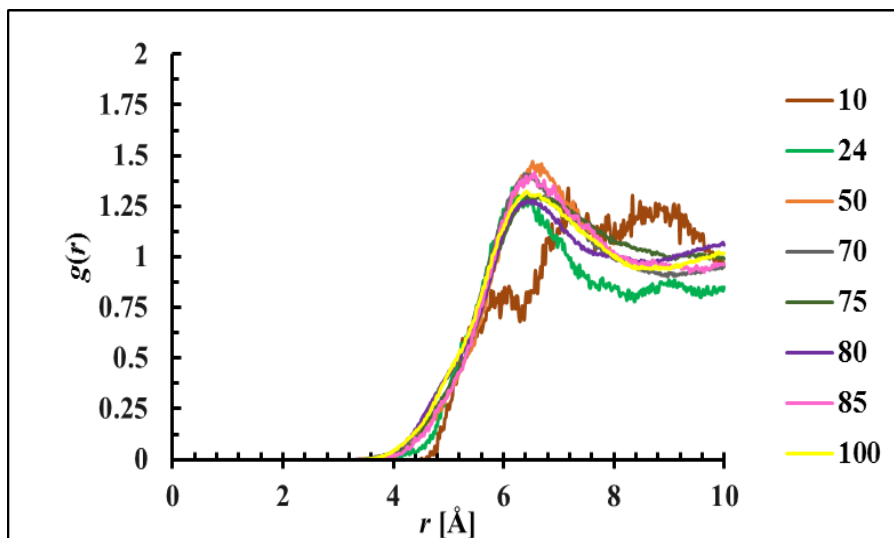


Figure 39. Partial radial distribution functions for nitrogen at various concentrations of IR3535. The indicated concentrations refer to the IR3535 content of the liquid phase

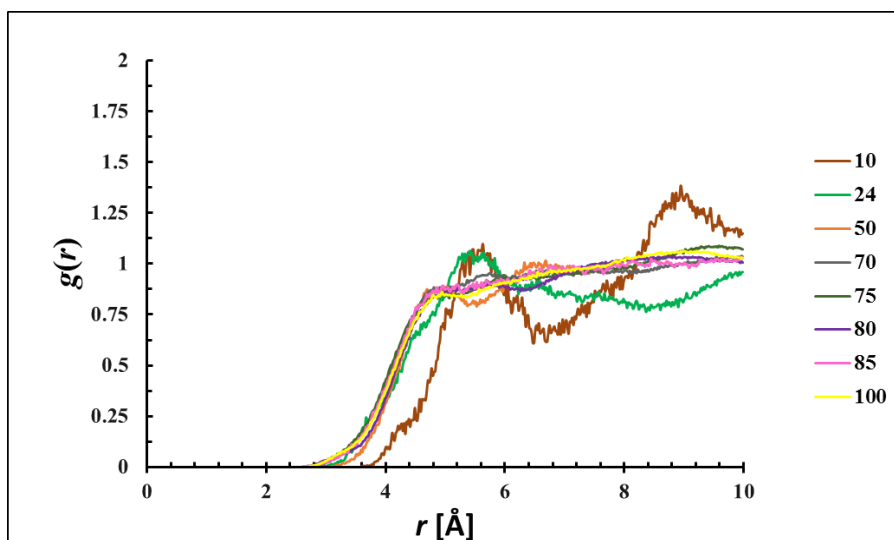


Figure 40. Partial radial distribution functions O(sp²-ester) - N at various concentrations of IR3535. The indicated concentrations refer to the IR3535 content of the liquid phase

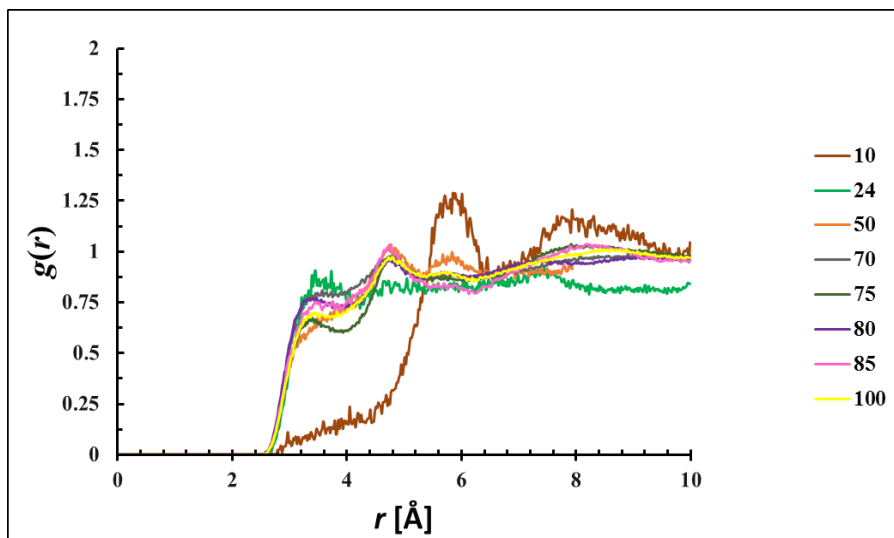


Figure 41. Partial radial distribution functions O(sp²-amide) - O(sp³-ester) at various concentrations of IR3535. The indicated concentrations refer to the IR3535 content of the liquid phase

Chapter 7

CONCLUSIONS

7. Conclusion

In this study, a novel approach to control the release rate of mosquito repellents was developed. The rationale behind the approach was to select a negative pseudo-azeotrope mixture of repellents in order to get a constant, reduced release rate.

The role of molecular interaction in the formation of pseudo-azeotrope mixture was investigated. The correlation between the possibility of azeotrope formation and intermolecular interactions revealed that hydrogen bonding has a pronounced impact on formation of azeotrope mixtures. Thus, hydrogen bonding was selected as the key means in the design of pseudo-azeotrope mixtures. General repellents were classified based on their chemical structure. Structural studies of known repellents revealed they generally have the ability to engage in hydrogen bonding, and thus they can potentially form pseudo-azeotrope mixtures in presence of appropriate azeotrope formers.

Selecting a suitable pair of repellents containing hydrogen bond donors and acceptors increases the likelihood of strong intermolecular interactions and obtaining the desired negative pseudo-azeotrope mixture.

In the current study, IR3535 and nonanoic acid were selected as model compounds to validate the concept. FTIR, Raman and UV-Vis spectroscopic techniques were applied as rough-and-ready techniques to rapidly determine the hydrogen bonding propensity and to establish whether pseudo-azeotrope formation is possible in the system. FTIR and Raman spectroscopic results revealed that in neat nonanoic acid, dimer rings are the predominant aggregates. Vibrational spectroscopic also indicated that when the molar concentration of nonanoic acid in the mixture exceeds 20 mol%, molecular interactions cause the amide carbonyl bond to become stronger. Formation of a new peak in the FTIR and Raman spectra of the mixtures also confirmed the existence of the intermolecular interactions in the system over a wide range of compositions. UV-Vis spectroscopic results indicated that there are at least two strong interactions with the maximum strength at the composition of 15 mol% IR3535 and 60 mol% IR3535.

Oven tests confirmed pseudo-azeotrope formation. This method is based on time-dependent measurements of the residual mass and FTIR spectra of the evaporating mixture. An inverse analysis approach was used to determine the composition of the evaporating mixture from the recorded FTIR spectra. The oven test confirmed that IR3535 and nonanoic acid form a negative pseudo-azeotrope at approximately 75 mol% IR3535 and a positive pseudo-azeotrope at ca. 10 mol% IR3535.

TGA and DSC results confirmed the existence of both pseudo-azeotropes. TGA results also illustrated that the evaporation profile of the negative pseudo-azeotrope mixture of IR3535-nonanoic acid mixture is significantly lower than that of the neat components.

A modified arm-in-cage test was used to evaluate the mosquito repellence properties of the controlled-release repellent formulation i.e. negative pseudo-azeotrope system of IR3535 and nonanoic acid. This bioassay test revealed that the repellence of the negative pseudo-azeotrope mixture was better than that achieved with the reference repellents DEET and IR3535. The improvement extended to both efficacy and persistence. Moreover, the negative pseudo-azeotrope formulation also had a knock down effect on the mosquitoes. Most mosquitoes even died during testing.

Molecular simulation techniques were applied to study the nature of the pseudo-azeotrope mixtures. Gibbs-Monte Carlo simulation results revealed that the rare phenomenon, of the presence of a double pseudo-azeotropes, could be due to composition-dependent reorganisation of molecular clusters.

The positive pseudo-azeotrope, at 10 mol% IR3535 was attributed to the breakdown of the IR3535 structures. The lower degree of molecular aggregation increases the freedom of IR3535 molecules allowing them to readily escape from the liquid phase and hence the mixture evaporates faster. On the other side, the negative azeotrope probably results from more extensive molecular clustering at 75 mol% IR3535. The larger sized aggregates present decreases the propensity to vaporise.

8. References

- MedeA®-GIBBS version 2.1, using Gibbs 9.5.6, IFP Energies Nouvelles, Rueil-Malmaison & Laboratoire de Chimie-Physique, Université Paris Sud, CNRS, France
- Abou-Donia, M. B., Goldstein, L. B., Jones, K. H., Abdel-Rahman, A. A., Damodaran, T. V., Dechkovskaia, A. M., Bullman, S. L., Amir, B. E. & Khan, W. A. 2001. Locomotor and sensorimotor performance deficit in rats following exposure to pyridostigmine bromide, DEET, and permethrin, alone and in combination. *Toxicological Sciences*, 60, 305-314.
- Akhtar, M. U. 2014. *Towards controlled release of a natural mosquito repellent from polymer matrices*. University of Pretoria.
- Akhtar, Y. & Isman, M. B. 2013. Plant natural products for pest management: the magic of mixtures. *Advanced technologies for managing insect pests*. Springer.
- Al-Jiboury, K. F. C. 2007. Correlation for fitting multicomponent vapor-liquid equilibria data and prediction of azeotropic behavior *Al-Khwarizmi Engineering Journal*, 3, 67-86.
- Alan R. Katritzky, J. M. L., J. A. T. Beard 1960. The Infrared Spectra of Esters. 1. Methyl, Ethyl, n- and i-Propyl, and n-, i- and s-Butyl Esters. *Spectrochimica Acta*, 16.
- Alex, S., Thanh, H. L. & Vocelle, D. 1992. Studies of the effect of hydrogen bonding on the absorption and fluorescence spectra of all-trans-retinal at room temperature. *Canadian Journal of Chemistry*, 70, 880-887.
- Allen, G. & Caldin, E. F. 1953. The association of carboxylic acids. *Quarterly Reviews, Chemical Society*, 7, 255-278.
- Anderson, C. E., Pickrell, A. J., Sperry, S. L., Vasquez Jr, T. E., Custer, T. G., Fierman, M. B., Lazar, D. C., Brown, Z. W., Iskenderian, W. S. & Hickstein, D. D. 2007. NMR detection of intramolecular OH/OH hydrogen bond networks: an approach using isotopic perturbation and hydrogen bond mediated OH... OH J-coupling. *Heterocycles*, 72, 469-495.
- Andrade-Garda, J. M. 2009. 4. Partial Least-Squares Regression. *Basic Chemometric Techniques in Atomic Spectroscopy*. Royal Society of Chemistry.
- Aparicio-Martínez, S. & Balbuena, P. B. 2007. On the properties of aqueous amide solutions through classical molecular dynamics simulations. *Molecular Simulation*, 33, 925-938.
- Apurba, K. B. & Raj, K. G. 2006. Discovery and Design of New Arthropod/Insect Repellents by Computer-Aided Molecular Modeling. *Insect Repellents*. CRC Press.

- Asaadi, E., Wilke, D. N., Heyns, P. S. & Kok, S. 2016. The use of direct inverse maps to solve material identification problems: pitfalls and solutions. *Structural and Multidisciplinary Optimization*, 1-20.
- Baba, H. & Suzuki, S. 1961. Electronic Spectra and Hydrogen Bonding. I. Phenol and Naphthols. *The Journal of Chemical Physics*, 35, 1118-1127.
- Barontini, F., Brunazzi, E. & Cozzani, V. 2002. A novel methodology for the identification of azeotropic binary mixtures by TG-FTIR techniques. *Thermochimica Acta*, 389, 95-108.
- Bell, J. W., Veltri, J. C. & Page, B. C. 2002. Human exposures to N,N-diethyl-m-toluamide insect repellents reported to the American Association of Poison Control Centers 1993-1997. *International Journal of Toxicology*, 21, 341-352.
- Bellamy, L. J., Lake, R. F. & Pace, R. J. 1963. Hydrogen bonding in carboxylic acids—II. Monocarboxylic acids. *Spectrochimica Acta*, 19, 443-449.
- Bershtein, V. A. & Egorov, V. M. 1994. *Differential scanning calorimetry of polymers: physics, chemistry, analysis, technology*, Prentice Hall.
- Bhattacharjee, A. K., Gupta, R. K., Ma, D. & Karle, J. M. 2000. Molecular similarity analysis between insect juvenile hormone and N, N-diethyl-m-toluamide (DEET) analogs may aid design of novel insect repellents. *J Mol Recognit*, 13, 213-20.
- Boeckh, J., Breer, H., Geier, M., Hoever, F. P., Kruger, B. W., Nentwig, G. & Sass, H. 1996. Acylated 1,3-aminopropanols as repellents against bloodsucking arthropods. *Pesticide Science*, 48, 359-373.
- Bohbot, J. D. & Dickens, J. C. 2010. Insect Repellents: Modulators of Mosquito Odorant Receptor Activity. *PLoS ONE*, 5, e12138.
- Bond, A. D. 2003. In situ co-crystallisation as a tool for low-temperature crystal engineering. *Chemical Communications*, 250-251.
- Bondesson, L., Mikkelsen, K. V., Luo, Y., Garberg, P. & Ågren, H. 2007. Hydrogen bonding effects on infrared and Raman spectra of drug molecules. *Spectrochimica Acta Part A: Molecular and Biomolecular Spectroscopy*, 66, 213-224.
- Bonds, J. A. S. 2012. Ultra-low-volume space sprays in mosquito control: a critical review. *Medical and Veterinary Entomology*, 26, 121-130.
- Bosch, O. J., Geier, M. & Boeckh, J. 2000. Contribution of fatty acids to olfactory host finding of female *Aedes aegypti*. *Chem Senses*, 25, 323-30.
- Boutard, Y., Ungerer, P., Teuler, J. M., Ahunbay, M. G., Sabater, S. F., Pérez-Pellitero, J., Mackie, A. D. & Bourasseau, E. 2005. Extension of the anisotropic united atoms intermolecular potential to amines, amides and alkanols: Application to the problems of the 2004 Fluid Simulation Challenge. *Fluid Phase Equilibria*, 236, 25-41.

- Bratož, S., Hadži, D. & Sheppard, N. 1956. The infra-red absorption bands associated with the COOH and COOD groups in dimeric carboxylic acid—II: The region from 3700 to 1500 cm^{-1} . *Spectrochimica Acta*, 8, 249-261.
- Breil, M. P. & Kontogeorgis, G. M. 2009. Thermodynamics of Triethylene Glycol and Tetraethylene Glycol Containing Systems Described by the Cubic-Plus-Association Equation of State. *Industrial & Engineering Chemistry Research*, 48, 5472-5480.
- Brown, T. L., Regan, J. F., Schuetz, R. D. & Sternberg, J. C. 1959. The Carbonyl Intensities of Some Simple Amides. *The Journal of Physical Chemistry*, 63, 1324-1325.
- Buera, M., Jouppila, K., Roos, Y. & Chirife, J. 1998. Differential scanning calorimetry glass transition temperatures of white bread and mold growth in the putative glassy state. *Cereal chemistry*, 75, 64-69.
- Bukhari, T., Takken, W. & Koenraadt, C. J. M. 2013. Biological tools for control of larval stages of malaria vectors - a review. *Biocontrol Science and Technology*, 23, 987-1023.
- Burgess, I. F. 2000. Dermatopharmacology of Antiparasitics and Insect Repellents. In: GABARD, B., SURBER, C., ELSNER, P. & TREFFEL, P. (eds.) *Dermatopharmacology of Topical Preparations: A Product Development-Oriented Approach*. Berlin, Heidelberg: Springer Berlin Heidelberg.
- Canfield, E. L., Dykstra, T. M., Soma, S. J., Rasmussen, R. E. & Alston, R. P. 2015. Radiating systems for affecting insect behavior. Google Patents.
- Chattopadhyay, P., Dhiman, S., Borah, S., Rabha, B., Chaurasia, A. K. & Veer, V. 2015. Essential oil based polymeric patch development and evaluating its repellent activity against mosquitoes. *Acta Tropica*, 147, 45-53.
- Chattopadhyay, P., Dhiman, S., Devi, K. A., Banerjee, S., Rabha, B., Chaurasia, A. & Veer, V. 2013. Ultra low concentration deltamethrin loaded patch development and evaluation of its repellency against dengue vector *Aedes (S) albopictus*. *Parasites & Vectors*, 6, 1-10.
- Chebaane, A., Hammami, F., Bahri, M. & Nasr, S. 2012. Intramolecular and intermolecular interactions in N-methylformamide–water mixture: X-ray scattering and DFT calculation study. *Journal of Molecular Liquids*, 165, 133-138.
- Chen, K. H., Lii, J. H., Fan, Y. & Allinger, N. L. 2007. Molecular mechanics (MM4) study of amines. *J Comput Chem*, 28, 2391-412.
- Choochote, W., Chaithong, U., Kamsuk, K., Jitpakdi, A., Tippawangkosol, P., Tuetun, B., Champakaew, D. & Pitasawat, B. 2007. Repellent activity of selected essential oils against *Aedes aegypti*. *Fitoterapia*, 78, 359-64.

- Chou, P. T., Martinez, M. L. & Clements, J. H. 1993. Reversal of excitation behavior of proton-transfer vs. charge-transfer by dielectric perturbation of electronic manifolds. *The Journal of Physical Chemistry*, 97, 2618-2622.
- Claxton, G., Benzole, N. & Association, A. P. 1958. *Physical and Azeotropic Data: Hydrocarbons and Sulphur Compounds Boiling Below 2000^oC*, National Benzole and Allied Products Association.
- Coates, J. 2000. Interpretation of infrared spectra, a practical approach. *Encyclopedia of analytical chemistry*.
- Colthup, N. 2012. *Introduction to infrared and Raman spectroscopy*, Elsevier.
- Comunian, T. A., Thomazini, M., Alves, A. J. G., de Matos Junior, F. E., de Carvalho Balieiro, J. C. & Favaro-Trindade, C. S. 2013. Microencapsulation of ascorbic acid by complex coacervation: Protection and controlled release. *Food Research International*, 52, 373-379.
- Conlon, J. 2011. Control of Mosquitoes in the United States. *Outlooks on Pest Management*, 22, 32-37.
- Cornell, W. D., Cieplak, P., Bayly, C. I., Gould, I. R., Merz, K. M., Ferguson, D. M., Spellmeyer, D. C., Fox, T., Caldwell, J. W. & Kollman, P. A. 1995. A Second Generation Force Field for the Simulation of Proteins, Nucleic Acids, and Organic Molecules. *Journal of the American Chemical Society*, 117, 5179-5197.
- Couch, J. N. 1972. Mass Production of Coelomomyces, a Fungus That Kills Mosquitoes. *Proceedings of the National Academy of Sciences*, 69, 2043-2047.
- Curtis, C., Lines, J., Lu, B. & Renz, A. 1990. Natural and synthetic repellents. *Appropriate technology in vector control.*, 75-92.
- Curtis, C. F. 1992. Personal protection methods against vectors of disease. *Review of Medical and Veterinary Entomology* 80, 543-553.
- da Silva, A. M., Ghosh, A. & Chaudhuri, P. 2013. Effect of Hydrogen Bond Formation on the NMR Properties of Glycine–HCN Complexes. *The Journal of Physical Chemistry A*, 117, 10274-10285.
- Dabiré, R. K., Diabaté, A., Baldet, T., Paré-Toé, L., Guiguemdé, R. T., Ouédraogo, J.-B. & Skovmand, O. 2006. Personal protection of long lasting insecticide-treated nets in areas of *Anopheles gambiae* ss resistance to pyrethroids. *Malar J*, 5, 12.
- Davis, E. E. 1976. A receptor sensitive to oviposition site attractants on the antennae of the mosquito, *Aedes aegypti*. *Journal of insect physiology*, 22, 1371-1376.
- Davis, E. E. & Sokolove, P. G. 1976. Lactic acid-sensitive receptors on the antennae of the mosquito, *Aedes aegypti*. *Journal of Comparative Physiology A: Neuroethology, Sensory, Neural, and Behavioral Physiology*, 105, 43-54.

- Debboun, M., Frances, S. P. & Strickman, D. 2006. *Insect repellents: principles, methods, and uses*, CRC Press.
- Debboun, M., Frances, S. P. & Strickman, D. 2014. *Insect repellents : principles, methods, and uses*, Boca Raton :, CRC Press.
- Debboun, M., Frances, S. P. & Strickman, D. 2015. *Insect repellents handbook*.
- Debboun, M., Strickman, D., Klein, T. A., Glass, J. A., Wylie, E., Laughinghouse, A., Wirtz, R. A. & Gupta, R. K. 1999. Laboratory evaluation of AI3-37220, AI3-35765, CIC-4, and deet repellents against three species of mosquitoes. *J Am Mosq Control Assoc*, 15, 342-7.
- Del Bene, J. E., Perera, S. A. & Bartlett, R. J. 1999. Hydrogen Bond Types, Binding Energies, and ¹H NMR Chemical Shifts. *The Journal of Physical Chemistry A*, 103, 8121-8124.
- Deletre, E., Martin, T., Campagne, P., Bourguet, D., Cadin, A., Menut, C., Bonafos, R. & Chandre, F. 2013. Repellent, Irritant and Toxic Effects of 20 Plant Extracts on Adults of the Malaria Vector *Anopheles gambiae* Mosquito. *PLoS ONE*, 8, e82103.
- Denney, R. C. 1982. *A dictionary of spectroscopy*, London, Macmillan.
- Desiraju, G. R. & Steiner, T. 1999. *The weak hydrogen bond : in structural chemistry and biology*, Oxford :, Oxford University Press.
- Dethier, V. G. 1948. Chemical Insect Attractants and Repellents. Philadelphia: The Blakiston Company, 1947. 289 p. *Science Education*, 32, 226-226.
- Dethier, V. G., Browne, B. L. & Smith, C. N. 1960. The Designation of Chemicals in Terms of the Responses They Elicit from Insects. *Journal of Economic Entomology*, 53, 134-136.
- Dickens, J. C. & Bohbot, J. D. 2013. Mini review: Mode of action of mosquito repellents. *Pesticide Biochemistry and Physiology*, 106, 149-155.
- Ditzen, M., Pellegrino, M. & Vosshall, L. B. 2008. Insect odorant receptors are molecular targets of the insect repellent DEET. *Science*, 319, 1838-1842.
- Dogan, E., Ayres, J. & Rossignol, P. 1999. Behavioural mode of action of deet: inhibition of lactic acid attraction. *Medical and veterinary entomology*, 13, 97-100.
- Dollish, F. R., Fateley, W. G. & Bentley, F. F. 1974. *Characteristic Raman frequencies of organic compounds*, Wiley.
- Eckl, B., Vrabec, J. & Hasse, H. 2008. Set of Molecular Models Based on Quantum Mechanical Ab Initio Calculations and Thermodynamic Data. *The Journal of Physical Chemistry B*, 112, 12710-12721.

- Eduljee, G. & Tiwari, K. 1976. Correlation of azeotrope data. *Chemical Engineering Science*, 31, 535-540.
- ES, N. 1985. Laboratory infection of mosquito larvae by Entomopathogenic fungi with particular reference to *Aspergillus parasiticus* and its effects on fecundity and longevity of mosquitoes exposed to conidial infections in larval stages. *Current Science*, 54, 1221-1228.
- Esposito, N., Bernal, Y. & Goss, G. 2015. Granular Carrier Effects on Volatility of Pesticide Formulations. *Pesticide Formulation and Delivery Systems: 34th Volume, Translating Basic Science into Products*. ASTM International.
- Ewell, R., Harrison, J. & Berg, L. 1944. Azeotropic distillation. *Industrial & Engineering Chemistry*, 36, 871-875.
- Federici, B., Park, H.-W., Bideshi, D., Wirth, M. & Johnson, J. 2003. Recombinant bacteria for mosquito control. *Journal of Experimental Biology*, 206, 3877-3885.
- Federici, B. A., Park, H.-W., Bideshi, D. K., Wirth, M. C., Johnson, J. J., Sakano, Y. & Tang, M. 2007. Developing recombinant bacteria for control of mosquito larvae. *Journal of the American Mosquito Control Association*, 23, 164-175.
- Feldmann, R. J. & Maibach, H. I. 1970. Absorption of some organic compounds through the skin in man. *Journal of investigative dermatology*, 54, 399-404.
- Ferrando, N., Lachet, V. & Boutin, A. 2010. Monte Carlo Simulations of Mixtures Involving Ketones and Aldehydes by a Direct Bubble Pressure Calculation. *The Journal of Physical Chemistry B*, 114, 8680-8688.
- Fillinger, U. & Lindsay, S. W. 2006. Suppression of exposure to malaria vectors by an order of magnitude using microbial larvicides in rural Kenya
- Suppression de l'exposition au vecteur de la malaria basée sur l'utilisation de larvicides microbiens en zone rurale au Kenya
- Supresión de la exposición a vectores de malaria en un orden de magnitud utilizando larvicidas microbianos en Kenya rural. *Tropical Medicine & International Health*, 11, 1629-1642.
- Fillinger, U., Ndenga, B., Githeko, A. & Lindsay, S. W. 2009. Integrated malaria vector control with microbial larvicides and insecticide-treated nets in western Kenya: a controlled trial. *Bull World Health Organ*, 87, 655-65.
- Focke, W. W., Nhlapo, N. S. & Vuorinen, E. 2013. Thermal analysis and FTIR studies of volatile corrosion inhibitor model systems. *Corrosion Science*, 77, 88-96.
- Fradin, M. & Auerbach, P. 2001. Protection from blood-feeding arthropods. *Wilderness medicine*, 754-768.

- Fradin, M. S. 1998. Mosquitoes and mosquito repellents: A clinician's guide. *Annals of Internal Medicine*, 128, 931-940.
- Fradin, M. S. 2001. *Protection from blood-feeding arthropods*.
- Fradin, M. S. & Day, J. F. 2002. Comparative Efficacy of Insect Repellents against Mosquito Bites. *New England Journal of Medicine*, 347, 13-18.
- Frances, S. P., Marlow, R. M., Jansen, C. C., Huggins, R. L. & Cooper, R. D. 2005. Laboratory and field evaluation of commercial repellent formulations against mosquitoes (Diptera: Culicidae) in Queensland, Australia. *Australian Journal of Entomology*, 44, 431-436.
- Freeman, S. K. 1974. *Applications of laser Raman spectroscopy*, Wiley.
- Frenkel, D. & Smit, B. 2002a. Chapter 3 - Monte Carlo Simulations. *Understanding Molecular Simulation (Second Edition)*. San Diego: Academic Press.
- Frenkel, D. & Smit, B. 2002b. Chapter 4 - Molecular Dynamics Simulations. *Understanding Molecular Simulation (Second Edition)*. San Diego: Academic Press.
- Frenkel, D. & Smit, B. 2002c. *Understanding molecular simulation : from algorithms to applications*, San Diego :, Academic Press.
- Gandolfo, F. G., Bot, A. & Flöter, E. 2003. Phase diagram of mixtures of stearic acid and stearyl alcohol. *Thermochimica Acta*, 404, 9-17.
- Garson, L. R. & Winnike, M. E. 1968. Relationships between insect repellency and chemical and physical parameters--a review. *J Med Entomol*, 5, 339-52.
- Garti, N., Sarig, S. & Wellner, E. 1980. Determination of the composition of mixtures of fatty acid polymorphs by DTA. *Thermochimica Acta*, 37, 131-136.
- Geyer, C. 2011. Introduction to Markov Chain Monte Carlo. *Handbook of Markov Chain Monte Carlo*, 3-48.
- Gilbert, I. H., Gouck, H. K. & Smith, C. N. 1955. New Mosquito Repellents. *Journal of Economic Entomology*, 48, 741-743.
- Goodyer, L. & Behrens, R. H. 1998. Short report: The safety and toxicity of insect repellents. *American Journal of Tropical Medicine and Hygiene*, 59, 323-324.
- Govere, J. M., Durrheim, D. N., Debboun, M., Frances, S. & Strickman, D. 2007. Techniques for evaluating repellents. *Insect repellents: principles, methods and uses*, 147-159.
- Graham, B. W. 2006. Terminology of Insect Repellents. *Insect Repellents*. CRC Press.

- Grieco, J. P., Vogtsberger, R. C., Achee, N. L., Vanzie, E., Andre, R. G., Roberts, D. R. & Rejmankova, E. 2005. Evaluation of habitat management strategies for the reduction of malaria vectors in northern Belize. *Journal of Vector Ecology*, 30, 235-243.
- Griffing, S. M., Villegas, L. & Udhayakumar, V. 2014. Malaria Control and Elimination, Venezuela, 1800s–1970s. *Emerging Infectious Diseases*, 20, 1691-1696.
- Gu, W., Utzinger, J. & Novak, R. J. 2008. Habitat-Based Larval Interventions: A New Perspective for Malaria Control. *The American Journal of Tropical Medicine and Hygiene*, 78, 2-6.
- Guillet, P., Alnwick, D., Cham, M. K., Neira, M., Zaim, M., Heymann, D. & Mukelabai, K. 2001. Long-lasting treated mosquito nets: a breakthrough in malaria prevention. *Bulletin of the World Health Organization*, 79, 0-0.
- Gupta, R. K. & Bhattacharjee, A. K. 2007. Discovery and design of new arthropod/insect repellents by computer-aided molecular modeling. *Insect Repellents: Principles, Methods, and Uses*, 195-228.
- Gupta, R. K. & Rutledge, L. C. 1993. Role of repellents in vector control and disease prevention. *The American journal of tropical medicine and hygiene*, 50, 82-86.
- Hadzi, D. & Sheppard, N. 1953. The Infra-Red Absorption Bands Associated with the COOH and COOD Groups in Dimeric Carboxylic Acids. I. The Region from 1500 to 500 cm^{-1} . *Proceedings of the Royal Society of London. Series A. Mathematical and Physical Sciences*, 216, 247-266.
- Haghtalab, A. & Yousefi Seyf, J. 2015. Vapor–Liquid and Solid–Liquid Modeling with a Universal Quasichemical Segment-Based Activity Coefficient Model. *Industrial & Engineering Chemistry Research*, 54, 8611-8623.
- Hao, H., Sun, J. & Dai, J. 2012. Preliminary Analysis of Several Attractants and Spatial Repellents for the Mosquito, *Aedes albopictus* using an Olfactometer. *Journal of Insect Science*, 12, 76.
- Hao, H., Wei, J., Dai, J. & Du, J. 2008. Host-seeking and blood-feeding behavior of *Aedes albopictus* (Diptera: Culicidae) exposed to vapors of geraniol, citral, citronellal, eugenol, or anisaldehyde. *Journal of Medical Entomology*, 45, 533-539.
- Helinski, M. E., Parker, A. G. & Knols, B. G. 2009. Radiation biology of mosquitoes. *Malaria journal*, 8, 1.
- Hieu, T. T., Kim, S. I., Lee, S. G. & Ahn, Y. J. 2010. Repellency to *Stomoxys calcitrans* (Diptera: Muscidae) of plant essential oils alone or in combination with *Calophyllum inophyllum* nut oil. *J Med Entomol*, 47, 575-80.
- Homocianu, M. 2011. Solvent effects on the electronic absorption and fluorescence spectra. *Journal of Advanced Research in Physics*, 2.

- Hoogerbrugge, P. & Koelman, J. 1992. Simulating microscopic hydrodynamic phenomena with dissipative particle dynamics. *EPL (Europhysics Letters)*, 19, 155.
- Horvath, H. 1988. Sixteenth Annual Conference of the Gesellschaft für Aerosolforschung Experimental investigation on the validity of the Lambert-Beer law at high particle concentrations. *Journal of Aerosol Science*, 19, 837-840.
- Iscan, Y., Hekimoglu, S., Sargon, M. F. & Hincal, A. A. 2006. DEET-loaded solid lipid particles for skin delivery: in vitro release and skin permeation characteristics in different vehicles. *J Microencapsul*, 23, 315-27.
- Jorgensen, W. L., Maxwell, D. S. & Tirado-Rives, J. 1996. Development and Testing of the OPLS All-Atom Force Field on Conformational Energetics and Properties of Organic Liquids. *Journal of the American Chemical Society*, 118, 11225-11236.
- Jorgensen, W. L. & Swenson, C. J. 1985. Optimized intermolecular potential functions for amides and peptides. Structure and properties of liquid amides. *Journal of the American Chemical Society*, 107, 569-578.
- Jouhara, H., Ajji, Z., Koulsi, Y., Ezzuddin, H. & Mousa, N. 2013. Experimental investigation of an inclined-condenser wickless heat pipe charged with water and an ethanol–water azeotropic mixture. *Energy*, 61, 139-147.
- Kang, J. S. & Caprio, J. 1991. Electro-olfactogram and multiunit olfactory receptor responses to complex mixtures of amino acids in the channel catfish, *Ictalurus punctatus*. *J Gen Physiol*, 98, 699-721.
- Karelson, M. & Zerner, M. C. 1990. On the n - π * blue shift accompanying solvation. *Journal of the American Chemical Society*, 112, 9405-9406.
- Karunamoorthi, K. 2011a. Vector control: A cornerstone in the malaria elimination campaign. *Clinical Microbiology and Infection*, 17, 1608-1616.
- Karunamoorthi, K. 2011b. Vector control: a cornerstone in the malaria elimination campaign. *Clin Microbiol Infect*, 17, 1608-16.
- Katritzky, A. R., Wang, Z., Slavov, S., Tsikolia, M., Dobchev, D., Akhmedov, N. G., Hall, C. D., Bernier, U. R., Clark, G. G. & Linthicum, K. J. 2008. Synthesis and bioassay of improved mosquito repellents predicted from chemical structure. *Proc Natl Acad Sci U S A*, 105, 7359-64.
- Kaya, K. & Nagakura, S. 1967. Vacuum ultraviolet absorption spectra of simple amides. *Theoretica chimica acta*, 7, 117-123.
- Khan, A., Maibach, H. I. & Skidmore, D. L. 1975a. Addition of perfume fixatives to mosquito repellents to increase protection time. *Mosquito News*, 35, 23-6.

- Khan, A., Maibach, H. I. & Skidmore, D. L. 1975b. Insect repellents: effect of mosquito and repellent-related factors on protection time. *Journal of economic entomology*, 68, 43-45.
- Killeen, G., Fillinger, U. & Knols, B. 2002a. Advantages of larval control for African malaria vectors: Low mobility and behavioural responsiveness of immature mosquito stages allow high effective coverage. *Malaria Journal*, 1, 8.
- Killeen, G. F. 2003. Following in Soper's footsteps: Northeast Brazil 63 years after eradication of *Anopheles gambiae*. *Lancet Infectious Diseases*, 3, 663-666.
- Killeen, G. F., Fillinger, U., Kiche, I., Gouagna, L. C. & Knols, B. G. J. 2002b. Eradication of *Anopheles gambiae* from Brazil: Lessons for malaria control in Africa? *Lancet Infectious Diseases*, 2, 618-627.
- Kiva, V., Hilmen, E. & Skogestad, S. 2003a. Azeotropic phase equilibrium diagrams: a survey. *Chemical Engineering Science*, 58, 1903-1953.
- Kiva, V. N., Hilmen, E. K. & Skogestad, S. 2003b. Azeotropic phase equilibrium diagrams: a survey. *Chemical Engineering Science*, 58, 1903-1953.
- Klun, J. A., Schmidt, W. F. & Debboun, M. 2001. Stereochemical effects in an insect repellent. *J Med Entomol*, 38, 809-12.
- Kofke, D. A. 1993. Gibbs-Duhem integration: a new method for direct evaluation of phase coexistence by molecular simulation. *Molecular Physics*, 78, 1331-1336.
- Kranias, S., Pattou, D., Levy, B. & Boutin, A. 2003. An optimized potential for phase equilibria calculation for ketone and aldehyde molecular fluids. *Physical Chemistry Chemical Physics*, 5, 4175-4179.
- Kroeger, A., Gerhardus, A., Kruger, G., Mancheno, M. & Pesse, K. 1997. The contribution of repellent soap to malaria control. *The American journal of tropical medicine and hygiene*, 56, 580-584.
- Kruger, T., Sibanda, M. M., Focke, W. W., Bornman, M. S. & de Jager, C. 2015. Acceptability and effectiveness of a monofilament, polyethylene insecticide-treated wall lining for malaria control after six months in dwellings in Vhembe District, Limpopo Province, South Africa. *Malaria Journal*, 14, 1-14.
- Kumar, S. 2006. *Spectroscopy of Organic Compounds*, New Delhi New Age International Pvt Ltd Publishers.
- Lajovic, A., Tomsic, M. & Jamnik, A. 2012. Structural study of simple organic acids by small-angle x-ray scattering and monte carlo simulations. *Acta Chim Slov*, 59, 520-7.
- Laurence, C. & Berthelot, M. 2000. Observations on the strength of hydrogen bonding. *Perspectives in Drug Discovery and Design*, 18, 39-60.

- Le Questel, J.-Y., Berthelot, M. & Laurence, C. 1997. Can semi-empirical calculations yield reasonable estimates of hydrogen-bonding basicity? The case of nitriles. *Journal of the Chemical Society, Perkin Transactions 2*, 2711-2718.
- Lei, Z., Chen, B. & Ding, Z. 2005. Special distillation processes. 1st ed. ed. Amsterdam :: Elsevier.
- Levine, I. N. 1991. *Quantum Chemistry*, Prentice Hall.
- Li, J., Lei, Z., Ding, Z., Li, C. & Chen, B. 2005. Azeotropic Distillation: A Review of Mathematical Models. *Separation & Purification Reviews*, 34, 87-129.
- Li, Y. F., Yu, Y. X., Zheng, Y. X. & Li, J. D. 2010. Shift of the azeotropic point of binary Lennard-Jones mixtures confined in a slit-like pore. *Fluid Phase Equilibria*, 292, 110-116.
- Liao, Y.-T. 1991. Differential scanning calorimetry heat capacity hysteresis of semicrystalline polymers. *Journal of Materials Science Letters*, 10, 706-708.
- Lin-Vien, D., Colthup, N. B., Fateley, W. G. & Grasselli, J. G. 1991. *The handbook of infrared and Raman characteristic frequencies of organic molecules*, Elsevier.
- Louis, C. R. & Raj, K. G. 2006. Animal Models for Research and Development of Insect Repellents for Human Use. *Insect Repellents*. CRC Press.
- Lourderaj, U., Giri, K. & Sathyamurthy, N. 2006. Ground and Excited States of the Monomer and Dimer of Certain Carboxylic Acids. *The Journal of Physical Chemistry A*, 110, 2709-2717.
- Lupi, E., Hatz, C. & Schlagenhauf, P. 2013. The efficacy of repellents against Aedes, Anopheles, Culex and Ixodes spp.–a literature review. *Travel medicine and infectious disease*, 11, 374-411.
- Ma, D., Bhattacharjee, A. K., Gupta, R. K. & Karle, J. M. 1999. Predicting mosquito repellent potency of N,N-diethyl-m-toluamide (DEET) analogs from molecular electronic properties. *Am J Trop Med Hyg*, 60, 1-6.
- Mackie, A. D., Tavitian, B., Boutin, A. & Fuchs, A. H. 1997. Vapour-Liquid Phase Equilibria Predictions of Methane–Alkane Mixtures by Monte Carlo Simulation. *Molecular Simulation*, 19, 1-15.
- Magnes, B. Z., Pines, D., Strashnikova, N. & Pines, E. 2004. Hydrogen-bonding interactions of photoacids: correlation of optical solvatochromism with IR absorption spectra. *Solid State Ionics*, 168, 225-233.
- Maharaj, R., Maharaj, V., Newmarch, M., Crouch, N. R., Bhagwandin, N., Folb, P. I., Pillay, P. & Gayaram, R. 2010. Evaluation of selected South African ethnomedicinal plants

- as mosquito repellents against the *Anopheles arabiensis* mosquito in a rodent model. *Malaria Journal*, 9, 301-301.
- Maia, F. M., Tsivintzelis, I., Rodriguez, O., Macedo, E. A. & Kontogeorgis, G. M. 2012. Equation of state modelling of systems with ionic liquids: Literature review and application with the Cubic Plus Association (CPA) model. *Fluid Phase Equilibria*, 332, 128-143.
- Maibach, H. I., Khan, A. A. & Akers, W. 1974. Use of insect repellents for maximum efficacy. *Archives of Dermatology*, 109, 32-35.
- Massey, T. S. & Langley, J. T. 2015. Microencapsulated volatile insect repellent and/or insecticide agent and methods of making and using the same. Google Patents.
- Materazzi, S. 1997. Thermogravimetry – Infrared Spectroscopy (TG-FTIR) Coupled Analysis. *Applied Spectroscopy Reviews*, 32, 385-404.
- Mayo, D. W., Miller, F. A. & Hannah, R. W. 2004. *Course notes on the interpretation of infrared and Raman spectra*, Wiley Online Library.
- McCabe, E. T., Barthel, W. F., Gertler, S. I. & Hall, S. A. 1954. INSECT REPELLENTS. III. N,N-DIETHYLAMIDES¹. *The Journal of Organic Chemistry*, 19, 493-498.
- McElroy, B., Wiseman, V., Matovu, F. & Mwengee, W. 2009. Malaria prevention in north-eastern Tanzania: patterns of expenditure and determinants of demand at the household level. *Malaria Journal*, 8, 1-10.
- McIver, S. B. 1982. Sensilla mosquitoes (Diptera: Culicidae). *J Med Entomol*, 19, 489-535.
- Metropolis, N., Rosenbluth, A. W., Rosenbluth, M. N., Teller, A. H. & Teller, E. 1953. Equation of state calculations by fast computing machines. *The journal of chemical physics*, 21, 1087-1092.
- Mikenda, W. 1986. Stretching frequency versus bond distance correlation of O□D(H)··Y (Y □ N, O, S, Se, Cl, Br, I) hydrogen bonds in solid hydrates. *Journal of Molecular Structure*, 147, 1-15.
- Mikenda, W. & Steinböck, S. 1996. Stretching frequency vs. bond distance correlation of hydrogen bonds in solid hydrates: a generalized correlation function. *Journal of Molecular Structure*, 384, 159-163.
- Miller, T. 2000. National pesticide telecommunications network (NPTN). Environmental & Molecular Toxicology, Oregon State University.
- Milutinović, R., Vuleta, G., Milić, J. & Stajković, N. 1999. Assessment of Efficiency of Repellent Formulations with N,N-diethyl-m-toluamide in Laboratory Conditions. *International Journal of Cosmetic Science*, 21, 7-14.

- Moore, S. J., Debboun, M., Debboun, M., Frances, S. & Strickman, D. 2007. History of insect repellents. *Insect Repellents: Principles, Methods, and Uses*, 3-29.
- Moore, S. J., Lenglet, A. & Hill, N. 2002. Field evaluation of three plant-based insect repellents against malaria vectors in Vaca Diez Province, the Bolivian Amazon. *J Am Mosq Control Assoc*, 18, 107-10.
- Moore, W. 1934. Esters as Repellents. *Journal of the New York Entomological Society*, 42, 185-192.
- Moreno, E., Cordobilla, R., Calvet, T., Cuevas-Diarte, M. A., Gbabode, G., Negrier, P., Mondieig, D. & Oonk, H. A. J. 2007. Polymorphism of even saturated carboxylic acids from n-decanoic to n-eicosanoic acid. *New Journal of Chemistry*, 31, 947-957.
- Morisawa, Y., Yasunaga, M., Fukuda, R., Ehara, M. & Ozaki, Y. 2013. Electronic transitions in liquid amides studied by using attenuated total reflection far-ultraviolet spectroscopy and quantum chemical calculations. *The Journal of Chemical Physics*, 139, 154301.
- Mortier, W. J., Ghosh, S. K. & Shankar, S. 1986. Electronegativity-equalization method for the calculation of atomic charges in molecules. *Journal of the American Chemical Society*, 108, 4315-4320.
- Mortier, W. J., Van Genechten, K. & Gasteiger, J. 1985. Electronegativity equalization: application and parametrization. *Journal of the American Chemical Society*, 107, 829-835.
- Muller, G. C., Junnila, A., Butler, J., Kravchenko, V. D., Revay, E. E., Weiss, R. W. & Schlein, Y. 2009. Efficacy of the botanical repellents geraniol, linalool, and citronella against mosquitoes. *J Vector Ecol*, 34, 2-8.
- Nakayama, A., Iwamura, H., Niwa, A., Nakagawa, Y. & Fujita, T. 1985. Development of insect juvenile hormone active oxime O-ethers and carbamates. *Journal of Agricultural and Food Chemistry*, 33, 1034-1041.
- Nakayama, A. & Richards, W. G. 1987. A Quantum Chemical Study of Insect Juvenile Hormone Mimics: The Active Conformation and the Electrostatic Similarities. *Quantitative Structure-Activity Relationships*, 6, 153-157.
- Nentwig, G. 2003. Use of repellents as prophylactic agents. *Parasitology Research*, 90, S40-S48.
- Nerio, L. S., Olivero-Verbel, J. & Stashenko, E. 2010. Repellent activity of essential oils: A review. *Bioresource Technology*, 101, 372-378.
- Nhlapo, N. S. 2013. *TGA-FTIR study of the vapours released by volatile corrosion inhibitor model systems*. PhD, University of Pretoria.

- Nhlapo, N. S., Focke, W. W. & Vuorinen, E. 2012. TGA–FTIR study of the vapors released by triethylamine–acetic acid mixtures. *Thermochimica Acta*, 546, 113-119.
- Nibbering, E. T. J., Dreyer, J., Kühn, O., Bredenbeck, J., Hamm, P. & Elsaesser, T. 2007. Vibrational dynamics of hydrogen bonds. In: KÜHN, O. & WÖSTE, L. (eds.) *Analysis and Control of Ultrafast Photoinduced Reactions*. Berlin, Heidelberg: Springer Berlin Heidelberg.
- Nielsen, E. B. & Schellman, J. A. 1967. The absorption spectra of simple amides and peptides. *The Journal of physical chemistry*, 71, 2297-2304.
- Nolen, J. A., Bedoukian, R. H., Maloney, R. E. & Kline, D. L. 2002. Method, apparatus and compositions for inhibiting the human scent tracking ability of mosquitoes in environmentally defined three dimensional spaces. Google Patents.
- Novak, A. 1974. Hydrogen bonding in solids correlation of spectroscopic and crystallographic data. *Large Molecules*. Berlin, Heidelberg: Springer Berlin Heidelberg.
- Nunes, N., Elvas-Leitao, R. & Martins, F. 2014. UV-Vis spectroscopic study of preferential solvation and intermolecular interactions in methanol/1-propanol/acetonitrile by means of solvatochromic probes. *Spectrochim Acta A Mol Biomol Spectrosc*, 124, 470-9.
- Nutting, H. S. & Horsley, L. H. 1973. Graphical Method for Predicting Effect of Pressure on Azeotropic Systems. *AZEOTROPIC DATA*. AMERICAN CHEMICAL SOCIETY.
- Ohannesian, L. & Streeter, A. 2001. *Handbook of pharmaceutical analysis*, CRC Press.
- Okorie, P., Okareh, O., Adeleke, O., Falade, C. & Ademowo, O. 2015. Effects of an in-built ultrasonic device on *Anopheles gambiae* sl mosquitoes in an indoor environment.
- Omrani, S. M., Vatandoost, H., Oshaghi, M. A., Shokri, F., Guerin, P. M., Ershadi, M. R. Y., Rassi, Y. & Tirgari, S. 2010. Fabrication of an olfactometer for mosquito behavioural studies. *Journal of Vector Borne Diseases*, 47, 17-25.
- Orozco, G. A., Nieto-Draghi, C., Mackie, A. D. & Lachet, V. 2012. Transferable force field for equilibrium and transport properties in linear and branched monofunctional and multifunctional amines. II. Secondary and tertiary amines. *J Phys Chem B*, 116, 6193-202.
- Otera, J. 1993. Transesterification. *Chemical reviews*, 93, 1449-1470.
- Pandit, S. P. & Kofke, D. A. 1999. Evaluation of a locus of azeotropes by molecular simulation. *AIChE Journal*, 45, 2237-2244.
- Papari, M. M., Moghadasi, J., Fadaei, F. & Campo, A. 2012. Modeling vapor–liquid equilibrium of various binary mixtures with a statistically based equation of state. *Journal of Molecular Liquids*, 165, 87-93.

- Park, B. S., Choi, W. S., Kim, J. H., Kim, K. H. & Lee, S. E. 2005. Monoterpenes from thyme (*Thymus vulgaris*) as potential mosquito repellents. *J Am Mosq Control Assoc*, 21, 80-3.
- Park, S.-K., Min, K.-C., Lee, C., Hong, S. K., Kim, Y. & Lee, N.-S. 2009. Intermolecular hydrogen bonding and vibrational analysis of N, N-dimethylformamide hexamer cluster. *Bull. Korean Chem. Soc*, 30, 2595.
- Pauling, L. 1939. *The Nature of the Chemical Bond*, NY, Cornell University, Press: Ithaca.
- Proniuk, S., Liederer, B. M., Dixon, S. E., Rein, J. A., Kallen, M. A. & Blanchard, J. 2002. Topical Formulation Studies with DEET (N,N- Diethyl- 3- methylbenzamide) and Cyclodextrins. *Journal of Pharmaceutical Sciences*, 91, 101-110.
- Raabe, G. & Koehler, J. 2002. Use of ab initio interaction energies for the prediction of phase equilibria in the system nitrogen-ethane. *Physical Chemistry Chemical Physics*, 4, 926-930.
- Rattan, R. S. 2010. Mechanism of action of insecticidal secondary metabolites of plant origin. *Crop protection*, 29, 913-920.
- Reid, E. E. 1937. Esterification A review of the recent past and a look towards the future. *Industrial & Engineering Chemistry*, 29, 1344-1350.
- Reifenrath, W., Hawkins, G. & Kurtz, M. 1990. In vitro evaluation of insect repellent formulations applied to pig skin. *Pharmacol Res*, 7, 192.
- Reifenrath, W. G. 2002. Natural insect repellent. Google Patents.
- Reifenrath, W. G. 2005. Natural insect repellent. Google Patents.
- Reifenrath, W. G., Hawkins, G. S. & Kurtz, M. S. 1989. Evaporation and skin penetration characteristics of mosquito repellent formulations. *J Am Mosq Control Assoc*, 5, 45-51.
- Reusch, W. June 2010 Virtual Text of Organic Chemistry. Michigan State University, Department of Chemistry.
- Reyes Labarta, J. A., Olaya López, M. d. M. & Marcilla Gomis, A. 2014. Mapping Binary Liquid-Vapor or Liquid-Liquid-Vapor Equilibria Regions, including the Different Azeotropic Behaviours, as a Function of the NRTL Binary Parameters.
- Robinson, J. W., Skelly Frame, E. M. & Frame, G. M. 2014. *Undergraduate instrumental analysis*, Boca Raton; London; New York, CRC Press, Taylor & Francis Group.
- Rueda, L. M., Rutledge, L. C. & Gupta, R. K. 1998. Effect of skin abrasions on the efficacy of the repellent deet against *Aedes aegypti*. DTIC Document.

- Ryckaert, J.-P., McDonald, I. R. & Klein, M. L. 1989. Disorder in the pseudohexagonal rotator phase of n-alkanes: molecular-dynamics calculations for tricosane. *Molecular Physics*, 67, 957-979.
- Samarasekera, R., Weerasinghe, I. S. & Hemalal, K. D. P. 2008. Insecticidal activity of menthol derivatives against mosquitoes. *Pest Management Science*, 64, 290-295.
- Sancho, M. I., Almandoz, M. C., Blanco, S. E. & Castro, E. A. 2011. Spectroscopic Study of Solvent Effects on the Electronic Absorption Spectra of Flavone and 7-Hydroxyflavone in Neat and Binary Solvent Mixtures. *International Journal of Molecular Sciences*, 12, 8895-8912.
- Satpute, K. 2015. A Review on Plant Based Mosquito Repellents. *Literati Journal of Pharmaceutical Drug Delivery Technologies*, 1, 8-13.
- Schlenk, H. 1961. Crystallization of fatty acids. *Journal of the American Oil Chemists Society*, 38, 728-736.
- Schlünder, E. U. 1989. Azeotropes and pseudo-azeotropes. *Fluid Phase Equilibria*, 51, 71-85.
- Schuster, P., Zundel, G. & Sandorfy, C. 1976. Hydrogen bond; recent developments in theory and experiments. *Hydrogen bond; recent developments in theory and experiments*. North-Holland Publishing Company.
- Service, M. 2008. *Medical Entomology for Students*, Cambridge University Press.
- Seyoum, A., Killeen, G. F., Kabiru, E. W., Knols, B. G. J. & Hassanali, A. 2003. Field efficacy of thermally expelled or live potted repellent plants against African malaria vectors in western Kenya. *Tropical Medicine & International Health*, 8, 1005-1011.
- Shousha, A. T. 1948. Species-eradication: The Eradication of Anopheles gambiae from Upper Egypt, 1942-1945. *Bull World Health Organ*, 1, 309-52.
- Singleton, D. L., Paraskevopoulos, G. & Irwin, R. S. 1987. UV absorption cross-sections of the monomer and dimer of formic acid. *Journal of Photochemistry*, 37, 209-216.
- Skinner, W. A., Tong, H. C., Maibach, H. I. & Skidmore, D. 1970. Human skin-surface lipid fatty acids — Mosquito repellents. *Experientia*, 26, 728-730.
- Skoog, D. A., Holler, F. J. & Crouch, S. R. 2014. *Principles of instrumental analysis*, Belmont, CA, Brooks/Cole Cengage Learning.
- Smith, R. 2003. *Chemical process design and integration*, Chichester :, Wiley.
- Soffientini, S., Bernasconi, L. & Imberti, S. 2015. The hydration of formic acid and acetic acid. *Journal of Molecular Liquids*, 205, 85-92.
- Solomon, B., Sahle, F. F., Gebre-Mariam, T., Asres, K. & Neubert, R. H. H. 2012. Microencapsulation of citronella oil for mosquito-repellent application: Formulation

- and in vitro permeation studies. *European Journal of Pharmaceutics and Biopharmaceutics*, 80, 61-66.
- Stanczyk, N. M. 2011. *An investigation of DEET-insensitivity in Aedes aegypti*. University of Nottingham.
- Subramoney, S. C., Nelson, W. M., Courtial, X., Naidoo, P., Coquelet, C., Richon, D. & Ramjugernath, D. 2015. Isothermal phase (vapour+ liquid) equilibrium data for binary mixtures of propene (R1270) with either 1, 1, 2, 3, 3, 3-hexafluoro-1-propene (R1216) or 2, 2, 3-trifluoro-3-(trifluoromethyl) oxirane in the temperature range of (279 to 318) K. *The Journal of Chemical Thermodynamics*, 90, 100-105.
- Suryanarayana, M., Pandey, K., Prakash, S., Raghuv eeran, C., Dangi, R., Swamy, R. & Rao, K. 1991a. Structure- activity relationship studies with mosquito repellent amides. *Journal of pharmaceutical sciences*, 80, 1055-1057.
- Suryanarayana, M. V., Pandey, K. S., Prakash, S., Raghuv eeran, C. D., Dangi, R. S., Swamy, R. V. & Rao, K. M. 1991b. Structure-activity relationship studies with mosquito repellent amides. *J Pharm Sci*, 80, 1055-7.
- Suryanarayana, M. V. S., Pandey, K. S., Prakash, S., Raghuv eeran, C. D., Dangi, R. S., Swamy, R. V. & Rao, K. M. 1991c. Structure-activity relationship studies with mosquito repellent amides. *Journal of Pharmaceutical Sciences*, 80, 1055-1057.
- Suzuki, S. & Baba, H. 1967. Polarization Study of the Fluorescent State of the Hydrogen Bonded α -Naphthol. *Bulletin of the Chemical Society of Japan*, 40, 2199-2200.
- Tanaka, N., Kitano, H. & Ise, N. 1990. Raman spectroscopic study of hydrogen bonding in aqueous carboxylic acid solutions. *The Journal of Physical Chemistry*, 94, 6290-6292.
- Tang, H., Zhu, C., Niu, W., Wang, H. & Hu, W. Mesoporous polyurea aerogel for large loading, uniform and slow release of insect repellent oil. 2015 IEEE Nanotechnology Materials and Devices Conference, NMDC 2015, 2016.
- Tawatsin, A., Wratten, S. D., Scott, R. R., Thavara, U. & Techadamrongsin, Y. 2001. Repellency of volatile oils from plants against three mosquito vectors. *J Vector Ecol*, 26, 76-82.
- Thakkar, S. V., Allegre, K. M., Joshi, S. B., Volkin, D. B. & Middaugh, C. R. 2012. An application of ultraviolet spectroscopy to study interactions in proteins solutions at high concentrations. *J Pharm Sci*, 101, 3051-61.
- Theodorou, D. N. 2010. Progress and outlook in Monte Carlo simulations. *Industrial and Engineering Chemistry Research*, 49, 3047-3058.
- Thompson, H. W. & Torkington, P. 1945. 171. The vibrational spectra of esters and ketones. *Journal of the Chemical Society (Resumed)*, 640-645.

- Toikka, A. On Thermodynamics of Evaporation Processes in Nonequilibrium Systems. INSTITUTION OF CHEMICAL ENGINEERS SYMPOSIUM SERIES, 2006. Institution of Chemical Engineers; 1999, 809.
- Toikka, A. M. & Jenkins, J. D. 2002. Conditions of thermodynamic equilibrium and stability as a basis for the practical calculation of vapour–liquid equilibria. *Chemical Engineering Journal*, 89, 1-27.
- Touré, Y. 2001. Malaria Vector Control in Africa: Strategies and Challenges. San Francisco.
- Toxvaerd, S. 1997. Equation of state of alkanes II. *The Journal of Chemical Physics*, 107, 5197-5204.
- Tuetun, B., Choochote, W., Kanjanapothi, D., Rattanachanpichai, E., Chaithong, U., Chaiwong, P., Jitpakdi, A., Tippawangkosol, P., Riyong, D. & Pitasawat, B. 2005. Repellent properties of celery, *Apium graveolens* L., compared with commercial repellents, against mosquitoes under laboratory and field conditions. *Tropical Medicine & International Health*, 10, 1190-1198.
- Turner, S. L., Li, N., Guda, T., Githure, J., Cardé, R. T. & Ray, A. 2011. Ultra-prolonged activation of CO₂-sensing neurons disorients mosquitoes. *Nature*, 474, 87-91.
- Turner, S. L. & Ray, A. 2009. Modification of CO₂ avoidance behaviour in *Drosophila* by inhibitory odorants. *Nature*, 461, 277-281.
- Ungerer, P. 2005. *Applications of Molecular Simulation in the Oil and Gas Industry*.
- Ungerer, P., Beauvais, C., Delhommelle, J., Boutin, A., Rousseau, B. & Fuchs, A. H. 2000. Optimization of the anisotropic united atoms intermolecular potential for n-alkanes. *The Journal of Chemical Physics*, 112, 5499-5510.
- Ungerer, P., Lachet, V. & Tavitian, B. 2006. Applications de la simulation moléculaire à la production et au traitement du pétrole et du gaz. *Oil & Gas Science and Technology - Rev. IFP*, 61, 387-403.
- Upstone, S. L. 2000. Ultraviolet/visible light absorption spectrophotometry in clinical chemistry. *Encyclopedia of Analytical Chemistry*.
- Utzinger, J., Tozan, Y. & Singer, B. H. 2001. Efficacy and cost-effectiveness of environmental management for malaria control. *Tropical Medicine & International Health*, 6, 677-687.
- Vahid, A. & Elliott, J. R. 2010. Transferable intermolecular potentials for carboxylic acids and their phase behavior. *AIC AIChE Journal*, 56, 485-505.
- Vale, G. A. 1980. Field studies of the responses of tsetse flies (Glossinidae) and other Diptera to carbon dioxide, acetone and other chemicals. *Bulletin of Entomological Research*, 70, 563-570.

- Van Genechten, K. A., Mortier, W. J. & Geerlings, P. 1987. Intrinsic framework electronegativity: A novel concept in solid state chemistry. *The Journal of Chemical Physics*, 86, 5063-5071.
- Varekova, R., Jirouskova, Z., Vanek, J., Suchomel, S. & Koca, J. 2007. Electronegativity Equalization Method: Parameterization and Validation for Large Sets of Organic, Organohalogen and Organometal Molecule. *International Journal of Molecular Sciences*, 8, 572.
- Vařeková, R. S. & Koča, J. 2006. Software news and update optimized and parallelized implementation of the electronegativity equalization method and the atom-bond electronegativity equalization method. *Journal of Computational Chemistry*, 27, 396-405.
- Walker, K. & Lynch, M. 2007. Contributions of Anopheles larval control to malaria suppression in tropical Africa: Review of achievements and potential. *Medical and Veterinary Entomology*, 21, 2-21.
- Wang, X., Gao, Z., Gao, X., Guan, W., Han, X. & Chen, G. 2015. Investigation on the Vapor–Liquid Equilibrium for the Ternary Mixture HFC-32+ HFC-125+ HFC-161 at Temperatures from 265.15 K to 303.15 K. *Journal of Chemical & Engineering Data*, 60, 2721-2727.
- Weaving, A., Sylvester, N. & 1967. Pyrethrum as an insect repellent, part II: a laboratory technique for its evaluation as a mosquito repellent, and the influence of formulation on persistence. 9, 31-35.
- Weeks, J. A., Guiney, P. D. & Nikiforov, A. I. 2012. Assessment of the environmental fate and ecotoxicity of N,N-diethyl-m-toluamide (DEET). *Integr Environ Assess Manag*, 8, 120-34.
- Weinhold, F. & Klein, R. A. 2014. What is a hydrogen bond? Resonance covalency in the supramolecular domain. *Chemistry Education Research and Practice*, 15, 276-285.
- WHO 1982. *Manual on Environmental Management for Mosquito Control with Special Emphasis on Malaria Vectors*, Geneva, Switzerland: World Health Organization, World Health Organization.
- WHO 2004. Global strategic framework for integrated vector management. Geneva, Switzerland: World Health Organization.
- WHO 2006a. Indoor residual spraying: Use of indoor residual spraying for scaling up global malaria control and elimination. Geneva, Switzerland: World Health Organization.
- WHO 2006b. WHO Specifications and Evaluations for Public Health Pesticides. Ethyl Butylacetylaminopropionate. Geneva, Switzerland: World Health Organization.
- WHO 2008. *World malaria report 2008*, Geneva, Switzerland: World Health Organization

World Health Organization.

WHO 2009. Guidelines for efficacy testing of mosquito repellents for human skins. *World Health Organization*. Geneva

WHO 2012. Summary of Evaluations Performed by the Joint FAO/WHO Expert Committee on Food Additives: Nonanoic acid.

WHO. 2014. *Fact sheet on the World Malaria Report 2014*

[Online]. Geneva, Switzerland: World Health Organization: World Health Organization. Available: http://www.who.int/malaria/media/world_malaria_report_2014/en/ [Accessed 6/22/2016 2016].

WHO 2015. *World Malaria Report 2015*, Geneva, Switzerland: World Health Organization, World Health Organization.

WHO 2016. Insect repellent 3535. Washington, D.C. .

Xie, W., Pu, J., MacKerell, A. D. & Gao, J. 2007. Development of a Polarizable Intermolecular Potential Function (PIPF) for Liquid Amides and Alkanes. *Journal of Chemical Theory and Computation*, 3, 1878-1889.

Xu, W. & Yang, J. 2010. Computer Simulations on Aggregation of Acetic Acid in the Gas Phase, Liquid Phase, and Supercritical Carbon Dioxide. *The Journal of Physical Chemistry A*, 114, 5377-5388.

Xue, R.-D., Muller, G. C. & Day, J. F. 2014. Commercially available insect repellents and criteria for their use. *Insect Repellents Handbook*, 339.

Yiannourakou, M., Ungerer, P., Leblanc, B., Ferrando, N. & Teuler, J.-M. 2013. Overview of MedeA®-GIBBS capabilities for thermodynamic property calculation and VLE behaviour description of pure compounds and mixtures: application to polar compounds generated from ligno-cellulosic biomass. *Molecular Simulation*, 39, 1165-1211.

Zare-Shahabadi, V., Lotfizadeh, M., Gandomani, A. R. A. & Papari, M. M. 2013. Determination of boiling points of azeotropic mixtures using quantitative structure–property relationship (QSPR) strategy. *Journal of Molecular Liquids*, 188, 222-229.

Zhang, J., Zhang, P., Ma, K., Han, F., Chen, G. & Wei, X. 2008. Hydrogen bonding interactions between ethylene glycol and water: density, excess molar volume, and spectral study. *Science in China Series B: Chemistry*, 51, 420-426.

Zhu, J., Zeng, X., Yanma, Liu, T., Qian, K., Han, Y., Xue, S., Tucker, B., Schultz, G., Coats, J., Rowley, W. & Zhang, A. 2006. Adult repellency and larvicidal activity of five plant essential oils against mosquitoes. *J Am Mosq Control Assoc*, 22, 515-22.

9. Appendices

9.1. Appendix A: Validated A and B parameters for $K= 2.75$ used for electric charge calculation based on EEM

Table A- 1. Parameters A and B for Kappa=2.75 (Vařeková and Koča, 2006)

	Multiplicity	Parameter A	Parameter B
H	1	2.3292	4.555
C	1	2.5642	3.583
N	1	3.4292	4.9706
O	1	3.5572	5.9164
C	2	2.4862	3.2606
N	2	2.9124	3.8762
O	2	3.2015	4.9212

9.2. Appendix B: Informed consent forms to practice in the repellence study

INFORMED CONSENT TO PARTICIPATE IN A RESEARCH STUDY
INSTITUTE: University of Pretoria; Institute of Applied Materials, Faculty of Engineering, Built Environment and Information Technology
RESEARCH COORDINATOR: <i>Homa Izadi</i>
STUDY TITLE: Mosquito repellent blends with reduced volatility

1) Introduction:

You have been invited to take part in our research study. Taking part in this research study is entirely voluntary. You may choose not to take part, or you may withdraw from the study at any time. You will be asked questions during the period of the study, but you may choose not to answer all questions. However, your answers will hopefully give us knowledge that may help many people in future. This whole document will be read out to you. Before you decide to take part, please take as much time as you need to ask any questions and discuss this study with me, the investigators, or your family. The proposal of this study has passed through the University of Pretoria's Health Sciences Research Ethics Committee and the Institute of Applied Materials. You will receive a copy of this informed consent form for future reference. Now I will describe this research study.

2) What is this research about and why is it being done?

The incidence of malaria in endemic areas can be reduced by preventing mosquito bites. Insect repellents provide a convenient way of protecting humans in this way. DEET, the most effective repellent in widespread use, has toxic side effects. Safe alternatives have been suggested but their high volatility prevents their use in topical skin applications.

This study aims to explore the ways of increasing the length of stay (Singleton et al.) of insect repellents so that people will be protected for longer against mosquito bites.

3) Why are you invited to participate in this study?

We need adult human volunteers exhibiting mild or no sensitivity to mosquito bites, preferably not be tobacco users, or at least to have refrained from tobacco use for 12 hours prior to and during testing. Equal numbers of male and female test volunteers are preferred.

4) How many people will take part in this research study?

We plan to enrol four participants.

5) How long will you take part in this research study?

We will study a series of formulation. It is anticipated that repellence tests may have to be conducted in cycles. During each cycle a set of at most four formulations will be tested.

In the first stage of such a test cycle, participants will be involved for a few hours to check the repellence of selected formulations.

In the second stage time lag studies will be conducted on those compositions that show good repellence performance. The time lag study for each composition will last 6 hours and one formulation will be tested per day. The maximum time is four days.

6) What procedures are involved in this research study?

The test area of the volunteers' skin will be washed with unscented soap and rinsed with water. 0.2 ml of acetone (for the control hand) or the prepared repellent formulations (for the test hand) should be applied evenly to 40 cm of the forearm skin and let to dry. We will prepare a special cup contain 25-30 active, host seeking female mosquitoes. The volunteers will be asked to keep the cup in contact with the treated area on their hand for 3 minutes. At the end of a three-minute exposure period the number of mosquitoes probing (attempting to feed on the volunteers) will be recorded.

In the case of time lag study this procedure should be repeated every hour and for the period of maximum 8 hours.

7) What are the risks and discomforts of this research study?

The fresh mosquitos are bred in MRC especially for research purposes and do not transfer parasites. There is no chance of any one getting malaria.

The only consequence of these mosquitoes feeding on human volunteers is transient discomfort, with no risk of infection by any known mosquito borne pathogens.

After each set of the tests the mosquitoes used will be frozen and kept for 2 nights before they will be discarded. This procedure guarantees the death of the mosquitoes without using any chemicals.

The materials may cause eye irritation in case of contact. In this case, one should rinse the eyes with plenty of water for several minutes. Remove contact lenses if present and easy to do and then continue rinsing.

8) What benefits are there for taking part in this study?

If you participate in this research, you may not get any personal benefits but your participation is likely to help us to introduce more effective repellent formulations.

9) Are there reasons that your participation may end early?

Your participation will end early for two reasons namely when withdrawing yourself from the study or when the researchers decide to withdraw you from the study. If you decide to withdraw from the study you will not be punished and refusing to participate will not affect you, your rights or your household in any way. If you do decide to withdraw, you should contact Homa Izadi on 0765970131 to tell her your decision. The researchers may decide to withdraw you from the study if it is determined that you are no longer able to meet the requirements of the study.

10) What will happen when the research study is over?

We will write a report about our findings and results will be published in scientific journals.

11) Will you have to pay to take part in this research study?

There will be no cost to you to participate. Also the researchers doing this study and the University of Pretoria will not make any money by doing this study.

12) What privacy and confidentiality procedures apply to the information gathered about you in this study?

All information that we collect from this research project will be kept strictly confidential. Information will be collected using a study identification number that will be assigned to you. Your name will not be on any data forms; instead we will use your study number. Your name will only be on the contact information sheet that will be locked away in an office at the University of Pretoria. Reports and articles in scientific journals will not include any information that may identify you.

13) Who can answer your questions about the research and your rights as a research subject?

If you have any problems or questions about this study or about your rights as a research participant, you may ask them now or later. If you wish to ask questions later, you may contact Homa Izadi on 0765970131. You may also call Mrs. Manda Smith at the Health Sciences Research Ethics Committee at the University of Pretoria on 012-354-1330.

14) Consent to participate in this research study

The above information had been read to me before signing this consent form. The content and meaning of this information have been explained to me. I have had the opportunity to ask questions and I am satisfied that my questions have been answered. I understand the study will last up to six months. I understand that it is my choice to participate in this study and that

I may withdraw from the study at any time. I hereby voluntarily consent that the repellent formulations may be tested on me as part of participating in this study. I have been provided with a copy of this consent form.

.....

Participant's signature

Participant's name

Date

.....

Witness' signature

Witness' name

Date

9.3. Appendix C: The initial compositions of mixtures used in the oven test

Table C- 1. Initial composition of prepared samples for oven test

Sample	Molar% of IR3535	Sample	Molar% of IR3535
O1	0	O8	50.8
O2	10	O9	60.1
O3	15.1	O10	70.6
O4	20.1	O11	75.3
O5	25.7	O12	81
O6	30	O13	90.1
O7	40.2	O14	100

9.4. Appendix D: Compositions used for constructing the training set for inverse mapping

Table D- 1. Compositions used for constructing the training set

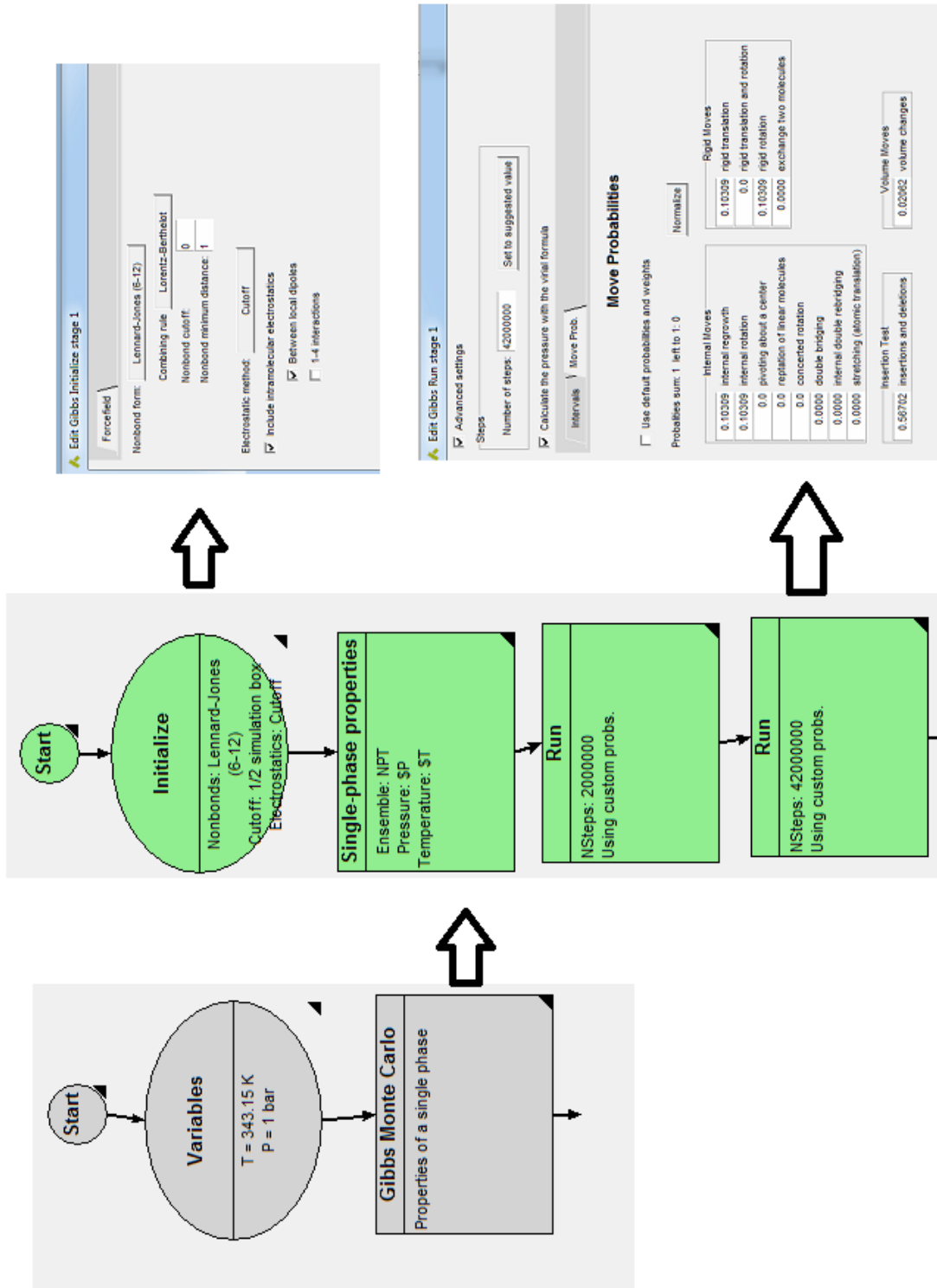
Sample	Molar% of IR3535	Sample	Molar% of IR3535
h0	0	h12	52.4
h1	4.2	h13	58.8
h2	12.3	h14	62.2
h3	12	h15	66.9
h4	15.9	h16	69.8
h5	20.1	h17	75.3
h6	24	h18	78.6
h7	32.6	h19	82.5
h8	36.1	h20	86.9
h9	40.6	h21	90.7
h10	44.3	h22	96
h11	48.4	h23	100

9.5. Appendix E: Considerations to minimize some of the possible sources of deviation of Beer-Lambert law

Table E- 1. Undertaken approaches to minimize possible source of deviation of Beer-Lambert law

Real deviation	In this case the solvent is the one of the analytes under study and interaction of solvent and solute is the issue of interest.
Chemical deviation	This is the desired deviation that we want to study.
Stray radiation	The spectrometer used in this study is a high performance-double beam instrument which guarantees the stray light is less than 0.01% of transmission.
Polychromatic source	Measurements were done at λ_{max} where the polychromatic deviation is minimal. Moreover, the spectral band pass in this instrument is 1 nm which is adequate to omit the polychromatic deviation.
Florescence	IR3535 and nonanoic acid do not florescence.
Turbidity	IR3535 and nonanoic acid and their mixtures are completely transparent.
Unequal path length	Since the instrument features a double beam system the path length is always constant.
Homogeneity	The mixtures were well mixed and homogenized.

9.6. Appendix F: GIBBS-Monte Carlo flowchart for calculation of density of liquids



9.7. Appendix G: Measured density of IR3535 over a range of temperature

Table G- 1. Measured density of IR3535 at the range of 20-100 °C

Temperature (°C)	Density (gr/cm ³)	Temperature (°C)	Density (gr/cm ³)
20.00	0.9982	60.00	0.9648
20.00	0.9982	60.00	0.9649
20.00	0.9982	70.00	0.9565
20.00	0.9982	70.00	0.9567
30.00	0.9899	70.00	0.9566
30.00	0.9899	70.00	0.9566
30.00	0.9899	80.00	0.9485
30.00	0.9899	80.00	0.9484
40.00	0.9815	80.00	0.9484
40.00	0.9816	80.00	0.9484
40.00	0.9816	90.00	0.9403
40.00	0.9816	90.00	0.9403
50.00	0.9732	90.00	0.9403
50.00	0.9734	90.00	0.9403
50.00	0.9733	100.00	0.9324

50.00	0.9733	100.00	0.9324
60.00	0.9648	100.00	0.9323
60.00	0.9649	100.00	0.9324

9.8. Appendix H: Validation of AUA model based on the reported density of N, N- dimethylacetamide

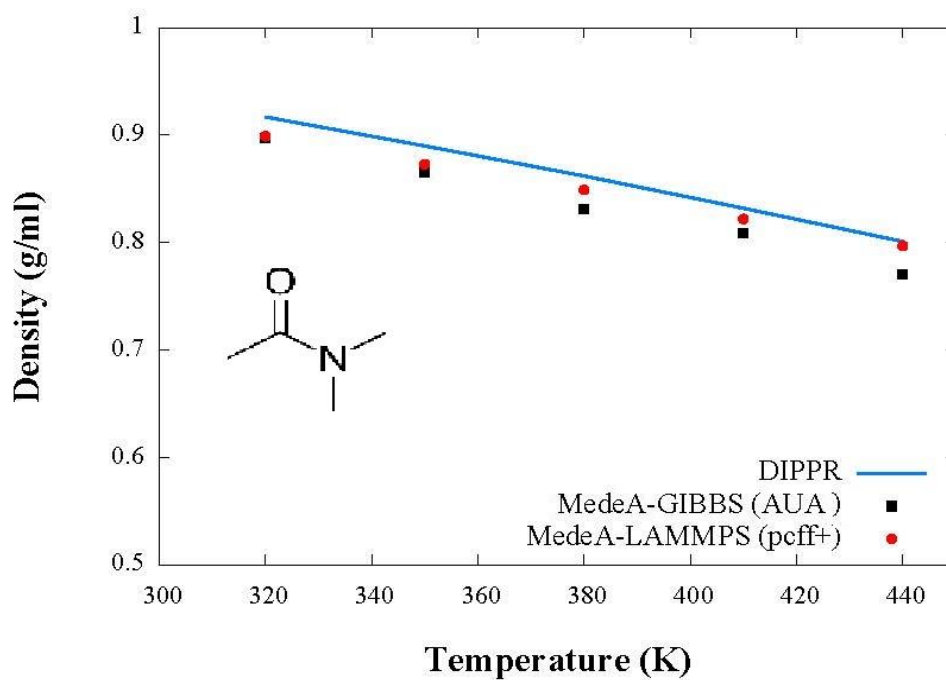


Figure H- 1. Comparison between (—) reported density of N,N-dimethylacetamide, (■) calculated density in MedeA[®]-GIBBS with AUA model and (●) calculated density in MedeA[®]-LAMMPS with the pcff+ model.

9.9. Appendix I: Validation of AUA model based on the reported radial distribution function of N, N- dimethylacetamide

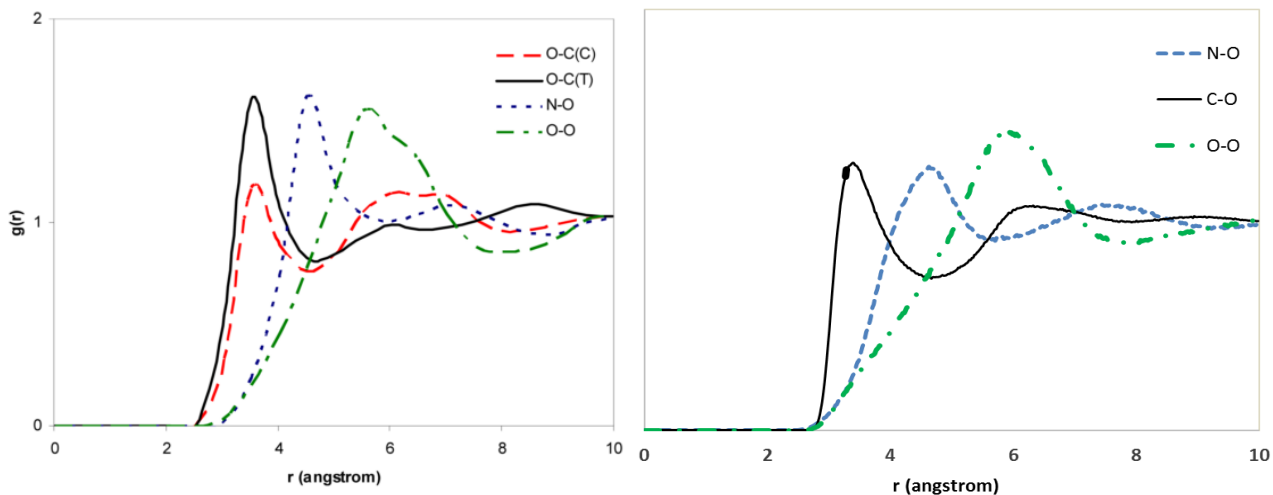


Figure I- 1. Radial distribution function for N, N- dimethylacetamide

(a) Reported in the literature (Xie *et al.*, 2007)

(b) Calculated with the new parameters.

9.10. Appendix J: GIBBS-Monte Carlo flowchart for calculation of single phase properties of IR3535-nonanoic acid binary mixtures

